POLY(VINYL ALCOHOL) RADIOCHROMIC DOSIMETERS

THE DEVEOLPMENT OF A TRANSPARENT POLY(VINYL ALCOHOL) RADIOCHROMIC CRYOGEL DOSIMETER AND OPTICAL DETECTION METHODS

by

MOLHAM MAJED, EYADEH, M.Sc. Physics.

A Thesis

Submitted to the School of Graduate Studies

in Partial Fulfillment of the Requirements

for the Degree

Doctor of Philosophy

McMaster University

© Copyright by MOLHAM MAJED EYADEH, October 2015.

DOCTOR OF PHILOSOPHY (2015) McMaster University

(Department of Medical Physics and
Applied Radiation Sciences) Hamilton, ON, Canada

TITLE: The Development of a Transparent Poly(vinyl alcohol) Radiochromic Cryogel Dosimeter and Optical Detection Methods

AUTHOR: MOLHAM MAJED EYADEH, M.Sc. Physics (Yarmouk University)

SUPERVISOR: Dr. Kevin R. Diamond

NUMBER OF PAGES: xix, 157

Abstract

In radiation therapy, gel dosimetry is used to measure radiation doses for treatment verification. Gel dosimeters have the ability to record dose information in three dimensions. The objective of this thesis was to fabricate a transparent cryogel radiochromic dosimeter with poly(vinyl alcohol) (PVA) as the gelling agent. A transparent dosimeter may be analyzed using an optical read out technique, which is desirable. PVA cryogels can be made transparent by adding dimethyl sulfoxide (DMSO).

Measurements of dose response were performed and various parameters were adjusted, including: numbers of freeze-thaw cycles (FTCs); concentrations of PVA; DMSO concentration. The measured absorption coefficient increased linearly with dose up to approximately 10 Gy. The sensitivity was increased for higher PVA concentrations, larger numbers of FTCs, and less DMSO. The resulting dosimeter was stable and showed no significant dose rate or photon energy dependence.

The cryogels were later formed into 5 mm thick films and used as a tool for performing *in vivo* dosimetry. The dose response of the radiochromic bolus was characterized by irradiating it on a flat surface at different gantry angles. The dose measured in the bolus was approximately 0.80 of the dose measured by Gafchromic film at the skin surface, taking the obliquity into account. IMRT treatments were delivered to a RANDO phantom. The radiochromic bolus was used to measure skin surface dose in two dimensions at various locations. The 0.80 factor was used to calibrate the bolus, which was then compared to an accompanying film measurement. Good agreement was

observed between the measurements (>95% gamma pass rate), suggesting the radiochromic bolus may be suitable for *in vivo* applications.

The radiochromic bolus was then used to evaluate errors associated with the breath hold technique often used with left chest wall tangential irradiation. Treatment plan incorporating the radiochromic bolus was delivered at the planned position and shifted anterior-posteriorly (A/P) up to 5 mm. Large discrepancies from the planned two dimensional skin surface distribution were observed for shifts as small as 3 mm in the A/P direction. The study demonstrated that the cryogel was sensitive to small positioning uncertainties for chest wall irradiations, potentially allowing for the detection of clinically relevant errors.

Other potential formulations of PVA-based radiochromic cryogels are discussed briefly as avenues to future research projects.

Keywords:

Gel Dosimetry, Radiation Dosimetry, Radiochromic Dosimeter, Radiotherapy, Poly(vinyl Alcohol) PVA, Cryogel

Acknowledgment

I would like to thank my supervisor, Dr. Kevin Diamond, for his invaluable guidance, support, encouragement, and patience during the full course of this work. I'm extremely grateful for the time he spent editing the content of this thesis. My deep appreciation goes to my supervisory committee members Dr. Tom Farrell and Dr. Marcin Wierzbicki for their assistance, advice, and constructive feeding back during my PhD. I must also record my gratitude to Pouria Ataei, Dr. Orest Ostapiak and Dr. Martin Shim for their assistance with the software used during my thesis. My appreciation goes to Dr Mark Weston for his invaluable assistance and guidance in the lab and during the irradiation of the chest wall phantom. I would like to thank Dr. Janos Juhasz for his advice and assistance in scanning the RANDO phantom. I would also like to thank our very own Juravinski Cancer Centre machine shop for their work of the custom moulds that were used in this thesis. Many thanks to the entire physics quality assurance staff at the Juravinski Cancer Centre for their patience during this work. I also thank administrative assistants Pauline Hiltz and Fiona Ahlang.

Finally I would also like to give special thanks to my parents, brothers, and sisters for all of their encouragement. Special thanks to my lovely wife for her support and patience as always.

Table of Contents

Abstract……iv

Acknowledgment……vi

Table of Contents……vii

List of Figures……xii

List of Tables……xvii

List of Abbreviations……xviii

1. Introduction……1

1.1 Radiotherapy……2

1.1.1 Breathing Adapted Radiotherapy Technique……4

1.2 Dosimetry……5

1.2.1 Gamma Analysis……6

1.2.2 *In vivo* Dosimetry……9

1.2.2.1 Film Dosimetry……10

1.3 Gel Dosimeters……11

1.3.1 Ferrous Sulphate (Fricke) Gel Dosimeter……12

1.3.2 Polymer Gel Dosimeter……14

1.3.3 Radiochromic Gel Dosimeter……..……16

1.3.3.1 Poly(vinyl alcohol) Cryogel Based Dosimeter…….……18

1.4 Clinical Applications of Gel Dosimetry……..……19

1.4.1 Intensity Modulated Radiation Therapy (IMRT)……...……...19

1.4.2 Volumtric Modulated Arc Therapy (VMAT)……..……..…..…22

1.4.3 Stereotactic Radiosurgery (SRS)……..…..……22

1.5 Thesis Proposal……..……...…..23

2. Paper I…….……..……..38

2.0.1 Introduction to Paper I……..……...……39

2.0.2 Content of Paper I…….……..……...…..40

2.1 Abstract…….……..……40

2.2 Introduction……..……40

2.3 Materials and Methods……..……44

2.3.1 Preparation of the FBX Cryogel Dosimeter ……..……...…44

2.3.2 Measurement of FBX Gel Dosimeter Stability……..……...46

2.3.3 Irradiation of FBX Cryogel Dosimeter ……..…...…48

2.3.4 Wavelengths Selection and Averaging ……..……..……...49

2.4 Results and Discussion……..……..……50

2.4.1 Stability of Dosimeter Before and After Irradiation……..……...……50

2.4.2 Dose Response of Typical PVA-C Formulations……...……59

2.4.3 Dose Rate Effect……...……70

2.4.4 Energy Effect……...……71

2.5 Conclusion……..……..72

3. Paper II……..……77

3.0.1 Introduction to Paper II……..……..78

3.0.2 Content of Paper II……...79

3.1 Abstract……..……79

3.2 Introduction……..……..…80

3.3 Materials and Methods……..……..…82

3.3.1 Translucent FBX PVA-C Dosimeter Preparation……..……..……82

3.3.2 Radiochromic Bolus Read out Apparatus……..……84

3.3.3 Calibration of Radiochromic Bolus and Film……..……85

3.3.4 Calibration of Radiochromic Bolus for Skin Surface Dosimetry……..…86

3.3.5 Validation of Skin Surface Dosimetry Using Radiochromic Bolus……88

3.4 Results and Discussion……..……..……89

3.4.1 Calibration of Radiochromic Bolus for Skin Surface Dosimetry..…....89

3.4.2 Validation of Skin Surface Dosimetry Using Radiochromic Bolus……..….95

3.5 Conclusion……..……104

4. Paper III……..……....110

4.0.1 Introduction to Paper III…….……...…111

4.0.2 Content of Paper III……..…..……..…112

4.1 Abstract……..……..…112

4.2 Introduction……..……..113

4.3 Materials and Methods……..……..….116

4.3.1 Treatment Planning System and Dose Delivery ……..……..…..116

4.3.2 Planar Dose Calculation Using Dose Evaluation Surfaces……..…..118

4.3.3 Radiochromic Cryogel Dosimeter Preparation…….....118

4.3.4 Measurement of Cryogel Dosimeter Using a Charged Coupled Device (CCD) Camera Apparatus……...……..119

4.3.5 Calibration of Cryogel Dosimeter……...…….120

4.3.6 Two Dimensional Dose Analysis……...……..…121

4.4 Results and Discussion……..……..…121

4.5 Conclusion……..…….....138

5. Conclusions and Future Directions……..……..….146

5.1 Summary and Conclusions……..……146

5.2 Future Directions……..……151

Appendix I……..…..…….155

LIST OF FIGURES

Chapter 1……

Figure 1.1 Gamma index concept illustration. The measured dose and position is denoted by $D_m(\mathbf{r}_m)$ and the calculated dose and position is denoted by $D_c(\mathbf{r}_c)$. The given acceptance criteria is represented by the black and orange ellipses. Based on (Low *et al.* 1998)……7

Paper I……

Figure 2.1 Schematic diagram of the measurement apparatus. Solid lines represent optical paths, while the broken line represents the electrical path……..……...47

Figure 2.2 The intensity of transmitted light for reference and pre-irradiation samples made from 5% PVA and one FTC with 20/80 water/DMSO……..……..……..…48

Figure 2.3 Absorption coefficients of different dosimeter formulations before irradiation for different concentrations of PVA. Different symbols represent different percentages of PVA used in the formulations. (a) Three FTCs, 20/80 water/DMSO formulation and (b) three FTCs 30/70 water/DMSO formulation. Each data point represents the mean absorption coefficient averaged over 590 – 600 nm for three independent preparations measured at five locations on each sample (*n* = 15). The error bars are the standard errors of the plotted measured values. The solid line is the average measured absorption coefficient and has been included to guide the eye……52-53

Figure 2.4 Absorption coefficient of the 15% (three FTCs) 20/80 water/DMSO gel dosimeter formulation for a seven day period prior to irradiation. Each data point represents the mean absorption coefficient averaged over 590 – 600 nm for three independent preparations measured at five locations on each sample (*n* = 15). The error bars are the standard errors of the plotted measured values. The solid line is the average measured absorption coefficient and has been included to guide the eye..……54

Figure 2.5 Box and whisker plots showing the measured absorption coefficients of different dosimeter formulations before irradiation for different concentrations of PVA. The bracketed numbers (1, 2, 3) represent independently prepared formulations. (a) Three FTCs, 20/80

water/DMSO formulation measured over a 2 day prior to irradiation; (b) three FTCs 30/70 water/DMSO formulation measured over a two day prior to irradiation; and (c) three FTCs, 20/80 water/DMSO formulation measured over a seven day period prior to irradiation……..…56-58

Figure 2.6 The fiducial markers show typical measurement locations used to obtain the average absorption coefficient of the sample……..…...59

Figure 2.7 A photograph of the reference, pre-irradiation, and post-irradiation for the 15% (three FTCs) 20/80 water/DMSO dosimeter system……..…59

Figure 2.8 Absorption coefficient behaviour versus time for samples of the 15% (three FTCs) 20/80 water/DMSO gel dosimeter formulation irradiated with 500 cGy of a 6, 10, and 18 MV photon beams……...……..…61

Figure 2.9 (a) The 20 positions used to evaluate sample heterogeneity of the 15% (three FTCs) 20/80 water/DMSO gel dosimeter formulation irradiated with 500 cGy of a 6 MV photon beam. (b) Measured absorption coefficient versus position for the sample shown in figure 2.9a.The solid line is the average measured absorption coefficient and has been included to guide the eye……...……..…62

Figure 2.10 (a) The change in FBX-PVA cryogel absorption spectrum of the 5% PVA (three FTCs) 20/80 water/DMSO formulation due to irradiation. The absorption spectra of the unirradiated gel (0 cGy curve) and the irradiated gels (100, 250, 500, 750 and 1000 cGy curves) were measured using a colourless and transparent PVA-C sample as reference. (b) Dose-response curves of different dosimeter formulations for different concentrations of PVA. Different symbols represent different percentages of PVA used in the formulations for three FTCs, 20/80 water/DMSO formulation, and (c) three FTCs 30/70 water/DMSO formulation. Different symbols represent different percentages of PVA used in the formulations. Each data point represents the mean absorption coefficient averaged over 590 – 600 nm for three independent preparations measured at five locations on each sample (n = 15). The error bars are the standard errors of the plotted measured values……..……..……53-65

Figure 2.11 Sensitivity of different concentrations of PVA dosimeters. (a) 20/80 and (b) 30/70. Different symbols represent the number of FTCs……66-67

Figure 2.12 Dose-response curve of 15% PVA (three FTCs) using a 20/80 water/DMSO ratio formulation up to 40 Gy. Each data point represents the mean absorption coefficient averaged over 590 – 600 nm taken over a three locations on each sample. The error bars are the standard errors of the plotted measured values……..……..……..…69

Figure 2.13 Absorbance of the gel dosimeter with different dose rate machine settings (100, 300, 400 and 600 MU/min), 6 MV, and 500 cGy delivered dose for sample of 15% (three FTCs) 20/80 water/DMSO dosimeter system. Each data point represents the mean absorption coefficient averaged over 590 – 600 nm and taken over a three day period post irradiation measured at three locations on each sample (*n* = 9). The error bars are the standard errors of the plotted measured values…….…...……70-71

Figure 2.14 Evaluation of energy response of FBX-PVA-C using a 15% (three FTCs) 20/80 water/DMSO formulation**.....**72

Paper II……...

Figure 3.1 In house 2D optical imaging apparatus. The lens is 61 cm away from the LED array, and the light box is 15.5 x 15.5 cm^2……...……..…85

Figure 3.2 Schematic of the radiochromic bolus and EBT-2 film irradiation. A 3 x 3 cm^2 field was formed using the jaw collimator and 1000 MU were delivered with a rate of 600 MU/min. The procedure was repeated with gantry rotations ranging from 0^o to 90^o..... 87

Figure 3.3 An example of radiochromic bolus definition for and AP/PA opposed pair. The bolus is 0.5 cm thick…….……..……..……...89

Figure 3.4 Photographs of irradiated radiochromic bolus and EBT-2 film arising from the configuration shown in figure 3.2: gantry angles of 0, 45, and 90^o from left to right……..……..90

Figure 3.5 The ratio of the measured dose distribution in a radiochromic bolus to the surface dose distribution estimated using Gafchromic EBT-2 film for gantry angles of a) 0 ,b) 22.5, c) 45, d) 67.5, and e) 90^o. The irradiated area regions of interest are included……...…….…...91-92

Figure 3.6 Cross line profiles (x-axis) of absolute dose distributions extracted from Gafchromic film, radiochromic bolus, calibrated radiochromic bolus using derived scaling factor of 0.80, and TPS surface dose for (a) 0 and (b) 90^{o} gantry angles……...…93

Figure 3.7 Inline profiles (y-axis) of absolute dose distributions extracted from Gafchromic film, radiochromic bolus, calibrated radiochromic bolus using derived scaling factor of 0.80, and TPS surface dose for (a) 0 and (b) 90^{o} gantry angles……...…94

Figure 3.8 Absorbed dose in cGy from calibrated measured radiochromic bolus (a,c) and the measured Gafchromic EBT-2 film (b,d) for two tangential POP static beams of (0^{o} / 180^{o}) and (90^{o} / 270^{o}) respectively……..……97-99

Figure 3.9 Absorbed dose in cGy from calibrated measured radiochromic bolus (panel a) and the measured Gafchromic EBT-2 film (panel b) for step-and-shoot IMRT larynx treatment……100-101

Figure 3.10 Absorbed dose in cGy from calibrated measured radiochromic bolus (panel a) and the measured Gafchromic EBT-2 film (panel b) for step-and-shoot IMRT neck treatment……..……102

Paper III……

Figure 4.1 Treatment planning used in this study. Three plan view of the two tangential beam arrangments……..……117

Figure 4.2 2D optical imaging apparatus consisting of a diffuse red light surface and a lens coupled CCD. Excess area on the light surface was masked using black construction paper to improve the dynamic range of the system……..…..…..……120

Figure 4.3 Absolute dose distributions maps in cGy calculated in Pinnacle at the phantom-cryogel interface at different A/P positions from the planned position. a) 0 mm, b) +2 mm, c) -3 mm, and d) +5 mm……..…..123-124

Figure 4.4 2D gamma maps (3%/3 mm, 10% threshold) that compare absolute dose planes at the phantom-cryogel interface generated in Pinnacle. The dose plane corresponding to the treatment position was compared to (A/P) shifts of a) +2 and b) -3 mm……..……..…...126

Figure 4.5 The fraction of chest wall target covered by the shifted 95% isodose levels as a function of A/P shift……128

Figure 4.6 Absolute dose distributions maps in cGy measured using the cryogel dosimeter at different A/P shifts from the planned position: a) 0 mm, b) +2 mm, c) -3 mm, and d) +5 mm……130-131

Figure 4.7 The 0 mm offset measured cryogel dose distribution map in cGy with black lines showing the cross line (horizontal) and inline (vertical) axes used to extract profiles at different A/P shifts, shown in figure 4.8……123

Figure 4.8 a) The cross line profiles and b) inline profiles extracted from absolute measured cryogel dose distribution images at different A/P shifts. The cross line profiles are taken from cryogels where the table was raised (+A/P couch shifts) and the inline profiles when the table was lowered (-A/P couch shifts)…….....133

Figure 4.9 2D gamma maps (3%/3 mm, 10% threshold) comparing dose measured using the cryogel dosimeter at the planned treatment position to A/P shifts of a) +2 and b) -3 mm……....135

LIST OF TABLES

Paper II……

Table 3.1 The mean ratio between surface dose and the dose measured in the radiochromic bolus at different gantry angles ranging from 0 to 90º……92

Table 3.2 Gamma pass rates for comparisons of calibrated radiochromic bolus and EBT-2 Gafchromic film (3%/3mm, 10% threshold) for different field arrangements……..……..103

Paper III……

Table 4.1 Gamma analyses (3%/3 mm, 10% threshold) of absolute dose planes created in Pinnacle for all A/P shifts compared to the planned A/P position……..……127

Table 4.2 Summary of gamma analyses (3%/3 mm, 10% threshold) comparing the measured absolute doses acquired at different A/P shifts to those acquired at the planned position. For each (A/P) shift a total of 9 gamma analyses were performed……..……..136

Table 4.3 Summary of gamma analyses (3%/3 mm, 10% threshold) comparing absolute doses measured at the same A/P position using the cryogel……137

LIST OF ABREVIATIONS

AAm	Monomer acrylamide
ABC	Active breathing coordinator
A/P	Anterior/posterior
BANANA	Bis, AAm, nitrous oxide and agarose
BANG	Bis, AAm, Nitrogen and Gelatin
BART	Breathing adapted radiotherapy
BH	Breath hold
Bis	N,N'-Methylene-bis-acrylamide
CCD	Charge coupled device
CTV	Clinical target volume
DIBH	Deep inspiration breath hold
DMSO	Dimethyl sulfoxide
3DCRT	Three dimensional conformal radiation therapy
EBRT	External beam radiation therapy
FB	Free breathing
FBX	Ferrous sulphate benzoic acid xylenol orange
FBX-PVA-C	Ferrous sulphate benzoic acid xylenol orange Poly (vinyl alcohol) cryogel
FTCs	Freeze-thaw cycles
FXG	Ferrous sulphate xylenol orange gelatin
IMRT	Intensity modulated radiation therapy
LED	Light emitting diode
MAGIC	Methacrylic acid, ascorbic acid, gelatin and copper
MLCs	Multileaf collimators
MOSFETs	Metal–oxide–semiconductor field-effect transistors

MRI	Magnetic resonance imaging
MU	Monitor Unit
OAR	Organs at risk
OD	Optical density
Optical CT	Optical computed tomography
OSL	Optically simulated luminescence
PAG	PolyAcrylamide gelatin gel
PTV	Planning target volume
PVA	Poly(vinyl alcohol)
PVA-C	Poly(vinyl alcohol) cryogel
POP	Parallel-opposed-pair
ROI	Region of interest
RPM	Real-time position management
SRS	Stereotactic radiosurgery
SSD	Source-to-surface distance
TLDs	Thermoluminescent detectors
TPS	Treatment planning system
VMAT	Volumetric modulated arc therapy
XO	Xylenol orange

Chapter 1

1. Introduction

In radiation therapy, a variety of dosimetry systems have been applied to different radiation delivery modalities and applications to monitor the deposited dose. One such system is the gel dosimeter, a measurement tool that features a radiosensitive material that undergoes changes in its chemical structures as a function of absorbed radiation dose (Schreiner 2009). Traditional *in vivo* dosimeters (diodes, thermoluminescent detectors (TLDs), and metal–oxide–semiconductor field-effect transistors (MOSFETs)) measure dose at discrete points. Radiosensitive films measure two dimensional dose distributions (Saur *et al.* 2009). Three dimensional dose distributions are the domain of gel dosimeters (McJury *et al.* 2000). These gels take the shape of the containers they are formed in, allowing for realistic irradiation conditions (De Deene *et al.* 1998, Hill *et al.* 2005). The development of gel dosimetry arose from the need of a method of verifying complicated dose distributions in three dimensions accurately and with good spatial resolution (McJury *et al.* 2000). These complex dose distributions arise naturally from techniques such as intensity modulated radiation therapy (IMRT) or stereotactic radiosurgery (SRS), where small or heavily modulated irradiation fields produce regions of steep dose gradients (McJury *et al.* 2000, Ibbott 2006, Baldock *et al.* 2010, Adline *et al.* 2014). Gel dosimeters can be used as quality assurance tools for the verification of dose distributions in a variety of settings, including end-to-end testing (Kron 2001); and as a bolus material that also monitors the surface dose distribution (Chu *et al.* 2000).

Most gel dosimeters are radiologically tissue-equivalent; their physical properties are also adjustable to a certain extent, depending on the material chosen. For example, many gel dosimeters use gelatin or agarose as the gelling agent (also referred to as the matrix material): these materials can be made more or less stiff by adjusting the matrix concentration. Poly(vinyl alcohol) (PVA) is another choice: its mechanical properties are tuneable by adjusting the concentration of PVA, and also by subjecting the PVA to thermal cycling; freezing and thawing the material to form a crystalline structure (Wang and Campbell 2009).

This chapter starts with a basic introduction to radiation therapy, followed by dosimetry, different types of gel dosimeters, and the clinical rationale behind gel dosimetry. Lastly, the thesis proposal is presented.

1.1 Radiation Therapy

Radiation therapy is a valuable tool in the management and treatment of tumours, where the aim is to deliver adequate doses to the tumour while minimizing the dose to the surrounding normal tissue (Jin *et al.* 2008, Schreiner 2009).

Conventional external beam radiation therapy (EBRT, also referred to as 3D conformal radiation therapy, 3DCRT) is usually restricted to co-planar, conformal beams of radiation delivered to the patient, where the radiation beams are shaped to match the shape of the tumour (Thwaites and Tuohy 2006, Camphausen and Lawrence 2008). These radiation fields may also be non-coplanar and lightly modulated. The tumour volume can be contoured using CT images, with a margin added for setup error and internal motions (Camphausen and Lawrence 2008).

Intensity modulated radiation therapy (IMRT) is the next generation of 3DCRT (Bakiu *et al.* 2013), where the radiation fields are modulated in order to improve the conformity of the dose delivered to the tumour. Concave and convex dose distributions are enabled by IMRT, allowing for the treatment of tumours that are wrapped around organs at risk (Brahme *et al.* 1982, Galvin *et al.* 2004, Bakiu *et al.* 2013). IMRT plans are typically developed using an inverse planning approach by a treatment planning system (TPS), where multiple gantry angles or couch angles are employed. IMRT plans may also be generated by manual segmentation, referred to as forward planned IMRT. The fluence is modulated for each of the different treatment fields, which is made possible by using a dynamic multileaf collimator (MLC) (Camphausen and Lawrence 2008, Sakhalkar and Oldham 2008). The MLC can be moved during the treatment and permit the fluence to be varied across the field by shielding different parts of the beam at different times. In IMRT, the high dose region conforms to the three dimension target volume geometry with fast fall off, sparing the surrounding healthy tissues, whereas conformal radiation therapy is more limited (Galvin *et al.* 2004).

Volumetric modulated arc therapy (VMAT) is an advanced EBRT technique that employs one or more arcs; it can realize highly conformal dose distributions while sparing surrounding normal tissues better and is delivered faster than IMRT in many cases (Wuu *et al*. 2015). The radiation intensity delivered by a VMAT treatment is modulated using three parameters: gantry rotation speed, MLC motions, and dose rate variation (Brtelsena *et al.* 2010, Wuu *et al.* 2015).

The use of these advanced radiation therapy techniques often involves complicated and interrelated gantry motions, as well as interplay between the gantry and patient motions.

The patient motions are difficult to correct in the linac-based setting; however, strategies have been developed to control some of these motions. An example is the use of gating to reduce the effects of breathing on thorax and abdominal irradiation (Korreman *et al.* 2005, Fassi *et al.* 2014).

1.1.1 Breathing Adapted Radiotherapy Technique

During treatment of the thorax and abdomen, the motion of target tissues due to respiration decreases the accuracy with which the dose and distribution in those tissues are known. Irradiation of lung and left-sided targets in the breast and chest wall raise additional concerns related to cardiac and pulmonary toxicity (Korreman *et al.* 2005, Månsson *et al.* 2006, Recht 2006, Shah *et al.* 2014, Latty *et al.* 2015). Breathing adapted radiotherapy (BART) of breast and lung cancers, using techniques such as respiratory gating, breath hold (BH), and deep inspiration breath hold (DIBH) techniques, allow for better control over where the dose is deposited, and may also decrease the dose absorbed in organs at risk (OAR) (Korreman *et al.* 2005, Fassi *et al*. 2014).

In BART the treatment beam is enabled only during a part of the patient's normal respiratory cycle. A treatment is said to be gated if the beam is on during a set phase of the breathing cycle (*e.g.* full exhale); during BH, a patient empties/fills their lungs to a predetermined point and holds their breath. DIBH refers to a situation where the patient fills their lungs completely (Ohara *et al*.1989, Korreman *et al*. 2005, Shah *et al*. 2014).

Free breathing gated radiotherapy systems use a camera to track an external fiducial marker (*e.g.* a gating block) as it rises and falls with abdominal or chest position. The

treatment is delivered when the fiducial falls within a certain range based on data acquired during the CT simulation process (Korreman *et al.* 2005, Månsson *et al*. 2006, Fassi *et al.* 2014).

During DIBH, the subject takes a deep breath and holds it during CT simulation and during treatment while radiation is being delivered. The treatment is delivered as long as the chest wall stays within a certain range of positions, usually 5 – 10 mm, tracked using an external fiducial on the thorax or abdomen (McCarter and Beckham 2000, Langen and Jones 2001). The main advantage of DIBH is a reduction in cardiac dose while maintaining target dose coverage (Korreman *et al.* 2005, Månsson *et al.* 2006, Fassi *et al.* 2014). DIBH can provide shorter treatment times compared with gated delivery due to increased beam on time while the breath is held compared to the beam being cycled on and off (Korreman *et al.* 2005, Fassi *et al.* 2014).

1.2 Dosimetry

Dosimetry, as it relates to the treatment fields used in radiation therapy, involves the measurement of absorbed dose delivered by the beams either to the patient or to a quality assurance phantom. An ideal radiation dosimeter should allow for absolute dose determination with high accuracy and precision. When used on a patient, the dosimeter should conform well to the body as to ensure accurate dose estimates in the underlying tissues of interest (Podgorsak 2005). Dosimeter systems can be described as being one dimensional, which is a point measurement (or a series of point measurements forming a line); two dimensional, which corresponds to a planar map of the dose distribution; or three dimensional, where the dose is recorded in a volume (IAEA 2009). Measurements

that are performed on a patient over the course of their treatment are referred to as *in vivo* dosimetry. The measurement of dose distributions may require comparison with those generated from a treatment plan to verify the agreement between measured and calculated doses. Gamma analysis is used for this purpose (Low *et al.* 1998, Low and Dempsey 2003, Ju *et al.* 2008, Low 2010).

1.2.1 Gamma Analysis

Dose distributions are compared for spatial accuracy (distance to agreement) and dosimetric performance (dose percent error). The gamma index (γ) is a parameter generated to describe the combined spatial and dosimetric performance. Gamma analysis is used routinely to judge the agreement between treatment plans and the dose measured using a quality assurance phantom (Low *et al.* 1998, Low and Dempsey 2003, Ju *et al.* 2008, Low 2010). Figure 1.1 shows an illustration of how the gamma index (γ) evaluation tool works.

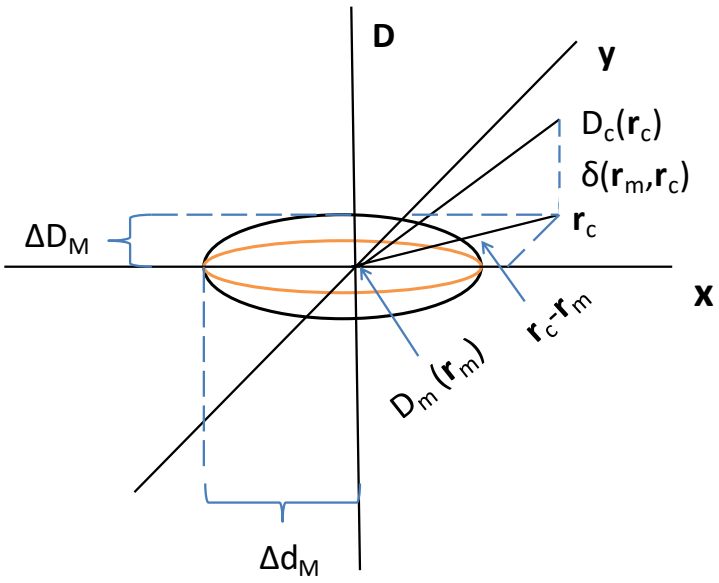

Figure 1.1 Gamma index concept illustration. The measured dose and position is denoted by $D_m(\mathbf{r}_m)$ and the calculated dose and position is denoted by $D_c(\mathbf{r}_c)$. The given acceptance criteria is represented by the black and orange ellipses. Based on (Low *et al.* 1998).

Figure 1.1 represents the evaluation of two dose distributions based on two acceptance criteria: tolerance on the distance Δd_M, and tolerance of the dose ΔD_M. The figure includes a measurement point $\mathbf{r}_m$, lying at the origin. The axis (x,y) represent the spatial location $\mathbf{r}_c$ of the calculated distribution relative to the measured point. The δ represents the difference between the measured doses $D_m(\mathbf{r}_m)$ and the calculated doses $D_c(\mathbf{r}_c)$.

Δd_M is the radius of a disk in the $\mathbf{r}_m - \mathbf{r}_c$ plane. If $D_c(\mathbf{r}_c)$ falls within the disk, the calculated distribution passes the tolerance on the distance test. The vertical line in the figure represents the tolerance of the dose; its length is $2\Delta D_M$. If $\delta \leq \Delta D_M$, the calculated distribution passes the dose difference test at the measurement point.

The combined acceptance criteria Δd_M and ΔD_M are represented by an ellipsoid defined by (Low *et al.* 1998, Low and Dempsey 2003, Ju *et al.* 2008, Low 2010):

$$\Gamma(\boldsymbol{r}_m, \boldsymbol{r}_c) = \sqrt{\frac{r^2(\boldsymbol{r}_m, \boldsymbol{r}_c)}{\Delta d_M{}^2} + \frac{\delta^2(\boldsymbol{r}_m, \boldsymbol{r}_c)}{\Delta D_M{}^2}} \qquad (1.1)$$

where

$\Gamma(\boldsymbol{r}_m, \boldsymbol{r}_c)$ is related to the gamma index (γ) by:

$$\gamma(\boldsymbol{r}_m) = \min\{\Gamma(\boldsymbol{r}_m, \boldsymbol{r}_c)\} \forall \{\boldsymbol{r}_c\}$$
$$r(\boldsymbol{r}_m, \boldsymbol{r}_c) = |\mathbf{r}_c - \mathbf{r}_m|, \text{ and} \qquad (1.2)$$
$$\delta(\boldsymbol{r}_m, \boldsymbol{r}_c) = D_c(\mathbf{r}_c) - D_m(\mathbf{r}_m)$$

If any $D_c(r_c)$ is within or on the ellipsoid defined by equation (1.1), the calculation passes r_m.

The pass fail-criterion is satisfied if

$\gamma(\boldsymbol{r}_m) \leq 1$, *i.e.* calculation passes, (1.3)

otherwise the calculation fails.

For the $\gamma(\boldsymbol{r}_m)$ values, 0 corresponds to an exact match between calculated and measured dose and 1 being the tolerance is met exactly. Values above one represent calculations that do not meet the acceptance criteria (Low *et al.* 1998, Low and Dempsey 2003, Ju *et al.* 2008, Low 2010).

1.2.2 *In vivo* Dosimetry

In vivo dosimetry is considered an important component of radiotherapy; it provides dose estimates to patients undergoing radiation treatments by employing external dosimeters such as TLDs and MOSFETs (point detectors), or radiosensitive film. It is used to validate and verify the dose distributions calculated by the TPS (Mijnheer 2008).

Point detectors and radiosensitive film dosimeters can measure radiation doses to high precision in one or two dimensions respectively. Dose distributions may be evaluated using numerous point dosimeters, such as TLDs and MOSFETs; however, these dose maps are quite coarse and may not be sufficient in some cases (Chan *et al.* 2006, Falco *et al.* 2015, Khanal *et al.* 2015). If a fine 2D distribution is desired, the only current option is to use a radiosensitive film. Film provides excellent resolution and is a good option to verify distributions arising from highly modulated fields (Chiu-Tsao and Chan 2010, Nakano *et al.* 2012, Morales *et al*. 2014).

1.2.2.1 Film Dosimetry

Historically, film has been primarily used in transmission radiography to identify bone damage, dense formations such as kidney stones, and dental caries (Heggie *et al*. 2001). In radiotherapy, film may be used to verify patient positioning prior to treatment and verify the location and dose distribution of the treatment fields (Mayles *et al.* 2007). Film dosimetry offers the ability to visualize dose distributions in a two dimension plane. Modern film is tissue equivalent, and has high spatial resolution, and therefore valuable for determining doses in small regions (Nakano *et al.* 2012, Morales *et al*. 2014). Two types of film have been used for dosimetry: radiographic and radiochromic.

Radiographic film consists of a transparent polyester base coated with a sensitive layer that consists of a silver halide. When the film is exposed to ionizing radiation, an incident photon interacts with the sensitive area, and a silver halide is ionized. The ionized silver halide is rendered visible through chemical processing, where the exposed silver halide is reduced to metallic silver. The amount of darkening is dependent on the amount of energy deposited during the ionization (Heggie *et al*. 2001). In contrast, radiochromic film changes colour upon being irradiated with ionizing radiation due to a polymerization process in which the film turns blue (Podgorsak 2005, Mayles *et al.* 2007). Radiochromic film is self developing and can be used over a higher dose range compared with radiographic film (Device *et al*. 2005, Podgorsak 2005).

For both types of film, the dose is determined by measuring the optical density (OD) of the film and comparing to a calibration. Ideally, dosimetry is restricted to the linear region of the film: above the level of the toe (base OD + post-processing fog) and below

the saturation point. The toe region represents the optical density of the unexposed film (Podgorsak 2005).

A type of radiochromic film called Gafchromic (ISP 2009) is used with EBRT. Gafchromic film is suitable for use in routine dose verification of highly modulated treatment plans (Martišíková *et al*. 2008).

While film works well in quality assurance phantoms, it does not conform well to most large and curved regions, where the fundamental problem is that flexible film cannot be prepared. In these situations, a more flexible material is desirable. Many of the limitations encountered with point detectors and radiosensitive film can be overcome using a deformable two dimensional dosimeter. One such solution is the gel dosimeter.

1.3 Gel Dosimeters

Gel dosimeters have a long history in radiation dosimetry (McJury *et al.* 2000). For many years authors have sought to measure the absorbed radiation dose distributions using gel dosimeters due to their ability to record dose in three dimensions, where the phantom itself represents the detector (Baldock 2006, Nazir *et al.* 2010). The study of gel dosimeters used in a clinical setting has been ongoing since the 1950s, where gel dosimeters were used for depth dose measurements (Day and Stein 1950, Andrews *et al.* 1957). The first development of a radiation sensitive gel was introduced by Day and Stein in 1950, where post-irradiation colour changes were observed through the use of chemical dyes (*e.g.* methylene blue and phenol indo dichlorophenol) suspended in a gelatin or agarose gelling agent. Gelatin is transparent and turns brittle when dry. Agarose is a jelly-like substance, a polymer made up of subunits of the sugar galactose.

Day and Stein. (1950) showed that the change in the colour was related to the change of chemical structures of the dyes once exposed to radiation. Later, in 1957, depth dose measurements for photons and electrons were studied and the nature of the colour change was investigated. It was shown that the chemical reaction responsible for the colour change was indirect, caused by free radicals created from water when it is irradiated (Andrews *et al.* 1957). Modern gel dosimeters do not only rely on colour changes; polymerization reactions can also be initiated when free radicals interact with certain monomers. In this section three types of gel dosimeters are introduced: ferrous sulphate (Fricke), polymer, and radiochromic.

1.3.1 Ferrous Sulphate (Fricke) Gel Dosimeter

For over 80 years in radiation dosimetry, ferrous sulphate (Fricke) solutions have been used in various forms (Fricke and Morse 1927, Fricke and Hart 1955). Fricke gel dosimeters are based on the oxidation of ferrous ions (Fe^{2+}) into ferric ions (Fe^{3+}) during irradiation (Fricke and Morse 1927). The concentration of ferric ions can be quantified and correlated to dose by measuring the optical density of the solution or using magnetic resonance imaging (MRI) techniques (Gore *et al.* 1984). Even though the aqueous system is sensitive to radiation, it cannot record spatial information. Gore *et al.* (1984) introduced a gel dosimeter that joined the aqueous Fricke system with a gel matrix, reducing ion mobility and enabling three dimensional radiation dosimetry. Gore *et al*. (1984) showed that the increase in the concentration of the ferric ions in the Fricke solution caused a shortening of the longitudinal relaxation time (T1) of the protons present in the solution. The graph of R1 (1/T1) plotted against absorbed dose increased

linearly up to 41 Gy. Fricke gel dosimeters are readily prepared and are readable shortly after irradiation (Schreiner 2004).

Chemically, upon irradiation, water decomposition takes place and resultant hydrogen atoms react with oxygen to produce the hydroperoxyl radical (HO_2•) (Fricke and Morse 1927, Fricke and Hart 1955, Lundstrom *et al*. 2004):

$$H_2O \rightarrow H\bullet + OH\bullet \qquad (1.4)$$
$$H\bullet + O_2 \rightarrow HO_2\bullet$$

Different reactions lead to the conversion of Fe^{2+} into Fe^{3+} :

$$Fe^{2+} + OH\bullet \rightarrow Fe^{3+} + OH^-$$
$$Fe^{2+} + HO_2\bullet \rightarrow Fe^{3+} + HO_2^- \qquad (1.5)$$
$$HO_2^- + H_3O+ \rightarrow H_2O_2 + H_2O, \text{ and}$$
$$2Fe^{2+} + H_2O_2 \rightarrow 2Fe^{3+} + OH\bullet + OH^-$$

The quantity of ferric ions produced depends on the energy absorbed by the Fricke solution, where the change in ferric ion concentration is related to the radiation dose by the following equation (Fricke and Hart 1955):

$$\Delta[Fe^{3+}] = \frac{D \times G(Fe^{3+}) \times 10\rho}{N_A \times e} \qquad (1.6)$$

where D is the dose, $G(Fe^{3+})$ is the chemical yield of Fe^{3+} (ions produced per 100 eV), ρ is the density of the solution, N_A is Avogadro's number, and *e* is the number of Joules per electron volt.

Fricke gel dosimeters are tissue equivalent over a wide range of photon energies (Ibbott 2006). Different attempts at producing a Fricke gel dosimeter established that the ferric ions were mobile, free to move throughout the gel matrix (ion diffusion). Ion diffusion, and the following loss of spatial dose information, is a serious limitation on the use of a Fricke gel dosimeter system (Schreiner 2004).

1.3.2 Polymer Gel Dosimeters

To overcome the diffusion problem inherent in Fricke gel dosimeters, a new approach was tried: the Fricke solution was replaced with radiosensitive monomers suspended in the gel matrix (Maryanski *et al.*1993, 1996). These monomers undergo a polymerization reaction after irradiation: the polymer appears cloudy in the translucent matrix, allowing for read out using optical systems or MRI (Oldham *et al.* 2001, 2003). The MRI characteristics of the monomer and polymer forms are distinct. One of the most common polymer gel dosimeters is prepared by adding the monomer acrylamide (AAm) and the cross-linking agent N,N'-Methylene-bis-acrylamide (Bis) to a simple agarose-based gel (BANANA: Bis, AAm, nitrous oxide and agarose). Maryanski *et al.* reported that these gels had a high MRI signal after irradiation (Maryanski *at al.* 1993, 1994). In 1994, gelatin replaced agarose in the BANANA formulation, which led to a new generation of polymer gel (BANG: Bis, AAm, Nitrogen and Gelatin). Polymer gel dosimetry provides a method to access three dimensional maps of complex radiotherapy dose distributions with up to 1 mm spatial resolution (McJury *et al.* 2000).

However, due to the nature of the free radical chemistry for these gels, they must be prepared and maintained in an anoxic environment; otherwise the polymerization

reaction will be inhibited (Baldock *et al.* 1998, De Deene *et al.* 2002, Baldock 2006). One option is to remove all of the oxygen from the gel by bubbling nitrogen through it, and then forming it in a sealed container. A more practical solution is to add oxygen scavengers to the formulation allowing for the gel to be made and used under normal atmospheric conditions (Baldock 2006). These “normoxic” gel dosimeters such as MAGIC (methacrylic acid, ascorbic acid, gelatin and copper) (Fong *et al.* 2001) employ antioxidants such as ascorbic acid or tetrakis (hydroxymethyl) phosphonium chloride to remove oxygen from the phantom (De Deene 2002, Baldock 2006). For example, in the MAGIC formulation the ascorbic acid links the free oxygen within the gelatin matrix (Fong *et al.* 2001). The development of normoxic gel dosimeters was an important step, allowing for gels to be manufactured in the clinic rather than a closely controlled laboratory (Ibbott 2004).

Comparing with Fricke gel dosimeters, polymer gels are relatively stable and have high sensitivity to radiation. However, polymer gels are more challenging to prepare and the monomers are toxic (Guo *et al.* 2006, Ibbott 2006).

Another potential drawback to polymer gel dosimeters is reading out the dose information post-irradiation. While optical computed tomography (optical CT) may be used in some cases (Gore *et al.* 1996), specialized collimators are required to reduce the effects of scattering; artefacts arising from gradients in the index of refraction may also distort the recovered dose map (Trapp *et al.* 2001, Oldham *et al.* 2003, Campbell *et al.* 2015). Therefore MRI tends to be used to read out these polymer gel dosimeters. Early work by Maryanski *et al.* (1994) established the relationship between MRI parameters and the radiation-induced polymerization reaction. The main disadvantage

for using MRI is that it is more costly than other readout methods (*i.e.* optical methods) as well as the lack of accessibility at many clinical sites. An alternative approach is to develop a non-turbid gel dosimeter that can be read optically.

1.3.3 Radiochromic Gel Dosimeter

The introduction of optical CT scanners has stimulated the development of 3D radiochromic dosimeters (Baldock *et al.* 2010). These dosimeters change colour when exposed to irradiation. As mentioned earlier, various groups in the 1950's noted colour changes in dyes exposed to radiation, arising from interactions with free radicals (Day and Stein 1950, Andrews *et al.* 1957). These dyes were suspended in gelling agents such as gelatin and agarose to immobilize them and enable dose recording in 3D.

Fricke-based dosimeters were improved significantly by the addition of an iron chelating agent. In 1985, Gupta and Narayan developed a solution Fricke dosimeter comprised of ferrous sulphate, benzoic acid, and chelator xylenol orange (FBX), where the xylenol orange (XO) absorption spectrum is modified by the binding of iron, and also the oxidation state of the bound iron. Chemically, XO binds the ferrous ions forming a coloured complex (XO-Fe^{3+}) that absorbs in the visible range and can be measured using accessible optical systems (Lundstrom *et al*. 2004, Davis and Baldock 2008).

$$Fe^{3+} + XO \rightarrow Fe^{3+}\text{-}XO \qquad (1.7)$$

The added benefit of XO is that the ferric ions are no longer free to diffuse throughout the gel, a problem with early Fricke gels (Smith *et al.* 2015). Gupta and Narayan indicated that the benzoic acid increases the radiolytic oxidation of ferrous ions.

Updated versions of this formulation drop the benzoic acid: an example is described in Bero *et al.* (2000) where the formulation was suspended in gelatin (FXG), as did Schreiner in 1999. The colour change after irradiation is the result of structural changes that may be caused by: direct absorption of penetrating radiation, a reduction of pH level by releasing H+ ions, or the action of free radicals generated by the absorption of the radiation (Bero *et al.* 2000).

In 2003 a new class of 3D radiochromic dosimeter (PRESAGE®) was introduced. These dosimeters comprise an optically clear polyurethane matrix loaded with a leuco dye (Adamovics and Maryanski 2003). The resulting dosimeter is usually a solid, machinable cylinder that is read using an optical CT scanner. The dose response has excellent linearity over a large dose range and long term stability, but the mechanical properties of the matrix material are not tissue-like (*e.g.* deformability, compressibility, texture): it is a hard polyurethane matrix (Ibbott 2006, Doran *et al.* 2013). However, a deformable formulation of the PRESAGE® dosimeter has also been reported (Juang *et al*. 2013).

Matrix materials such as gelatin and agarose are relatively weak and still permit a degree of diffusion of the radiochromic components. By looking for a simple chemistry model that overcomes the diffusion problem, Chu *et al*. (2000) proposed using poly(vinyl alcohol) (PVA) as the gelling agent rather than gelatin or agarose. Chu noted some improvement in the diffusion characteristics of FX when the PVA is thermally cycled, resulting in a cryogel. A PVA cryogel (PVA-C) is a turbid, rubber like material that will maintain the shape of the mould it is formed in.

1.3.3.1 Poly(vinyl alcohol) Cryogel Based Dosimeter

Poly(vinyl alcohol) is a water soluble polymer that, when dissolved, forms a transparent hydrogel. The hydrogel can be made rigid by crosslinking polymer chains using chemicals or large doses of radiation (kGy), or by crystallization achieved through successive cycles of freezing and thawing. The result in each case is a rubbery turbid sample that has a high modulus of elasticity and superior strength compared with organic gelling agents (Kharine *et al.* 2003). PVA-C is an excellent choice for a gel dosimeter matrix material owing to its lifelike mechanical properties such as: deformability, compressibility, texture, shearing, and needle penetration; it can also be moulded into any desired shape. The mechanical properties of PVA-C are controlled by adjusting PVA concentration, and the number of freeze-thaw cycles the hydrogel is subjected to (Wang and Campbell 2009). Standard formulations of PVA-C are opaque, so scanning them optically may be challenging (Chu *et al.* 2000). Ideally, an optically scanned gel should be as transparent as possible, that is to say it should not be turbid (Olding and Schreiner 2011). The turbidity PVA-C tends to restrict its readout to MRI-based methods.

However, PVA-C can be made transparent by adding dimethyl sulfoxide (DMSO) to the formulation. Hyon *et al*. (1989) developed a transparent PVA cryogel formulation using a combination of DMSO and water as the solvent for dissolving PVA powder. DMSO is a clear liquid; it dissolves polar and non polar compounds as well as water does. The addition of DMSO to the hydrogel formulation brings down the freezing point of the solution, allowing PVA crystallization to progress without phase separation and volume expansion. This results in a cryogel whose transparency arises from the presence of

smaller pores than its turbid rival (Hyon *et al.* 1989). This transparent cryogel may then be used as a matrix for radiochromic chemicals, such as the FBX formulation. One potential disadvantage to employing DMSO is that it has been reported to act as a free radical scavenger (Silva *et al*. 2011).

1.4 Clinical Applications of Gel Dosimetry

Clinical applications of gel dosimetry started out with simple measurements of beam characteristics, such as depth dose profiles (Day and Stein 1950, Andrews *et al.* 1957). Since then, the body of science with respect to gel dosimetry has extended considerably (Gore *et al.* 1984). In general, gel dosimeters are still considered to be research projects and its clinical use is proceeding slowly (Ibbott 2006, Schreiner 2009, Wuu *et al.* 2015).

Demonstrated clinical applications of gel dosimeters in EBRT include dose distributions from imaging techniques, conformal radiation therapy, IMRT, VMAT, and stereotactic radiosurgery (SRS).

1.4.1 Intensity Modulated Radiation Therapy (IMRT)

Gel dosimeters have been used to evaluate conformal and IMRT dose distributions (Haas *et al.* 1997, Oldham *et al.* 1998, De Deene *et al.* 1999, Low *et al.* 1999, De Neve *et al.* 1999, De Deene 2002, Ibbott *et al.* 2002, Beach *et al.* 2003, Gustavsson *et al.* 2003, Ibbott *et al.* 2003, Vergote *et al.* 2003, Oldham *et al.* 2004, Molineu *et al.* 2005, Oldham *et al*. 2006, Higgins *et al*. 2007, Vandecasteele and De Deene 2013). These studies were performed using simple geometric and anthropomorphic phantoms in

arrangements that allowed for direct comparisons of gel dosimeters with measurements using other dosimeters such as film and TLDs, as well as comparisons directly with the TPS-derived distributions.

In 1997, Haas *et al*. compared measurements of polymer gel and film dosimeters to confirm conformal dose distributions produced by static compensators for treatment of a simulated pelvis, finding good qualitative agreement between film and gel. In 1999, De Neve *et al*. used a polymer gel dosimeter with IMRT delivery for head and neck radiation therapy. The measurements of gel were performed on an anthropomorphic phantom and compared with film measurements. Good agreement was reported between film and gel. In 1999, Low *et al*. evaluated an MRI-read polymer gel as a 3D dosimeter for IMRT. Ionization chambers, film, and TLD measurements were also performed. A tolerance of 3% and 3 mm distance-to-agreement criteria were used for gamma comparisons: more than 90% of the TLD measurements agreed with gel; the ionization chamber was within 1% of the dose measured by the gel; and within 2 mm localization compared with film. In 2000, De Deene *et al*. reported measurements of polymer gel and film dosimeters for a conformal irradiation treatment of a tumour located near the esophagus. They found the film and gel dose distributions maps agreed, with deviations of less than 3%.

Several studies compared the results of polymer and radiochromic gel dosimeter measurements of IMRT delivery performed on an anthropomorphic phantom directly with TPS derived distributions (Oldham *et al.* 1998, Vergote *et al.* 2003, Oldham *et al.* 2004, Sakhalkar *et al.* (2009a, 2009b), Vandecasteele and De Deene 2013, Jackson *et al.* 2015). These studies were performed using either MRI or optical CT read out to

recover the stored dose information from gel dosimeters used to verify different IMRT patient treatment plans, such as Tomotherapy irradiation (Oldham *et al.* 1998), head and neck (Sakhalkar *et al.* 2009a, 2009b), brain (Vandecasteele and De Deene 2013), and prostate treatment (Oldham *et al.* 2004). These studies showed that it is feasible to perform IMRT treatment verification using three dimension gel dosimeters.

Oldham *et al.* (1998) used a polymer gel to examine the performance of the Tomotherapy TPS. The gel measurements were found to agree well for medium and high doses although differences up to 10% at lower doses were observed. In 2009b, Sakhalkar *et al.* demonstrated the three dimensional verification of IMRT using a head and neck phantom and radiochromic dosimeter. A tolerance of 4% and 3 mm distance-to-agreement was used for gamma comparisons: 98% and 94% of the gel measurements agreed with TPS in 2D and 3D gamma comparisons respectively. In 2013, Vandecasteele and De Deene studied 3D gel dosimetry in a clinical setting. The gel dosimeter was evaluated for a brain tumour IMRT treatment and compared against TPS. The gel dosimeter was able of measuring the absolute dose within 5% in the whole 3D volume. Recently, Jackson *et al*. (2015) investigated a radiochromic gel dosimeter for IMRT radiation therapy treatment verification. The treatment plans were delivered to a cylindrical gel phantom and read using an optical CT scanner: 99.6% of pixels passed a 3D gamma test using 3% tolerance and 3 mm distance-to-agreement criteria. All of these studies suggest that the gel dosimeter is a useful method of 3D dose verification.

1.4.2 Volumetric Modulated Arc Therapy (VMAT)

Polymer and radiochromic gel dosimeters have been used for dosimetric verifications of RapidArc^{TM} treatments (Ceberg *et al.* 2009, Ceberg *et al.* 2010, Jackson *et al.* 2015). In 2009, Ceberg *et al*. reported polymer gel dosimeter measurements that compared TPS dose distributions for VMAT prostate treatments delivered to a gel phantom. The gel measurements agreed well with the TPS within the treated volume showing differences of less than 5%. In 2010, Ceberg *et al*. evaluated VMAT prostate treatment with a polymer gel phantom system. For the comparisons between gel measurements and TPS, the mean value was within 1% and the standard deviation was within 2.5%. More than 95% of pixels passed a 3D gamma test using 3% tolerance and 3 mm distance-to-agreement criteria. The study successfully demonstrated that the RapidArc^{TM} treatment plan was delivered as planned. In 2015, Jackson *et al*. used a radiochromic gel dosimeter for VMAT radiation therapy treatment verification, demonstrating that accurate three dimensional dosimetry of VMAT treatments is possible using gel dosimeter phantoms: 94.5% of pixels passed a 3D gamma test using 3% tolerance and 3 mm distance-to-agreement criteria.

1.4.3 Stereotactic Radiosurgery (SRS)

The obvious advantage of a gel dosimeter is that they can record the dose distribution in 3D, particularly those highly conformal distributions generated by SRS techniques (Olsson *et al.* 1992, Schulz *et al.* 1993, Ibbott *et al.* 1997, Novotny *et al.* 2002, Scheib and Gianolini 2002, Thomas *et al.* 2013). In one example (Ibbott *et al.* 1997), the gel dosimeters were prepared in flasks chosen for their size and shape, comparable to that

of a human head. Head mimicking phantoms have also been irradiated to verify the dosimetry of slim shaped lesions in the brain (Pfaender *et al.* 1999).

In the case of Ibbott *et al*. (1997) good agreement between the SRS TPS calculations and the polymer gel dosimeter dose distributions was found, where the agreement between isodose lines was within a few millimetres. Pfaender *et al*. (1999) used a polymer gel dosimeter to evaluate the dosimetry of stereotactic radiation treatment of slim shaped lesions of the brain compared with the planned treatment. Similarly, in 1999, Hilts *et al*. demonstrated that the polymer gel can provide accurate localization of high dose regions for SRS treatment. In 2000, Cosgrove *et al*. examined the reproducibility of polymer gel dosimetry applied to the stereotactic treatment using 6 MV photons beams. They found that the measured gel dose distributions were consistent and reproducible, and the distributions were within a few millimetres of the planned isodose lines. VMAT SRS treatments have also been evaluated using a head phantom containing a cylindrical radiochromic gel dosimeter. The three dimension gamma maps show that the predicted and measured dose agreed well, with a 98.0% passing rate for a tolerance of 3% and 2 mm distance-to-agreement (Thomas *et al.* 2013).

1.5 Thesis proposal

Advanced techniques in radiation therapy, such as IMRT or VMAT, are routinely employed to conform high doses to tumours while sparing surrounding normal tissues in order to improve tumour control (Jin *et al.* 2008, Wuu *et al.* 2015). The high degree of conformity places additional weight on choosing the correct planning target volume (PTV) margin (Jin *et al.* 2008). Often there is a trade off between complexity and

treatment plan quality when reaching the desired objectives (Craft *et al.* 2007). For example, sparing normal tissues reduces toxicities but may increase treatment complexity, resulting in a highly modulated treatment (Jin *et al.* 2008, McNiven *et al.* 2010). The TPS may force excessive dose close to the skin surface where the accuracy of the calculation may be quite poor, with an accuracy of ±25% (Dogan and Glasgow 2003, Court *et al.* 2008, Panettierei *et al.* 2009). Therefore accurate dose evaluation tools are essential.

Gel dosimeters have the ability to record dose information in multiple dimensions since they take the shape of the container in which they are formed. This is a key advantage in favour of gel dosimeters. The research presented in this thesis addresses the development of a transparent PVA radiochromic cryogel dosimeter and evaluates its potential to perform *in vivo* dosimetry. Compared to a water based PVA radiochromic cryogel dosimeter, the transparent cryogel can be read optically rather than using MRI; optical apparatus is more accessible and far less expensive.

Chapter 2 (Paper I) examines a deformable radiochromic cryogel dosimeter using ferrous benzoic xylenol orange (FBX) in a translucent poly(vinyl alcohol) cryogel matrix. It is a robust gel dosimeter that can be read optically; with adjustable, tissue-like mechanical properties. A natural question is: do the mechanical properties affect the radiosensitivity of the gel dosimeter? The temporal stability of the dosimeter pre- and post-irradiation is also important to understand, so that the dosimeter may be imaged appropriately. The radiochromic dose response of the gel dosimeter was characterized for a wide range of parameters related to the mechanical properties, including: number of freeze-thaw cycles (FTCs); concentration of PVA; DMSO concentration; photon

energy and dose rate dependence was also evaluated. Measurements were performed using a simple optical instrument developed in house.

Chapter 3 (Paper II) examines the ability of radiosensitive bolus material to monitor the dose distribution at the skin surface in two dimensions (referred to as “surface dose”). The measurement of surface dose in radiotherapy may be of interest to ensure superficial targets are treated appropriately. PVA-C is very flexible, and wraps easily around curved regions of the body (*e.g.* head and neck region), where it is not easy to get the same coverage with film or TLDs. Translucent FBX-PVA-C was used in place of bolus to simulate *in vivo* dosimetry measurements on an anthropomorphic phantom. First, a series of open fields with gantry angles ranging from 0^o to 90^o were delivered to a stack of radiochromic bolus and film on the surface of a polystyrene phantom. These measurements established the relationship between skin surface dose (estimated using Gafchromic EBT-2 film) and the dose measured in a 5 mm thick piece of radiochromic bolus. These measurements were used to compute a calibration factor that converted dose in the bolus to dose at the underlying surface. Proof-of-principle *in vivo* dosimetry measurements were performed on clinical head and neck IMRT treatment plans that were delivered to a RANDO phantom.

Chapter 4 (Paper III) employs the radiochromic bolus developed in Chapter 3 to investigate uncertainties in patient chest wall position during treatment delivery for patients performing DIBH. The irradiations, which consisted of a forward planned IMRT tangential pair, were conducted on a RANDO phantom at both the planned position and with A/P shifts up to 5 mm. The 2D dose distributions recorded by the cryogel at the planned position were compared with the distributions at all A/P shifts. The dose planes

at the skin surface and mid-cryogel were also computed using the TPS for all A/P shifts to validate the cryogel measurements.

Chapter 5 summarizes the results of the thesis and recommends possible future directions of the research.

References

Adamovics J and Maryanski M 2003 “New 3D radiochromic solid polymer dosimeter from leuco dyes and a transparent polymeric matrix”, *Med. Phys*. 30(6) 1349-1349

Adliene D, Jakstas K and Vaiciunaite N 2014 “Application of optical methods for dose evaluation in normoxic polyacrylamide gels irradiated at two different geometries”, *Nucl. Instru. Meth. Phys.* A*(*741) 88-94

Andrew H L. Murphy R E and LeBrun E J 1957 “Gel dosimeter for depth dose measurements”, *Sci. Instrum*. 28(5) 329 – 332

Bakiu E, Telhaj E, Kozma E, Ruçi F and Malkaj P 2013 “Comparison of 3D CRT and IMRT treatment plans”, *Acta. Inform. Medi.* 21(3) 211-212

Baldock C, De Deene Y, Doran S, Ibbott G, Jirasek A, Lepage M, McAuley K B, Oldham M and Schreiner L J 2010 “Polymer gel dosimetry”. *Phys. Med. Biol*. 55(5), R1-R63

Baldock C 2006 “Historical overview of the development of gel dosimetry: a personal prespective”, *J. Phys. Conf* (Vol. 56, pp. 14-22). Institute of Physics Publishing

Baldock C, Burford R P, Billingham N, Wagner G S, Patval S, Badawi R D and Keevil S F 1998 “Experimental procedure for the manufacture and calibration of polyacrylamide gel (PAG) for magnetic resonance imaging (MRI) radiation dosimetry”, *Phys. Med. Biol.* 43(3) 695–702

Beach M, Ibbott G, Followill D, Hanson W, Bloch C, Jackson E and Tucker S 2003 “Implementation of a polymer gel dosimetry insert for an anthropomorphic phantom used to evaluate head and neck intensity-modulated radiation therapy”, *Med. Phys.* 30(6) 1396-1396

Bero M A, Gilboy W B and Glover P M 2000 “An optical method for three-dimensional dosimetry”, *J. Radiol. Prot.* 20(3) 287–294

Bertelsen A, Hansen C R, Johansen J and Brink C 2010 “Single arc volumetric modulated arc therapy of head and neck cancer”. *Radiother. Oncol.* 95(2) 142-148

Brahme A, Roos J E and Lax I 1982 “Solution of an integral equation encountered in rotation therapy”, *Phys. Med. Biol*. 27(10) 1221-1229

Campbell W G, Wells D M and Jirasek A 2015 “Destructive backscatter-based readout of polymer gel dosimeters: proof of principle”. *World. Congr. Med. Phys. Bio. Engin*, June 7-12, Toronto, Canada (pp. 629-632). *Springer*

Camphausen K A and Lawrence R C 2008 “Principles of Radiation Therapy” in Pazdur R, Wagman L D, Camphausen K A and Hoskins W J (Eds) Cancer Management: A Multidisciplinary Approach 11 ed.

Ceberg S, Gagne I, Gustafsson H, Scherman J B, Korreman S S, Kjær-Kristoffersen F, Hilts M and Bäck, S Å J 2010 “Rapid Arc treatment verification in 3D using polymer gel dosimetry and Monte Carlo simulation”, *Phys. Med. Biol.* 55(17) 4885-4898

Ceberg S, Gustavsson H, Korreman S, Medin J, Kjær-Kristoffersen F and Bäck S Å 2009 “RapidArc™ treatment verification using polymer gel dosimetry”, *J. Phys. Conf* (Vol. 164, No. 1, p. 012052). IOP Publishing

Chan M, Song Y, Meli J, Huang Y and Burman C 2006 “TU-FF-A1-02: Estimating Dose to ICD outside the Treatment Fields Using Skin QED Diode”, *Med. Phys.* 33(6) 2218-2218

Chiu-Tsao S T and Chan M F 2010 “Evaluation of two-dimensional bolus effect of immobilization/support devices on skin doses: A radiochromic EBT film dosimetry study in phantom”, *Med. Phys*. 37(7) 3611-3620

Chu K C, Jordan K J, Battista J J, Van Dyk J and Rutt B K 2000 “Polyvinyl alcohol Fricke hydrogel and cryogel:two new gel dosimetry systems with low Fe^{+3} diffusion”, *Phys. Med. Biol.* 45(4) 955-969

Cosgrove V P, Murphy P S, McJury M, Adams E J, Warrington A P Leach M O and Webb S 2000 “The reproducibility of polyacrylamide gel dosimetry applied to stereotactic conformal radiotherapy”, *Phys. Med. Biol.* 45(5) 1195-1210

Court LE, Tishler RB, Xiang H, Allen A M, Makrigiorgos M and Chin L 2008 “Experimental evaluation of the accuracy of skin dose calculation of a commercial treatment planning system” *J. Appl. Clin. Med. Phys*. 9(1) 29-35

Craft D, Süss P and Bortfeld T 2007 “The tradeoff between treatment plan quality and required number of monitor units in intensity-modulated radiotherapy”, *Int. J. Radiat. Oncol. Biol. Phys.* 67(5) 1596-1605

Day and Stein 150 “Chemical effects of ionizing radiation in some gels”, *Nature*, 166(4212) 146 – 147

Davies J B and Baldock C 2008 “Sensitivity and stability of the Fricke-gelation-xylenol orange gel dosimter”, *Radiat. Phys. Chem.* 77(6) 690-699

De Deene Y, De Wagter C, Van Duyse B, Derycke S, De Neve W and Achten E 1998 “Three-dimensional dosimetry using polymer gel and magnetic resonance imaging applied to the verification of conformal radiation therapy in head-and-neck cancer”, *Radiother. Oncol.* 48(3) 283–291

De Deene Y, De Wagter C, Van Duyse B, Derycke S, Mersseman B, De Gersem W, Voet T, Achten E and De Neve W 2000 “Validation of MR-based polymer gel dosimetry as a preclinical three-dimensional verification tool in conformal radiotherapy”, *Magn. Reson. Med*. 43(1) 116–125

De Neve W, De Gersem W, Derycke S, De Meerleer G, Moerman M, Bate M T, Duyse B V, Vakaet L, De Deene Y, Mersseman B and De Waeter C 1999 “Clinical delivery of intensity modulated conformal radiotherapy for relapsed or second-primary head and neck cancer using a multileaf collimator with dynamic control”, *Radiother. Oncol.* 50(3) 301-314

Dogan N and Glasgow G P 2003 “Surface and build-up region dosimetry for obliquely incident intensity modulated radiotherapy 6 MV x rays”, *Med. Phys.* 30(12) 3091-3096

Doran S J, Rahman A A, Bräuer-Krisch E, Brochard T, Adamovics J, Nisbet A and Bradley D 2013 “Establishing the suitability of quantitative optical CT microscopy of PRESAGE® radiochromic dosimeters for the verification of synchrotron microbeam therapy”, *Phys. Med. Biol*. 58(18) 6279-6297

Falco M D, Masala S, Stefanini M, Fiori R, Gandini R, Bagalà P, Morosetti D, Calabria E, Tonnetti A, Verona-Rinati G, Santoni R and Simonetti G 2015 “Patient skin dose measurements using a cable free system MOSFETs based in fluoroscopically guided percutaneous vertebroplasty, percutaneous disc decompression, radiofrequency medial branch neurolysis, and endovascular critical limb ischemia”, *J. Appl. Clin. Med. Phys*. 16(1) 298-310

Fassi A, Ivaldi G B, Meaglia I, Porcu P, de Fatis P T, Liotta M, Ribold M and Baroni G 2014 “Reproducibility of the external surface position in left-breast DIBH radiotherapy with spirometer-based monitoring”. *J. Appl. Clin. Med. Phys*. *15*(1) 130-140

Fong P M, keil D C, Does M D and Gore J C 2001 “Polymer gels for magnetic resonance imaging of radiation dose distributions at normal room atmosphere”, *Phys. Med. Biol*. 46(12) 3105 – 3113

Frick H and Hart E 1955 “Radiation Dosimetry*”* vol 2 ed F h Attix and W C Roesch (New York: Academic) (Chemical Dosimetry)

Frick H and Morse S 1927 “The chemical action of Roentgen on dilute ferrous sulphate solutions as a measure of dose”, *Am. J. Roent. Radium. Ther. Nucl. Med.* 18 430-432

Galvin J M, Ezzell G, Eisbrauch A, Yu C, Butler B, Xiao Y Rosen I and Palta J 2004 “Implementing IMRT in clinical practice: a joint document of the American Society for Therapeutic Radiology and Oncology and the American Association of Physicists in Medicine”, *Int. J. Radiat. Oncol. Biol. Phys.* 58(5) 1616-1634

Gore J C and Kang Y S 1984 “Measurement of radiation dose distributions by nuclear magnetic resonance (NMR) imaging”, *Phys. Med. Biol.* 29(10) 1189-1197

Gore J C, Ranade M, Maryanski M J and Schulz R J 1996 “ Radiation dose distributions in three dimensions from tomographic optical density scanning of polymer gels: I. Development of an optical scanner”, *Phys. Med. Biol*. 41(12) 2695-2704

Guo P Y, Adamovics J A and Oldham M 2006 “Characterization of a new radiochromic three dimensional dosimeter”, *Med. Phys*. 33(5) 1338 – 1345

Gupta B L and Narayan G R 1985 “G(Fe+3) values in the FBX dosemeter” *Phys. Med. Biol*. 30(4) 337-340

Gustavsson H, Karlsson A, Bäck S Å J, Olsson L E, Haraldsson P, Engstrom P and Nystrom H 2003 “MAGIC-type polymer gel for three-dimensional dosimetry: Intensity-modulated radiation therapy verification”, *Med. Phys.* 30(6) 1264-1271

Haas O C L, Mills J A, Burnham K J, Bonnett D E, Farajollahi A R, Fisher M H, Glendinning A G and Aukett R J 1997 “Experimental verification of beam intensity modulated conformal radiotherapy using patient specific compensators”, *Br. J. Radiol*. 70 Supple S16

Heggie J CP, Liddell N A and Maher K P 2001 “Applied Imaging Technology” School of Medical Sciences RMIT University. (vol.4) st. Vincent’s Hospital Melbourne

Higgins P D, Han E Y, Yuan J L, Hui S and Lee C K 2007 “Evaluation of surface and superficial dose for head and neck treatments using conventional or intensity-modulated techniques”, *Phys. Med. Biol*. 52(4) 1135-1146

Hill B, Venning A and Baldock, C 2005 “The dose response of normoxic polymer gel dosimeters measured using X-ray CT”. *Br. J. Radiol*. 78(931) 623-630

Hilts M, Audet C, Duzenli C and Jirasek A 1999 “Polymer gel dosimetry using x-ray computer tomography: feasibility and potential application to stereotactic radiosurgery”, DOSGEL 1999 Proceedings of the *1st. Int. Workshop on Radiation Therapy Gel Dosimetry* (Lexington, Kentucky)

Hyon S H, Cha W I and Ikada Y 1989 “Preparation of transparent poly(vinyl alchohol) hydrogel”, *Polym. Polym. Bull* 22(2) 119-122

International Atomic Energy Agency 2009 “Quality Assurance in Radiation Dosimetry: Achievement and Trends” Vienna

Ibbott G, Beach M and Maryanski M 2002 “An anthropomorphic head phantom with a BANG® polymer gel insert for dosimetric evaluation of IMRT treatment delivery”, Standards and Codes of Practice in Medical Radiation Dosimetry, Proceedings of an *Int Symp*, Vienna. 2 361-368

Ibbott, G S 2004 “Applications of gel dosimetry”, *J. Phys. Conf* (Vol. 3, No. 1, p. 58). IOP Publishing

Ibbott, G S 2006 “Clinical applications of gel dosimeters”, *J. Phys. Conf* (Vol. 56, No. 1, p. 108). IOP Publishing

Ibbott G S, Beach M L and Maryanski M J 2003 “IMRT QA with an anthropomorphic phantom employing a polymer gel dosimeter”. *Int. Org. Med. Phys. Proc.* Vol 1

Ibbott G S, Maryanski M J, Eastman P, Holcomb S D, Zhang Y, Avison R G, Sanders M, Gore J C 1997 “Three dimensional visualization and measurement of conformal dose distributions using magnetic resonance imaging of BANG polymer gel dosimeters”, *Int. J. Radiat. Oncol. Biol. Phys.* 38(5) 1097-1103

International Specialty Products Gafchromic® EBT2 2009 “Self developing film for radiotherapy dosimetry” Wayne, NJ, USA

Jackson J, Juang T, Adamovics J and Oldham M 2015 “An investigation of PRESAGE® 3D dosimetry for IMRT and VMAT radiation therapy treatment verification”, *Phys. Med. Biol.* 60(6) 2217-2230

Jin H, Palta J, Suh T S, and Kim S 2008 “A generalized a priori dose uncertainty model of IMRT delivery”, *Med. Phys.* 35(3) 982-996

Ju T, Simpson T, Deasy J O and Low D A 2008 “Geometric interpretation of the γ dose distribution comparison technique: Interpolation-free calculation”, *Med. Phys.* 35(3) 879-887

Juang T, Newton J, Das S, Adamovics J and Oldham M 2013 “Preliminary investigation and application of a novel deformable PRESAGE® dosimeter”, *J. Phys. Conf* (Vol. 444, No. 1, p. 012080). IOP Publishing

Khanal S P, Ouhib Z, Benda R K and Leventouri T 2015 “Evaluation of surface dose outside the treatment area for five breast cancer irradiation modalities using thermo-luminescent dosimeters”, *Int. J. Canc. Thera. Oncol.* 3(1) ISSN 2330-4049

Kharine A, Manohar S, Seeton R, Kolkman R G, Bolt R A, Steenbergen W and de Mul F F 2003 “Poly (vinyl alcohol) gels for use as tissue phantoms in photoacoustic mammography”, *Phys. Med. Biol.* 48(3) 357-370

Korreman S S, Pedersen A N, Nottrup T J, Specht L and Nystrom H 2005 “Breathing adapted radiotherapy for breast cancer: Comparison of free breathing with the breath hold-technique”, *Radiother. Oncol.* 76(3) 311-318

Kron T “What do we expect from gel dosimetry”, DOSGEL, 2nd international conference of gel dosimetry, 2001

Langen K M and Jones D T L 2001 “Organ motion and its management”, *Int. J. Radiat. Oncol. Biol. Phys* 50(1) 265-278

Latty D, Stuart K E, Wang W and Ahern V 2015 “Review of deep inspiration breath-hold techniques for the treatment of breast cancer” *J. Med. Radiat. Sci.* 62(1) 74-81

Low D A 2010 “Gamma dose distribution evaluation tool”, *J. Phys. Conf* (Vol. 250, No. 1, p. 012071)

Low D A and Dempsey J F 2003 “Evaluation of the gamma dose distribution comparison method”, *Med. Phys.* 30(9) 2455-2464

Low D A, Dempsey J F, Venkatesan R, Mutic S, Markman J, Haacke E M and Purdy J A 1999 “Evaluation of polymer gels and MRI as a 3D dosimeter for intensity-modulated radiation therapy” *Int. J. Radiat. Oncol. Biol. Phys*. 26(8) 1542-1551

Low D A, Harms W B, Mutic S and Purdy J A 1998 “A technique for the quantitative evaluation of dose distributions”, *Med. Phys.* 25(5) 656-661

Lundstrom T, Christensen H and Sehested K 2004 “Reaction of the HO_2 radical with OH, H, Fe^{2+} and Cu^{2+} at elevated temperature”, *Radiat. Phys. Chem.* 69(3) 211-216

Månsson S, Karlsson A, Gustavsson H, Christensson J and Bäck S Å J 2006 “Dosimetric verification of breathing adapted radiotherapy using polymer gel”, *J. Phys. Conf* (Vol. 56, No. 1, p. 300). IOP Publishing

Martišíková M, Ackermann B and Jäkel O 2008 “Analysis of uncertainties in Gafchromic® EBT film dosimetry of photon beams”, *Phys. Med. Biol.* 53(24) 7013-7027

Maryanski M J, Gore J C, Kennan R P, Schulz R J 1993 “NMR relaxation enhancement in gels polymerized and cross-linked by ionization radiation: a new approach to 3D dosimetry by MRI”, *Magn. Reson. Imag.* 11(2) 253-258

Maryanski M J, Ibbott, G S, Eastman P, Shulz RJ and Gore J C 1996 “Radiation therapy dosimetry using magnetic resonance imaging of polymer gels”, *Med. Phys.* 23(5) 699-705

Maryanski M J, Schulz R J, Ibbot G S, Gatenby J C , Xie J, Horton D and Gore J C1994 “Magnetic Resonance Imaging of radiation dose distribution using a polymer-gel dosimeter”, *Phys. Med. Biol.* 39(9) 1437-1455

Mayles P, Nahum A E and Rosenwald J C 2007 “Handbook of Radiotherapy Physics: Theory and Practice. CRC Press.

McCarter S D and Beckham W A 2000 “Evaluation of the validity of a convolution method for incorporating tumour movement and set-up variations into the radiotherapy treatment planning system”, *Phys. Med. Biol.* 45(4) 923-931

McJury M , Oldham M, Cosgrove V P, Murrphy P S, Doran S, Leach M O and Webb S 2000 “Radiation dosimetry using polymer gels: methods and application”, *Br. J. Radiol.* 73(873) 919-929

McNiven A L, Sharpe M B and Purdie T G 2010 “A new metric for assessing IMRT modulation complexity and plan deliverability”, *Med. Phys.* 37(2) 505-515

Mijnheer B 2008 “State of the art of in vivo dosimetry”, *Radiat. Protect. Dosim.* 131(1) 117-122

Molineu A, Followill D S, Balter P A, Hanson W F, and Ibbott G S 2005 “Design and Implementation of an Anthropomorphic Quality Assurance Phantom for Intensity Modulated Radiation Therapy”, *Int. J. Radiat. Oncol. Biol. Phys.* 63(2) 577-583

Morales J E, Hill R, Crowe S B, Kairn T and Trapp J V 2014 “A comparison of surface doses for very small field size x-ray beams: Monte Carlo calculations and radiochromic film measurements”, *Austr. Phys. Eng. Sci. Med.* 37(2) 303-309

Nakano M, Hill R F, Whitaker M, Kim J H and Kuncic Z 2012 A “study of surface dosimetry for breast cancer radiotherapy treatments using Gafchromic EBT2 film”, *J. Appl. Clinic. Med. Phys*. 13(3) 3727-3727

Nazir A, Afzal M and Buzdar S A 2010 “Effects of variation of MRI parameters of signal homogeneity: A qualitative analysis for ferrous benzoic xylenol orange gel”, *JPMA* 60(6) 470-473

Novotny J, Dvorak P, Spevacek V, Tintera J, Cechak T and Liscak R 2002 “Quality control of the stereotactic radiosurgery procedure with the polymer-gel dosimetry”, *Radiother. Oncol*. 63(2) 223-230

Ohara K, Okumura T, Akisada M, Inada T, Mori T, Yokota H and Calaguas M J 1989 “Irradiation synchronized with respiration gate”, *Int. J. Radiat. Oncol. Biol. Phys*. 17(4) 853-857

Oldham M, Baustert I, Lord C, Smith T A, McJury M, Warrington A P, Leach M O and Webb S 1998 “An investigation into the dosimetry of a nine-field tomotherapy irradiation using BANG-gel dosimetry”, *Phys. Med. Biol.* 43(5) 1113–1132

Oldham M, Gluckman G and Kim L 2004 “3D verification of a prostate IMRT treatment by polymer gel-dosimetry and optical-CT scanning”, *J. Phys. Conf* (Vol. 3, No. 1, p. 293). IOP Publishing

Oldham M, Sakhalkar H, Oliver T, Wang Y M, Kirpatrick J, Cao Y, Badea C, Johnson A and Dewhirst M 2006 “Three-dimensional imaging of xenograft tumors using optical computed and emission tomography”, *Med. Phys.* 33(9) 3193-3202

Oldham M, Siewerdsen J H, Kumar S, Wong J and Jaffray D A 2003 “Optical-CT gel dosimetry I: Basic investigations”, *Med. Phys.* 30(4) 623–634

Oldham M, Siewerdsen J H, Shetty A and Jaffray D A 2001 “High resolution gel-dosimetry by optical-CT and MR scanning”, *Med. Phys.* 28(7) 1436–1445

Olding T and Schreiner L J 2011 “Cone-beam optical computed tomography for gel dosimetry II: imaging protocols”, *Phys. Med. Biol*. 56(5) 1259-1279

Olsson L E, Arndt J, Fransson A, and Nordell B 1992 “Three-dimensional dose mapping from gamma knife treatment using a dosimeter gel and MR-imaging”, *Radiother. Oncol.* 24(2) 82-86

Penettierei V, Barsoum P, Westermark M, Brulla L and Lax I 2009 “AAA and PBC calculation accuracy in the surface build-up region in tangential beam treatments. Phantom and breast case study with the Monte Carlo code PE-NELOPE”, *Radiother. Oncol.* 93(1) 94-101

Pfaender M Grebe G Budac V and Wurm R 1999 “Dosimetry with BANG-dosimeters regarding slim shaped parts of lesions for stereotactic radiation with a linac and micro-multi-leaf-collimator”, In Proceedings of the *1st Int workshop on radiation gel dosimetry* (pp. 190-2)

Podgorsak, E B 2005 “Radiation oncology physics. a handbook for teachers and students”, Vienna: *IAEA*, 657

Recht A 2006 “Which breast cancer patients should really worry about radiation-induced heart disease — and how much?”, *J. Clin. Oncol.* 24(25) 4059–4061

Sakhalkar H S, Adamovics J, Ibbott G and Oldham M 2009a “A comprehensive evaluation of the PRESAGE/optical-CT 3D dosimetry system”, *Med. Phys*, 36(1), 71-82.

Sakhalkar H S and Oldham M 2008 “Fast, high-resolution 3D dosimetry utilizing a novel optical-CT scanner incorporating tertiary telecentric collimation”, *Med. Phys.* 35(1) 101-111

Sakhalkar H, Sterling D, Adamovics J, Ibbott G and Oldham M 2009b “Investigation of the feasibility of relative 3D dosimetry in the Radiologic Physics Center Head and Neck IMRT phantom using presage/optical-CT”, *Med. Phys.* 36(7) 3371-3377

Saur S, Fjellsboe L M B, Lindmo T and Frengen J 2009 “Contralateral breast doses measured by film dosimetry: tangential techniques and an optimized IMRT technique”, *Phys. Med. Biol*. 54(15) 4743 -4758

Scheib S G and Gianolini S 2002 “Three-dimensional dose verification using BANG gel: a clinical example”, *J. Neurosur*. 97(5) 582-587

Schreiner L J 1999 “Gel dosimetry: Motivation and historical foundation”, In DOSGEL 1999 Proceedings of the *1st Int Workshop on Radiation Therapy Gel Dosimetry* (Lexington, Kentucky) (pp. 1-10)

Schreiner L J 2004 “Review of Fricke gel dosimeters”, *J. Phys. 3rd Int. Conf. on Radiotherapy Gel Dosimetry* pp 9-21

Schreiner L J “Where does gel dosimetry fit in the clinic?”, 2009 *J. Phys. 5th Int. Conf. on Radiotherapy Gel Dosimetry* , Conf series 164

Schulz R J, Maryanski M J, Ibbott G S and Bond JE 1993 “Assessment of the Accuracy of Stereotactic Radiosurgery Using Fricke-Infused Gels and MRI”, *Med. Phys.* 20(6) 1731-1734

Shah C, Badiyan S, Berry S, Khan A J, Goyal S, Schulte K, Nanavati A, Lynch M and Vicini F A 2014 “Cardiac dose sparing and avoidance techniques in breast cancer radiotherapy”, *Radiother. Oncol.* 112(1) 9-16

Silva P P, Cuerra W, Silveria J N, Ferreira A M D C, Bortolotto T, Fischer F L, Terenzi H, Neves A and Pereira-Maia E C 2011 Two new ternary complexes of copper(II) with tetracycline or doxycycline and 1,10-phenanthroline and their potential as antitumoral : cytotoxicity and DNA cleavage *Inorg. Chem*. 50(14) 6414-6424

Smith S T, Masters K S, Hosokawa K, Blinco J, Crowe S B, Kairn T and Trapp J V 2015 “A reduction of diffusion in PVA Fricke hydrogels”, *J. Phys. Conf*: (Vol. 573, No. 1, p. 012046). IOP Publishing

Thomas A, Niebanck M, Juang T, Wang Z and Oldham M 2013 “A comprehensive investigation of the accuracy and reproducibility of a multitarget single isocenter VMAT radiosurgery technique”, *Med. Phys*. 40(12) 121725-121725

Thwaites D I and Tuohy J B 2006 “Back to the future: the history and development of the clinical linear accelerator”, *Phys. Med. Biol.* 51(13) R343-R362

Trapp J V, Bäck S Å J, Lepage M, Michael G and Baldock C 2001 “An experimental study of the dose response of polymer gel dosimeters imaged with x-ray computed tomography”, *Phys. Med. Biol.* 46(11) 2939-2951

Vandecasteele J and De Deene Y 2013 “Evaluation of radiochromic gel dosimetry and polymer gel dosimetry in a clinical dose verification”, *Phys. Med. Biol.* 58(18) 6241-6262

Vergote K, De Deene Y, Claus F, De Gersem W, Van Duyse B, Paelincka L, Achten E, De Neve W, De Wagter C 2003 “Application of monomer/polymer gel dosimetry to study the effects of tissue inhomogeneities on intensity-modulated radiation therapy (IMRT) dose distributions”, *Radiother. Oncol.* 67(1) 119–128

Wang B H and Campbell G 2009 “Formulations of polyvinyl alcohol cryogel that mimic the biomedical properties of soft tissues in the natural lumbar intervertebral disc”, *Spine* 34(25) 2745-2753

Wuu C S 2015 “Clinical applications of 3-D dosimeters”, *J. Phys. Conf* (Vol. 573, No. 1, pp. 12011-12017). IOP Publishing

Chapter 2

Paper I - Evaluation of a ferrous benzoic xylenol orange transparent PVA cryogel radiochromic dosimeter

Molham M Eyadeh, Thomas J Farrell and Kevin R Diamond

Department of Medical Physics and Applied Radiation Sciences, McMaster University and Juravinski Cancer Centre, 699 Concession St, Hamilton, ON, L8V 5C2, Canada

Published in Physics in Medicine and Biology 59 (2014) 1773-1787

Printed with Permission

© 2014 Institute of Physics and Engineering in Medicine 0031-9155/14/071773

2.0.1 Introduction to Paper I

The following paper considers an evaluation of ferrous benzoic xylenol orange (FBX) in a translucent poly(vinyl alcohol) (PVA) cryogel matrix with adjustable tissue-like mechanical properties, using a simple optical instrument developed in house. The work presented in this paper examines the cryogel for a group of parameters, including different considerations of PVA, ratios of water/DMSO, and numbers of FTCs. The stability of the dosimeter at pre- and post-irradiation, dose response, photon energy response, and dose rate effect were evaluated. Related studies evaluated opaque versions of PVA cryogel dosimeters (Chu *et al.* 2000, Hill *et al.* 2002) recovering the stored dose information using MRI. Adding DMSO to the PVA cryogel formulation makes it optically transparent or translucent, enabling the use of optical read out techniques (Hyon *et al.* 1989). In this paper, a deformable radiochromic cryogel dosimeter with good stability and sensitivity that can be read optically was obtained.

The experiments, apparatus design, and analysis presented in this paper were performed by the author of this thesis under the supervision of Dr. Diamond. The manuscript was written by the author of this thesis and edited by Dr. Diamond and Dr. Farrell. The manuscript has been changed slightly to conform to the style of the thesis.

2.0.2 Content of Paper I

2.1 Abstract

A stable cryogel dosimeter was prepared using ferrous benzoic xylenol Orange (FBX) in a transparent poly(vinyl alcohol) (PVA) cryogel matrix. Dose response was evaluated for different numbers of freeze-thaw-cycles (FTCs), different concentrations of PVA, and ratios of water/dimethyl sulfoxide. Linear relationships between dose and absorbance were obtained in the range of 0-1000 cGy for all formulations. Increasing the concentration of PVA and number of FTCs resulted in increased absorbance and sensitivity. The number of crosslinks that form in a cryogel increases with additional PVA and FTCs. There may be some interaction between the physical properties of the polymer and FBX material that lead to increased sensitivity. The effects of energy and dose rate were also evaluated. No significant dose rate dependence was observed over the range 1.05 to 6.33 Gy/min. No energy response was observed over photon energies of 6, 10, and 18 MV.

2.2 Introduction

Ferrous sulphate (Fricke) solutions have been used in various forms for over 40 years (Fricke and Morse 1927, Fricke and Hart 1955). In Fricke dosimetry, Fe^{2+} ions are dissolved in an acidic solution and are oxidized to Fe^{3+} upon irradiation (Fricke and Morse 1927). The concentration of Fe^{3+} can then be probed optically or using magnetic resonance imaging techniques and correlated to dose (Gore *et al.* 1984). While the aqueous system is sensitive to radiation dose, it cannot record spatial information.

Gel dosimeters have a long history in radiation dosimetry (McJury *et al.* 2000). Gore addressed the dose distribution problem experienced by aqueous dosimeters by introducing a gel dosimeter that combined the aqueous Fricke solution with a gel matrix, reducing ion mobility and allowing for the possibility of three dimensional radiation dosimetry (Gore *et al.* 1984). Fricke gel dosimeters have some desirable properties, such as ease of preparation and they can be read shortly after irradiation (Schreiner 2004). However, early attempts at creating a Fricke gel dosimeter found that the Fe^{3+} ions were mobile. This ion diffusion and the subsequent loss of spatial dose resolution is a serious restriction on the use of this type of system (Schreiner 2004). Several studies have been performed on Fricke-like dosimeters examining the effect of different gelling substances on ion diffusion (see, for example, Chu *et al.* 2000). Many systems have been proposed using gelling agents such as gelatin or agarose (Olsson *et al.* 1990, Hazle *et al.* 1991, Gambarini *et al.* 1994, Schreiner *et al.* 1994), or more recently poly(vinyl alcohol) PVA (Chu *et al.* 2000, Hill *et al.* 2002). Chu demonstrated that a Fricke PVA-FX cryogel dosimeter, read out using magnetic resonance imaging, had excellent stability and decreased the diffusion of the ferric ions significantly. The PVA cryogel (PVA-C) is a hydrogel that has been subjected to cycles of freezing and thawing, which induces thermal crosslinking and leads to greater opacity (Chu *et al.* 2000, Hill *et al.* 2002). Several studies are focused on incorporating chemicals such as Xylenol Orange (XO) that produce a visible colour change in the presence Fe^{3+} that can be measured using more accessible optical systems (Gupta and Narayan 1985, Appleby and Leghrouz 1991, Kelly *et al.* 1998, Davies and Baldock 2008).

Optically scanned gels must be manufactured with as little turbidity as possible to minimize light scattering, which is complicated to model (Farrell *et al.* 1992, Olding and Schreiner 2011). The turbidity requirement restricts the choice of matrix materials to clear plastics and natural gelling agents (such as gelatin). It would be advantageous to use a matrix material that can be made with lifelike mechanical properties (*e.g.* deformability, compressibility, texture), such as a cryogel, that is also transparent or translucent.

Contemporary radiochromic gel dosimetry formulations have excellent linearity and long-term stability of the radiochromic response, such as PRESAGE®, but the matrix materials are not tissue-like. For example, PRESAGE® uses a hard polyurethane matrix (Doran *et al.* 2013). Deformable gel dosimeters such as nPAG (Niu *et al.* 2012, Yeo *et al.* 2012), use gelatin as the matrix material. Gelatin will take the shape of the container it is set in and is deformable, but its mechanical properties are inferior to PVA-C: PVA cryogels have a high modulus of elasticity, where as matrices like gelatin and agarose tend to be somewhat fragile; larger gelatin phantoms may break with handling (Kharin *et al.* 2003).

PVA cryogel is an excellent choice of matrix material because it can be manufactured to mimic the mechanical properties of a wide variety of tissues and moulded into any shape. The mechanical properties (such as shear, compressibility, and needle penetration) of PVA cryogel are controlled by adjusting the amount of PVA, the number of freeze-thaw-cycles the hydrogel is subjected to, and the isotherms used during the temperature cycling (Wang and Campbell 2009). This allows for the development of biomechanically accurate models of deformable organs, which may be useful for

situations where intrafraction deformation and motion are of interest. PVA cryogels are gaining in popularity for surgical simulators specifically because of their tissue-like mechanical properties (see, for example, Jiang *et al.* 2013). In principle it is possible to embed a "tumour" PVA cryogel into a large dose limiting volume, also a PVA cryogel, each with different mechanical properties, as would be the case of a solitary metastasis in a liver. The challenge, then, is to incorporate a radiochromic material into such a gelling matrix, with the condition that it should be read optically (Olding and Schreiner 2011).

One of the major obstacles when employing gel dosimeters is recovering the stored dose information: PVA hydrogels are optically transparent, and can be read with either MRI or optical detection methods, while PVA cryogel is opaque, so the internal concentration of Fe^{3+} is measured using MRI (Chu *et al.* 2000, Hill *et al.* 2002). PVA cryogels can be made optically transparent or translucent by adding DMSO to the formulation, allowing for the use of optical read out techniques (Hyon *et al.* 1989). (Refractive index of PVA is 1.52-1.55, for DMSO is 1.48). These DMSO-bearing PVA cryogels are stiffer than the equivalent water-based PVA cryogels, but may still be produced with a broad range of mechanical properties. The purpose of the work presented here was to evaluate transparent PVA cryogel loaded with ferrous benzoic xylenol orange (FBX) for its potential use as a gel dosimetry material. Radiochromic (FBX) (Kelly *et al.* 1989, Nazir *et al.* 2010) was suspended in a translucent PVA cryogel. The cryogel was prepared from a mixture of PVA, water, and DMSO. The resulting cryogel is high in tensile strength and light transmittance (Hyon *et al.* 1989). Different water/DMSO ratios may lead to changes in light transmittance as well as differences in

sensitivity arising from DMSO's free radical scavenging properties (Silva *et al.* 2011). In our study, dose response was evaluated for a wide range of PVA concentrations (5%, 7.5%, 10%, 12.5%, and 15% by weight), one, three, and six FTCs, and for two different ratios of water/DMSO in 25 mM sulphuric acid (20/80 and 30/70 by weight). Dose rate and photon energy responses were examined using a dosimeter comprising 15% PVA by weight, 20/80 water/DMSO ratio, and crosslinked for three FTCSs.

2.3 Materials and Methods

2.3.1 Preparation of the FBX Cryogel Dosimeter

FBX radiochromic dosimeters were prepared using PVA cryogels comprising 99+% hydrolyzed PVA (MW 146000-188000, Sigma Aldrich) in distilled water with Dimethyl Sulfoxide (Sigma Aldrich, St. Louis, USA ≥99%), ferrous ammonium sulphate (Aldrich ammonium iron (II) sulphate hexahydrate, 99% A.C.S Reagent), sulphuric acid (Sigma Aldrich, 95-98% A.C.S Reagent), XO tetrasodium salt (Sigma Aldrich, A.C.S Reagent), and benzoic acid (Sigma Aldrich, ≥99.5% A.C.S Reagent).

A stock solution of 5 mM benzoic acid, 1 mM XO, and 25 mM sulphuric acid was prepared in a 100 mL volumetric flask and kept at room temperature. An additional stock solution of water, DMSO, and sulphuric acid was prepared at 25 mM ('water/DMSO'). The benzoic acid was added to the dosimeter to facilitate comparisons with previous studies (Kelly *et al.* 1989, Nazir *et al.* 2010), even though it was not included with other PVA gel formulations (Chu *et al*. 2000, Hill *et al*. 2002).

Gel preparation began with the addition of PVA (5%, 7.5%, 10%, 12.5%, or 15% by weight) to 70 mL of water/DMSO stock. Two ratios of water/DMSO were studied: 20/80 and 30/70 by weight. The mixture was stirred at 90-120^{o}C for 90-120 min under normal atmospheric pressure using a hot plate stirrer. The volume of the hydrogel was monitored during stirring and water/DMSO mixture was added to replace any evaporated liquid.

In another beaker, 0.55 mM of ferrous ammonium sulphate was dissolved in 10 mL of the stock solution (benzoic acid, XO, and sulphuric acid) and then added to the PVA hydrogel after it had cooled to 50 ^{o}C. The process was completed by adding enough sulphuric water/DMSO mixture to the hydrogel to make up 100 mL total volume and mixing slowly at 50 ^{o}C for another 10 min.

To obtain high optical uniformity, the warm hydrogel was evacuated for 15 min to remove unwanted air bubbles. Finally, the solution was poured into round sample plates (35 mm diameter x 10 mm thick).

The samples were then subjected to one, three, or six FTCs, each cycle comprising a period of freezing for 18 hours at -80 ^{o}C and thawing at room temperature for 6 h. The final samples ranged between 4-8 mm in thickness, depending on the formulation (higher concentrations of PVA yielded thicker cryogels). The thickness of each sample was measured using a vernier calliper.

Clear and colourless reference samples were also produced using the same procedure as above omitting the stock solution and ferrous ammonium sulphate (*i.e.* PVA, water, DMSO, and sulphuric acid without XO, ferrous ammonium sulphate, and benzoic acid).

These reference samples were similar to transparent PVA-C described by Hyon *et al*. Reference samples were prepared to match each of the FBX-PVA-C formulations tested in this study.

2.3.2 Measurement of FBX Gel Dosimeter Stability

Absorbance measurements were performed using a simple transmission apparatus, illustrated in figure 2.1. The apparatus was composed of two optical fibres coupled to collimating lenses (ThorLabs F220SMA-B), a white light source (Ocean Optics LS-1), a measurement platform to support the sample plates, and a spectrometer (Ocean Optics HR4000). The collimating lenses image a 2 mm diameter circle, which is a fraction of the 20 – 25 mm diameter samples. Multiple measurements were taken on each sample to obtain average absorption coefficients. Pre-irradiation stability was evaluated over 48 hours for most samples. Three independent preparations were measured at five locations on each sample for a total of 15 measurements at each time point for each formulation. Samples comprising 15% PVA and three FTCs were also observed for a seven day period prior to irradiation. A colourless and transparent PVA-C sample was measured as reference (PVA, water, DMSO, *i.e.* the same formulation of cryogel without FBX added). The measured spectra were later exported from the measurement system and analyzed. Figure 2.2 is an example of the spectrally resolved light transmitted through the reference sample and the associated FBX-PVA-C dosimeter before irradiation. All measurements and irradiations were performed at ambient room temperature.

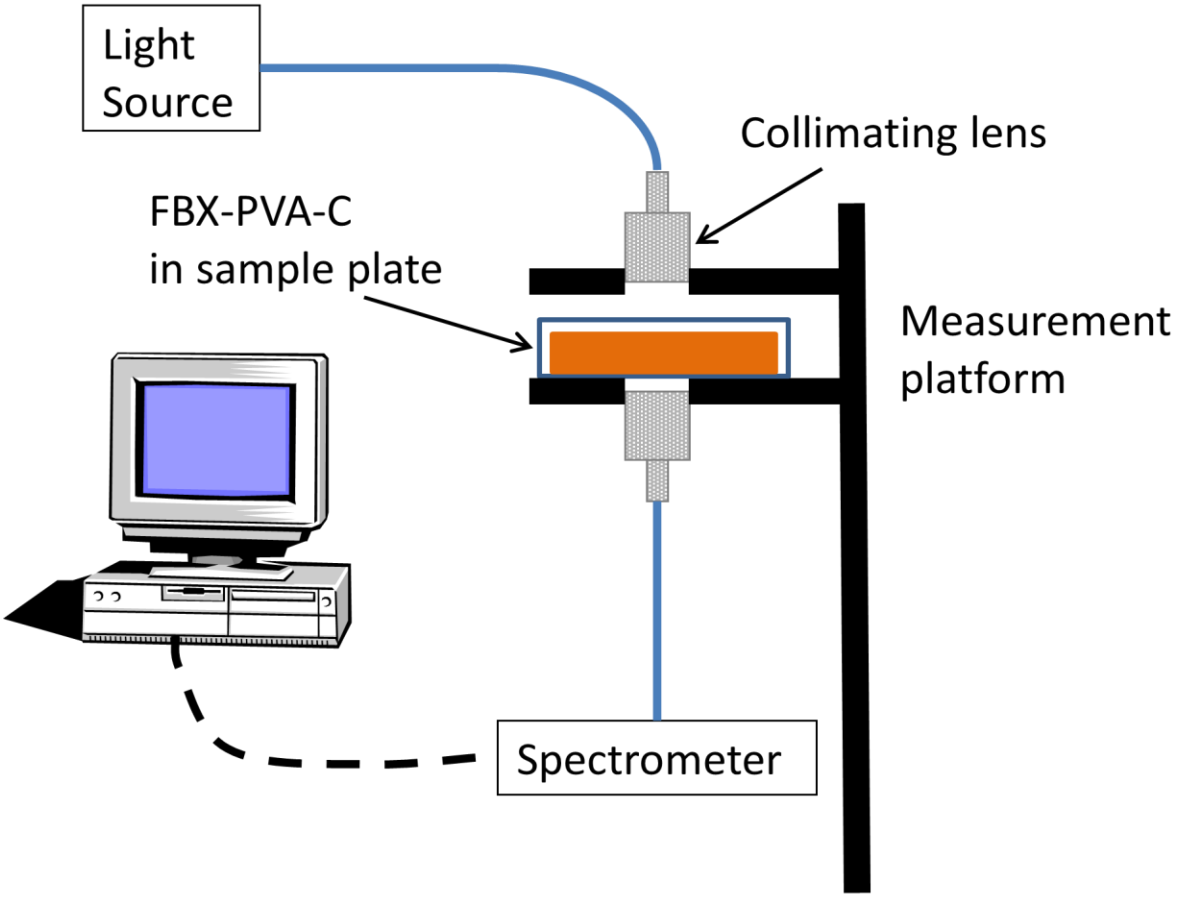

Figure 2.1. Schematic diagram of the measurement apparatus. Solid lines represent optical paths, while the broken line represents the electrical path.

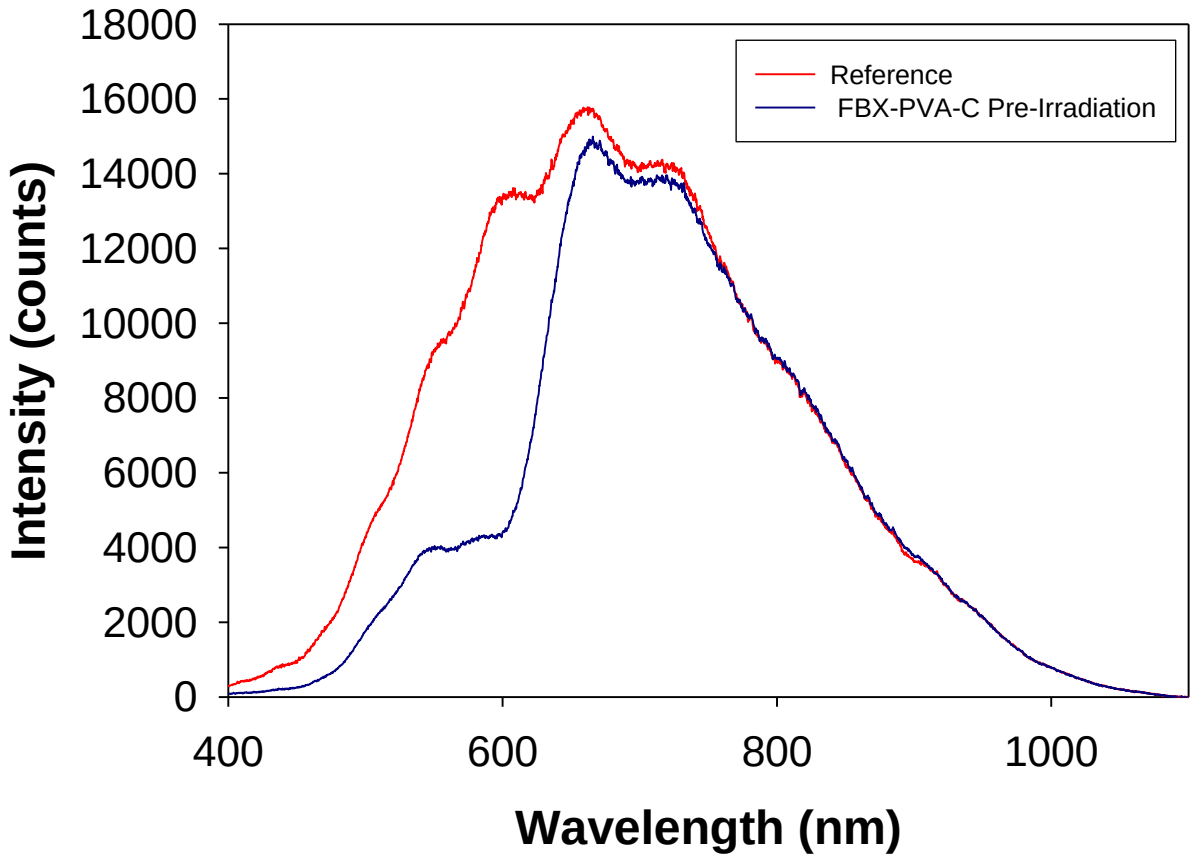

Figure 2.2. The intensity of transmitted light for reference and pre-irradiation samples made from 5% PVA and one FTC with 20/80 water/DMSO.

2.3.3 Irradiation of FBX Cryogel Dosimeter

All samples were irradiated using Varian iX linear accelerators with a 20 x 20 cm^2 field size. Samples were placed at isocentre height between 5.6 cm slabs of polystyrene. Multiple samples were irradiated in the field and were assumed to receive the same dose. Wet gauze was placed around the sample plates in an attempt to maintain electronic equilibrium conditions in the gap between polystyrene plates in all cases. The

effect of PVA concentration and number of FTCs on dose response was studied using 6 MV photons. The number of Monitor Units needed to obtain doses of 100, 250, 500, 750, and 1000 cGy were computed with Pinnacle 9.2 (Philips Radiation Oncology System) using a CT dataset of the polystyrene phantom, samples, and wet gauze. A dose rate of 422 cGy/min (corresponding to a machine setting of 400 monitor units per minute, MU/min) was employed for these irradiations. To clearly identify the linear dose range and the chemical saturation regime, the measurements were extended to 4000 cGy using 15% PVA-C (three FTCs) dosimeters, with 6 MV photons at a dose rate of 422 cGy/min**.** Dose rate and photon energy responses were evaluated using 15% PVA-C (three FTCs) dosimeters. Dose rate was studied using 6 MV photons, delivering 500 cGy at dose rates of 105, 316, 422, and 633 cGy/min (corresponding to machine settings of 100, 300, 400, and 600 MU/min). Energy dependence was evaluated by measuring the dose response curves for 6, 10, and 18 MV photons, at a dose rate setting of 400 MU/min with doses ranging from 100-1000 cGy. The treatment planning system, as described above, was used for monitor unit computation.

2.3.4 Wavelengths Selection and Averaging

It is interesting to note that the broad absorption peak is centred over the range of 590-600 nm, which is different than the 585 nm peak observed in the hydrogel (data not shown) and other formulations, such as Fricke PVA glutaraldehyde xylenol orange (FPGX), Fricke-gelatin-xylenol orange (FGX), and Fricke xylenol gel dosimeter (FXG) (Jin *et al.* 2012, Davis and Baldock 2008, Oliveira *et al.* 2009). The 10 nm difference is likely due to the interaction of the chromic components of FBX with the crystalline PVA-C.

The absorption coefficient μ_a was calculated using Beer-Lambert Law:

$$\mu_{a} = -\frac{1}{x} ln(\frac{I}{I_O}) \quad (2.1)$$

where

x is the thickness of sample in mm, I is the intensity of either irradiated or un-irradiated samples, and I_O is the intensity of the transparent reference sample.

Based on the measured spectra, the absorption coefficient was averaged over the range of 590-600 nm for all measurements. Averaging over the absorption peak resulted in reduced noise in the measured dose response curves.

2.4 Results and Discussion

2.4.1 Stability of Dosimeter Before and After Irradiation

No clear trend with time was observed prior to irradiation for different concentrations of PVA and for number of FTCs. An example of this shown in figure 2.3 for formulations prepared with three FTCs. This was also observed over an extended seven day period for a sample of 15% PVA and three FTCs (figure 2.4).

The gel that contained 30/70 ratio of water/DMSO was more attenuating (*i.e.* more DMSO leads to presence of smaller pores, which increases the transparency of cryogel). The absorbance also increased with increasing concentrations of PVA and

number of FTCs, as did the stiffness of the cryogel (Griffiths *et al.* 1996). A Pearson's chi-squared test was performed on the pre-irradiation data in order to establish if the data were substantially different from a constant value. The calculated *p*-value typically ranged from 0.90-0.95, with a worst case of 0.1 for 5% PVA and one FTC, suggesting that the transmittance of samples prior to irradiation was stable over time. The absorption coefficient of the unirradiated dosimeter (relative to the same formulation of cryogel without FBX added) is high (0.2 to 0.4 mm^{-1}); the water-based PVA cryogels typically have scattering coefficients in the range of 2 – 10 mm^{-1} depending on their formulation. The transparent cryogels do not scatter light, allowing for more accurate optical measurements compared to the water-based PVA cryogels.

a)

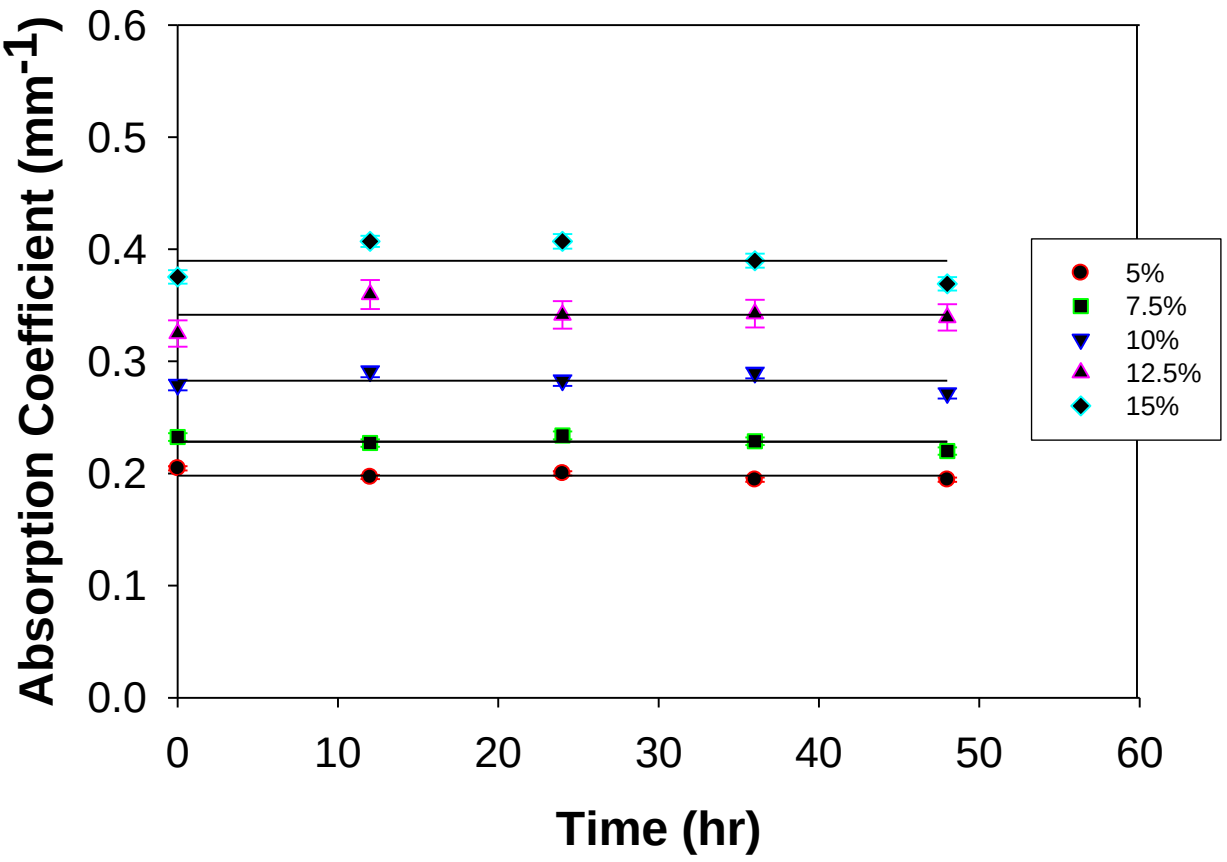
Absorption Coefficient (mm-1)
0.6
0.5
0.4
0.3
0.2
0.1
0.0
0
10
20
30
40
50
60
Time (hr)
5%
7.5%
10%
12.5%
15%

b)

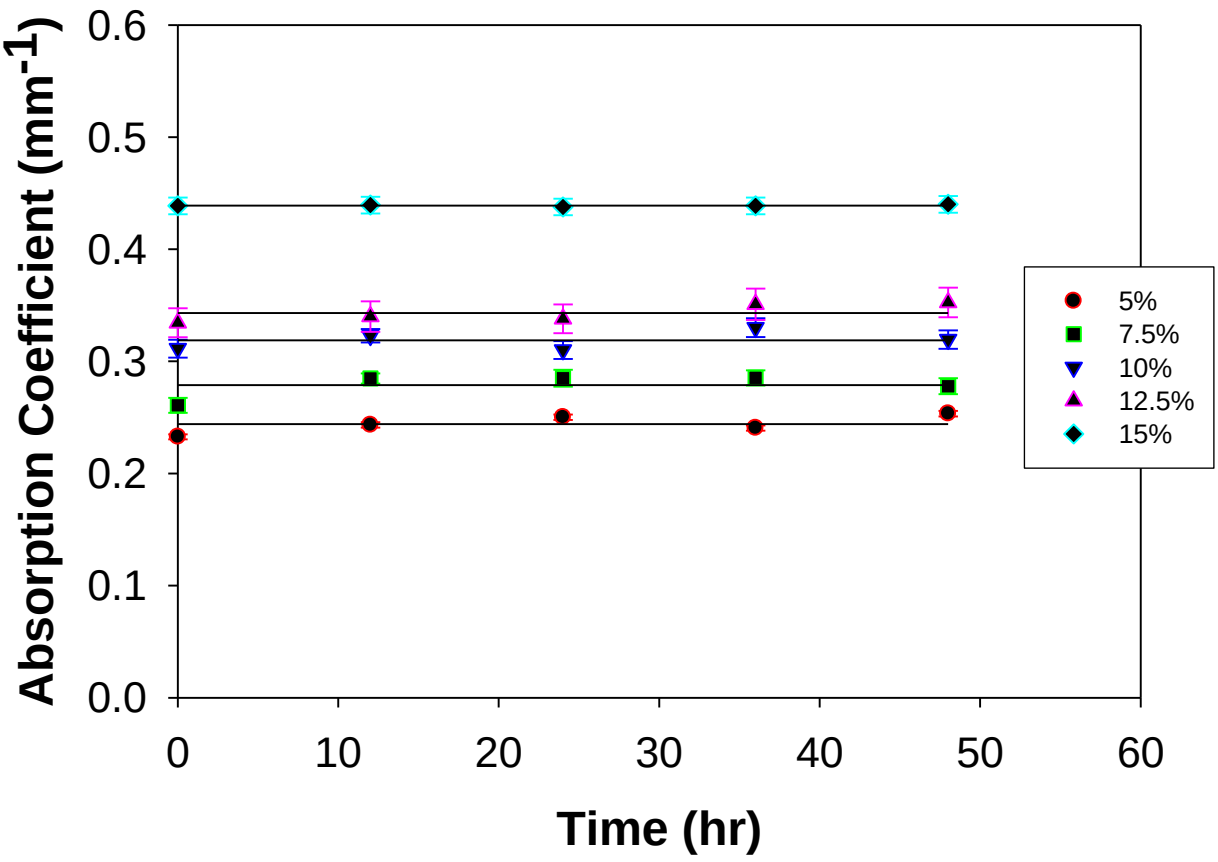

Figure 2.3. Absorption coefficient of different dosimeter formulations before irradiation for different concentrations of PVA. Different symbols represent different percentages of PVA used in the formulations. (a) Three FTCs, 20/80 water/DMSO formulation and (b) three FTCs 30/70 water/DMSO formulation. Each data point represents the mean absorption coefficient averaged over 590 – 600 nm for three independent preparations measured at five locations on each sample (n = 15). The error bars are the standard errors of the plotted measured values. The solid line is the average measured absorption coefficient and has been included to guide the eye.

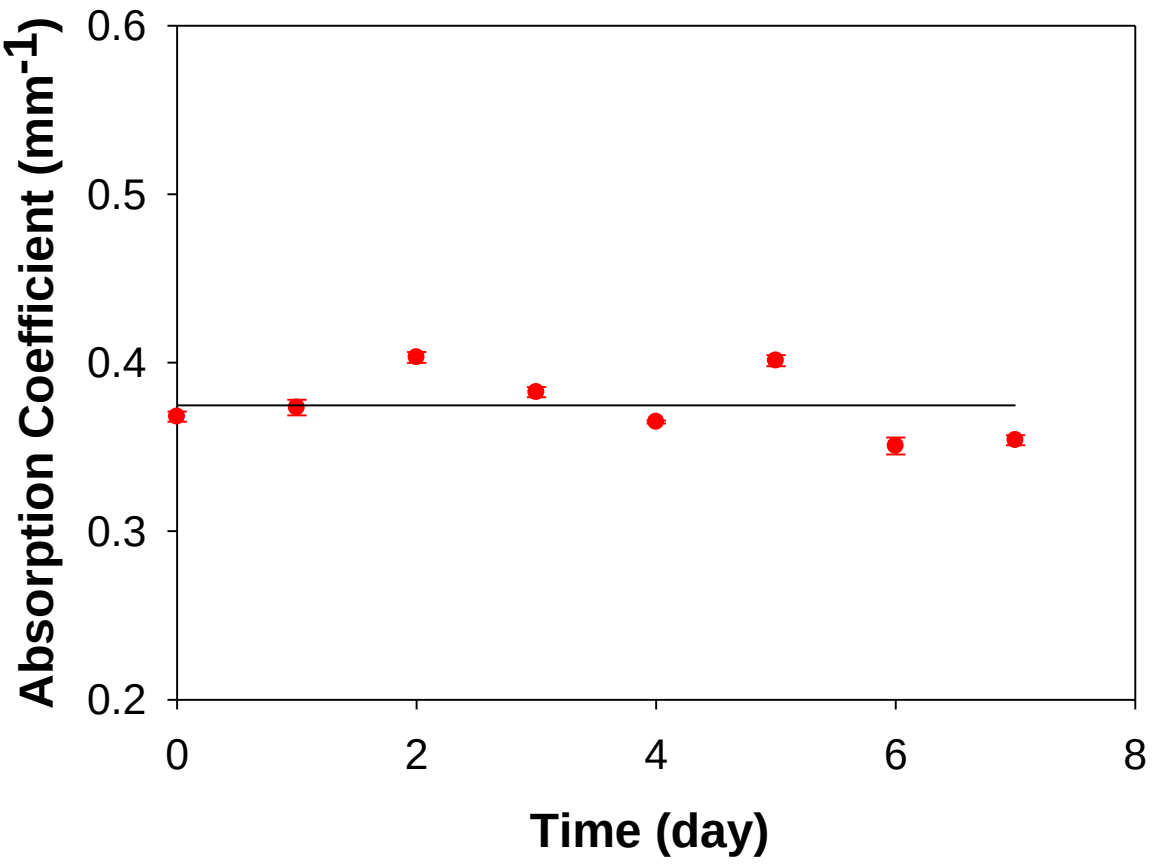

Figure 2.4. Absorption coefficient of the 15% (three FTCs) 20/80 water/DMSO gel dosimeter formulation for a seven day period prior to irradiation. Each data point represents the mean absorption coefficient averaged over 590 – 600 nm for three independent preparations measured at five locations on each sample (n = 15). The error bars are the standard errors of the plotted measured values. The solid line is the average measured absorption coefficient and has been included to guide the eye.

Larger than expected differences were observed in some measurements; figure 2.5 attempts to capture inter-batch and inter-location variability in the form of a box-and-whisker plot. It appears that a large proportion of the variability may have resulted from inconsistencies in sample preparation given the vertical separation of the boxes shown

in figure 2.5 panels (a) and (b). This is especially true at higher PVA concentrations (12.5% and 15%), where it was challenging to remove very small bubbles from the samples during the evacuation process. This may have been additional variation in the absorption coefficient from day-to-day if the measurement positions could not be replicated exactly. It is also possible that there was some heterogeneity in the thickness of the samples, which would result in differences in the measured absorption coefficient since a single thickness was used for each sample. The errors connected with the averaging over the multiple regions of the samples can be related to the error of different thicknesses. The error in thickness was approximately 3% for all samples, except for those cases where there was a visible imperfection. The physical thicknesses of the cryogel samples were taken using a Vernier calliper: the thickness of each sample were computed by averaging three independent measurements.

To demonstrate the sampling methodology, spectroscopic measurements were performed at the locations indicated by the five fiducials as shown in figure 2.6.

a)

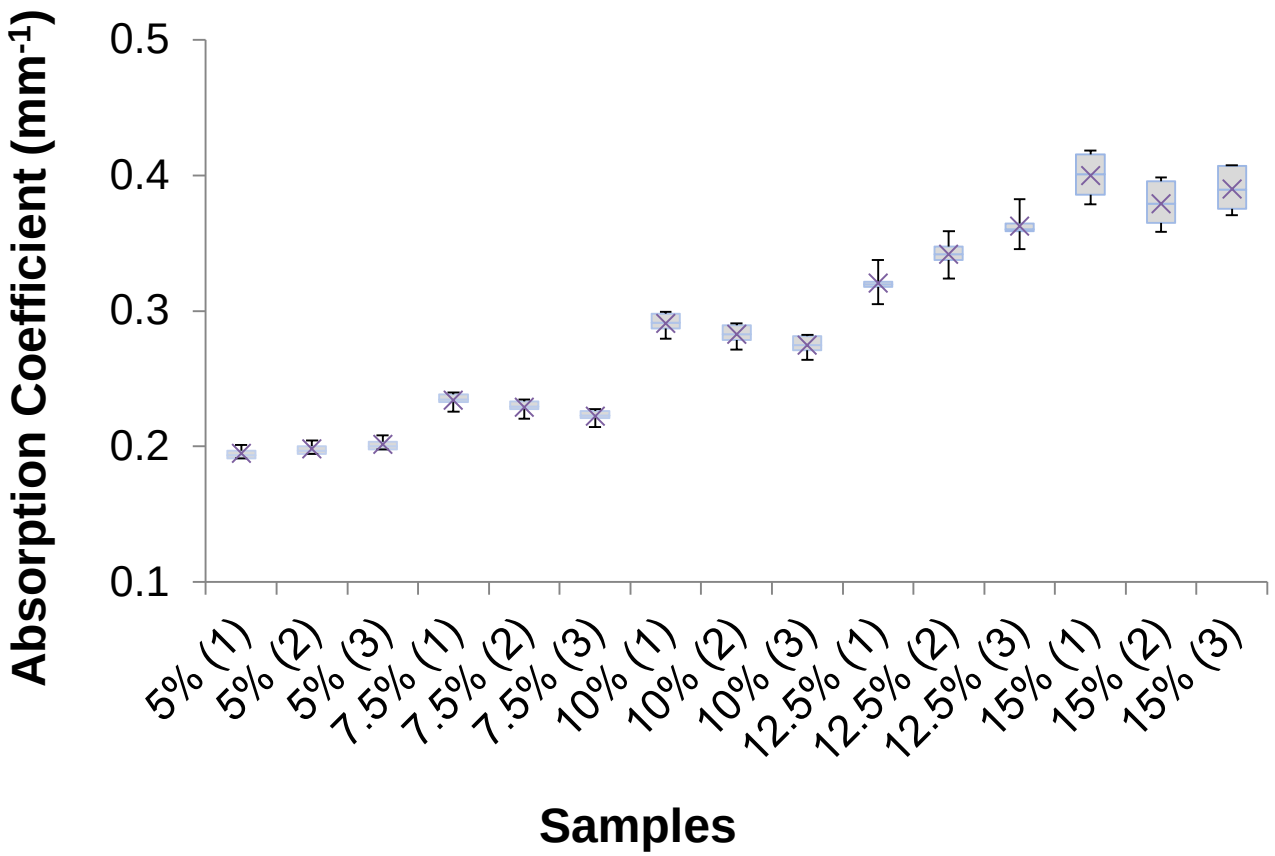
Absorption Coefficient (mm-1)
0.5
0.4
0.3
0.2
0.1
5% (1)
5% (2)
5% (3)
7.5% (1)
7.5% (2)
7.5% (3)
10% (1)
10% (2)
10% (3)
12.5% (1)
12.5% (2)
12.5% (3)
15% (1)
15% (2)
15% (3)
Samples

b)

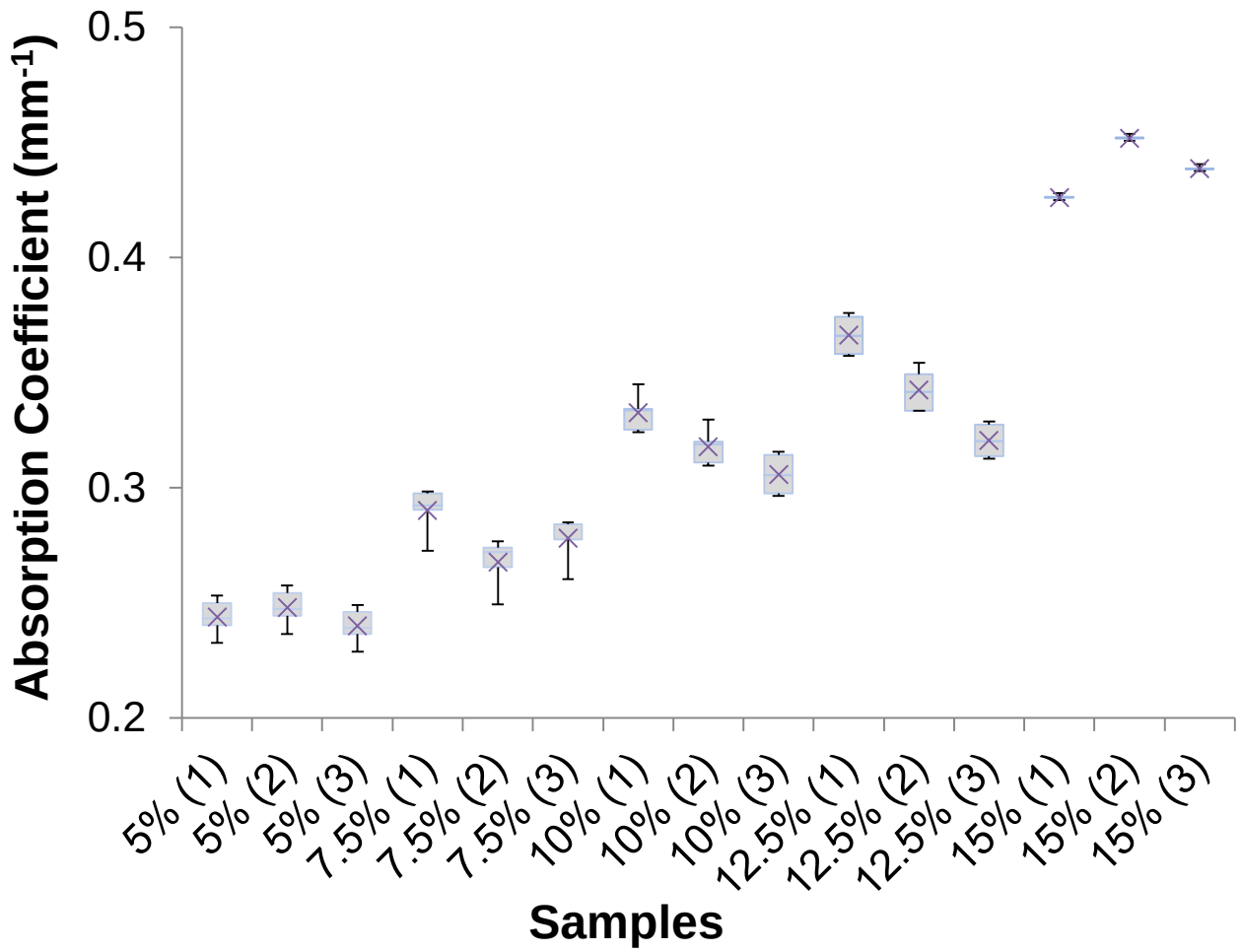
Absorption Coefficient (mm-1)
0.5
0.4
0.3
0.2
5% (1)
5% (2)
5% (3)
7.5% (1)
7.5% (2)
7.5% (3)
10% (1)
10% (2)
10% (3)
12.5% (1)
12.5% (2)
12.5% (3)
15% (1)
15% (2)
15% (3)
Samples

c)

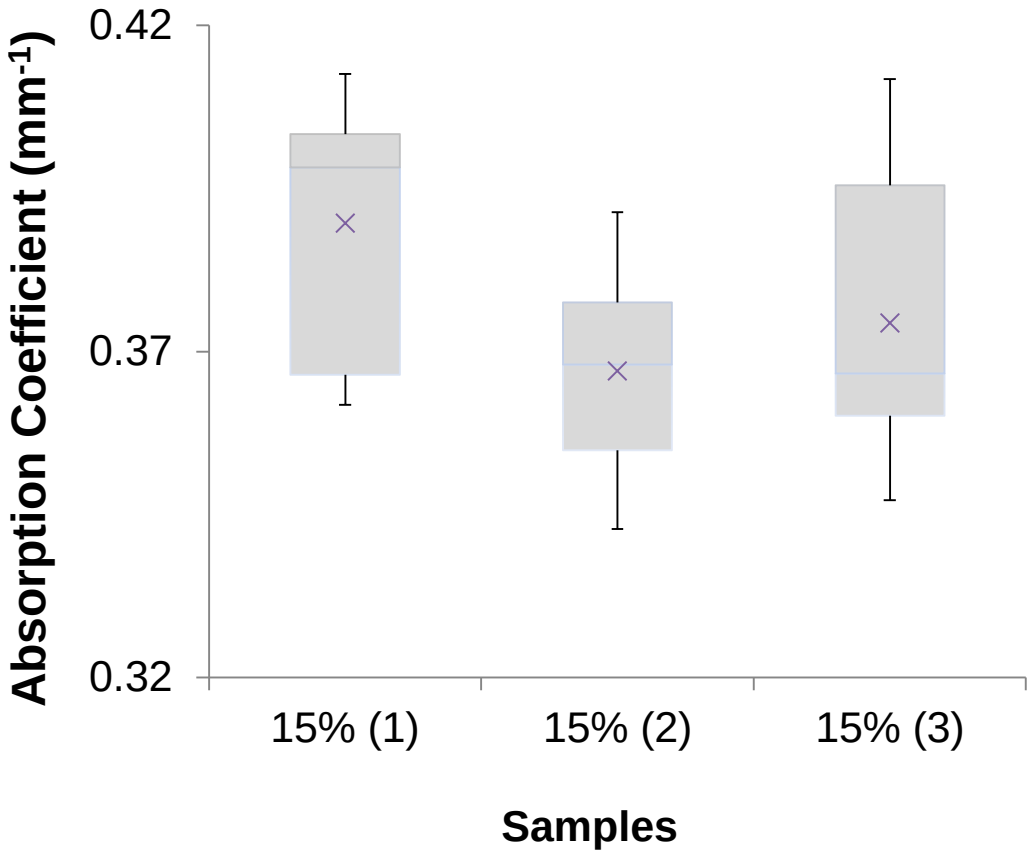

Figure 2.5. Box and whisker plots showing the measured absorption coefficients of different dosimeter formulations before irradiation for different concentrations of PVA. The bracketed numbers (1, 2, 3) represent independently prepared formulations. (a) Three FTCs, 20/80 water/DMSO formulation measured over a 2 day prior to irradiation; (b) three FTCs 30/70 water/DMSO formulation measured over a two day prior to irradiation; and (c) three FTCs, 20/80 water/DMSO formulation measured over a seven day period prior to irradiation.

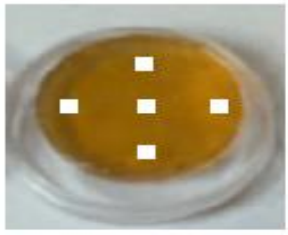

Figure 2.6. The fiducial markers show typical measurement locations used to obtain the average absorption coefficient of the sample.

2.4.2 Dose Response of Typical PVA-C Formulations

The effect of PVA concentration on dose response was investigated for samples prepared with 20/80 and 30/70 water/DMSO ratios by weight. A sample photograph (figure 2.7) shows a reference sample, pre-irradiation, and irradiated samples up to 1000 cGy.

Figure 2.7. A photograph of the reference, pre-irradiation, and post-irradiation for the 15% (three FTCs) 20/80 water/DMSO dosimeter system.

Additional measurements were performed at early time points after irradiation (0.5-7 hours) for 6, 10, and 18 MV photon beams, shown in figure 2.8. There is a small increase in measured optical density within the first two hours, after which the signal was approximately constant. For scheduling convenience, all gels were read approximately 16 hours after irradiation (*i.e.* measurements performed the morning after

an evening irradiation). The rate of base line drift can be calculated using the following equation:

$$Response\ rate = \frac{\mu_a(D) - \mu_a(0)}{\Delta D} \quad (2.2)$$

where

$\mu_a(D)$ is the absorption coefficient at the irradiated dose, $\mu_a(0)$ is pre- irradiation absorption coefficient, and ΔD is the change in absorbed dose.

Using equation (2.2) the sensitivity was calculated to be 2.8 X 10^{-4} mm^{-1} cGy^{-1}.

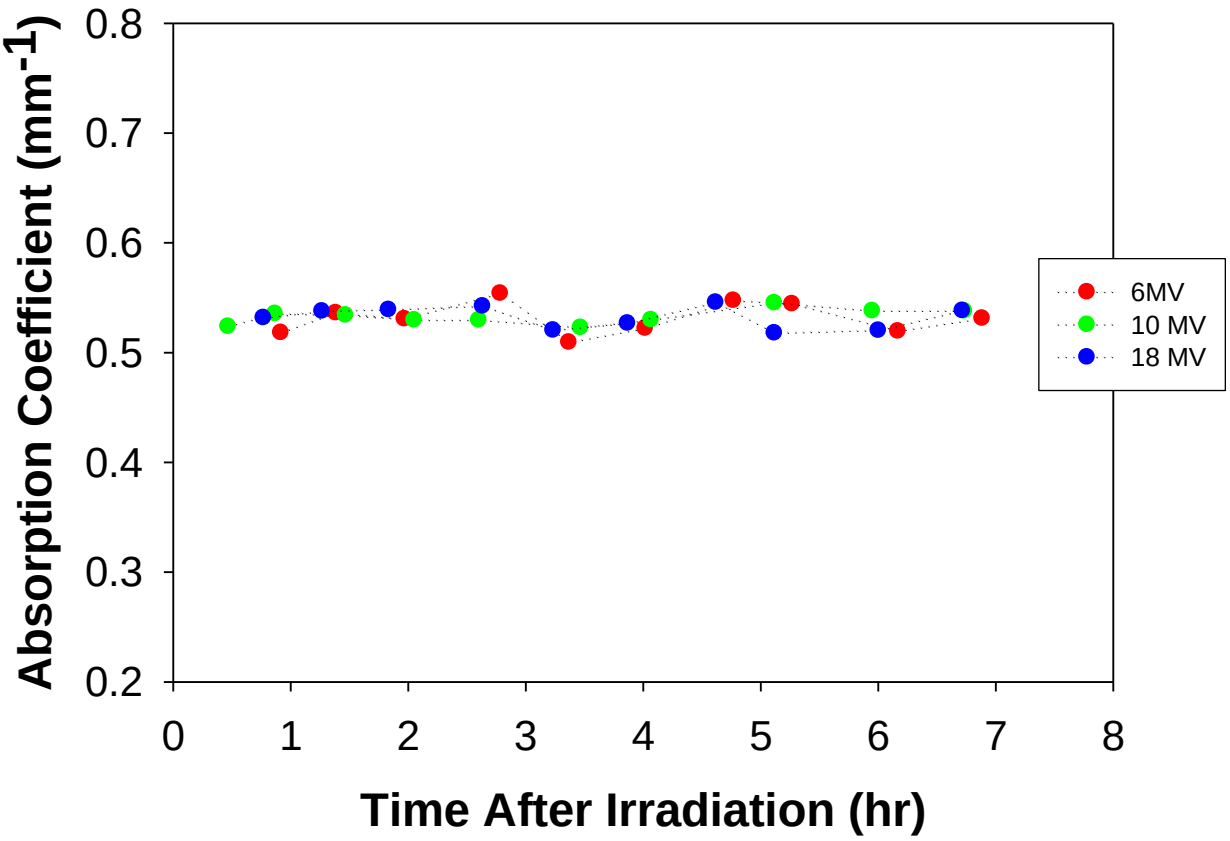

Figure 2.8. Absorption coefficient behaviour versus time for samples of the 15% (three FTCs) 20/80 water/DMSO gel dosimeter formulation irradiated with 500 cGy of a 6, 10, and 18 MV photon beams.

Spatial heterogeneity measurements were also performed on representative samples. The measurement points are shown in figure 2.9a. Figure 2.9b shows the typical level of heterogeneity within a given sample.

a)

b)

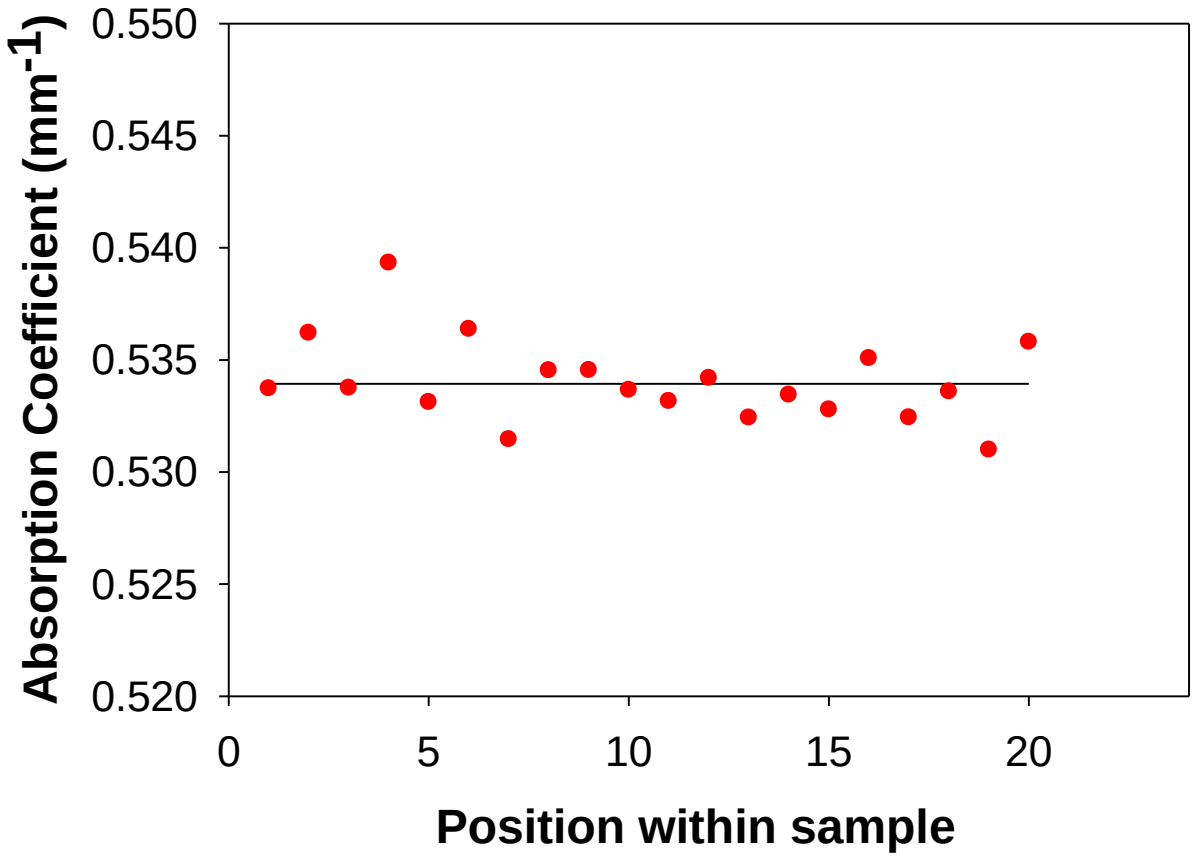

Figure 2.9. (a) The 20 positions used to evaluate sample heterogeneity of the 15% (three FTCs) 20/80 water/DMSO gel dosimeter formulation irradiated with 500 cGy of a 6 MV photon beam. (b) Measured absorption coefficient versus position for the sample shown in figure 2.9a. The solid line is the average measured absorption coefficient and has been included to guide the eye.

Figure 2.10 shows the change in absorption spectrum due to irradiation using a completely transparent sample as reference (panel a) with the measured dose response for formulations prepared with three FTCs (panel b,c). The slope of the line of best fit (sensitivity) increased with increasing concentration of PVA, number of FTCs, and decreasing the amount of DMSO used in the formulation.

a)

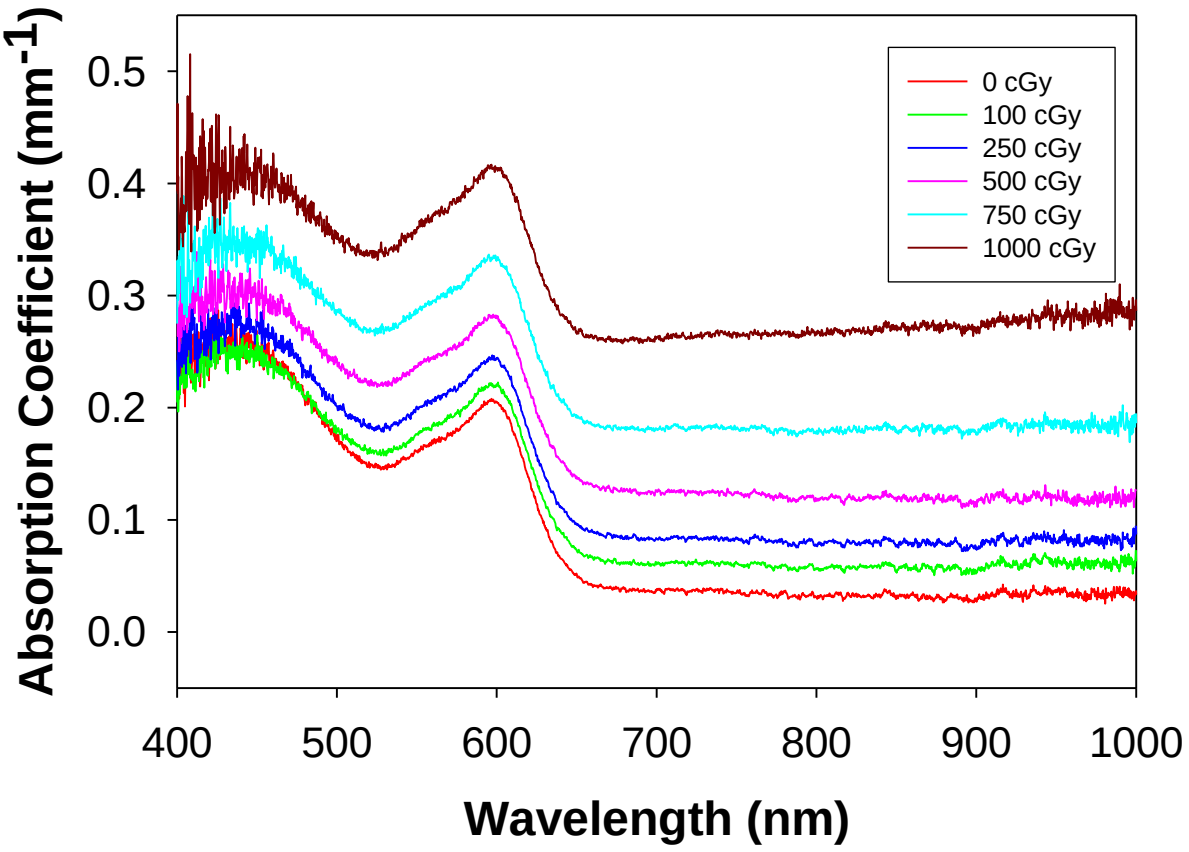

b)

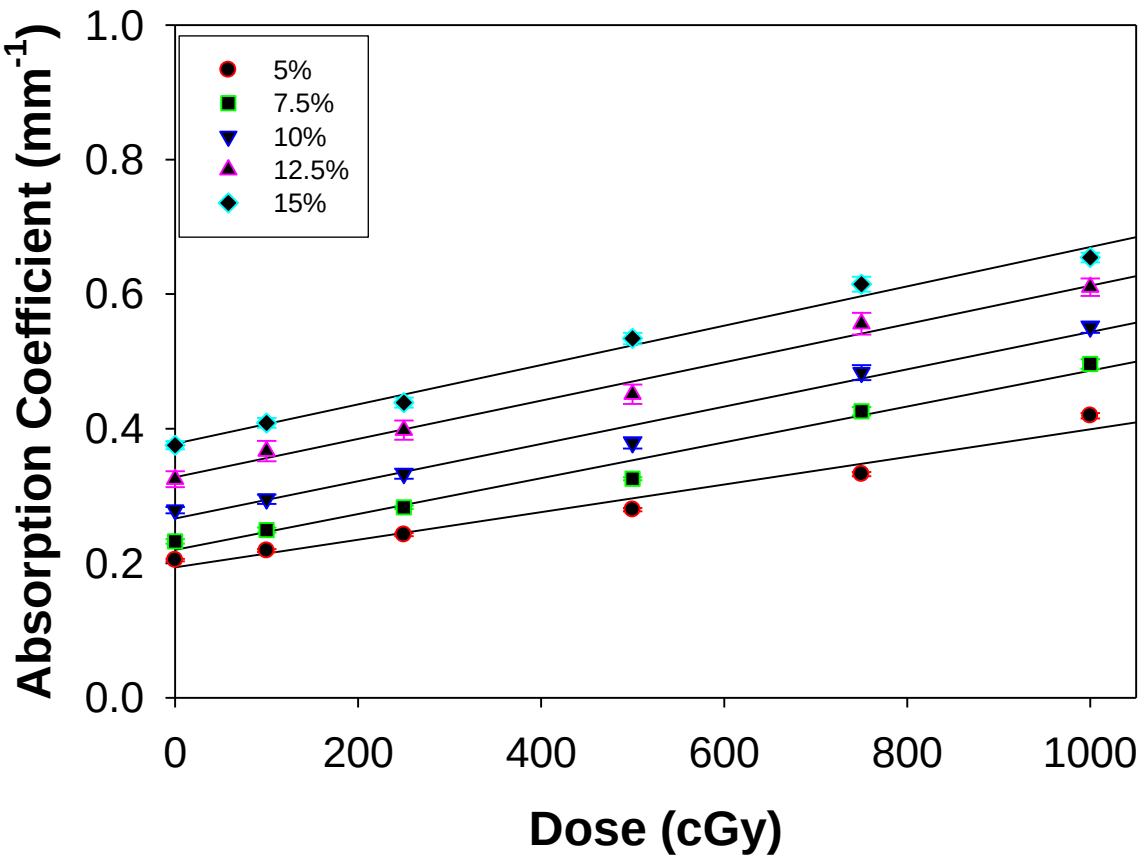
Absorption Coefficient (mm-1)
1.0
0.8
0.6
0.4
0.2
0.0
0
200
400
600
800
1000
Dose (cGy)
5%
7.5%
10%
12.5%
15%

c)

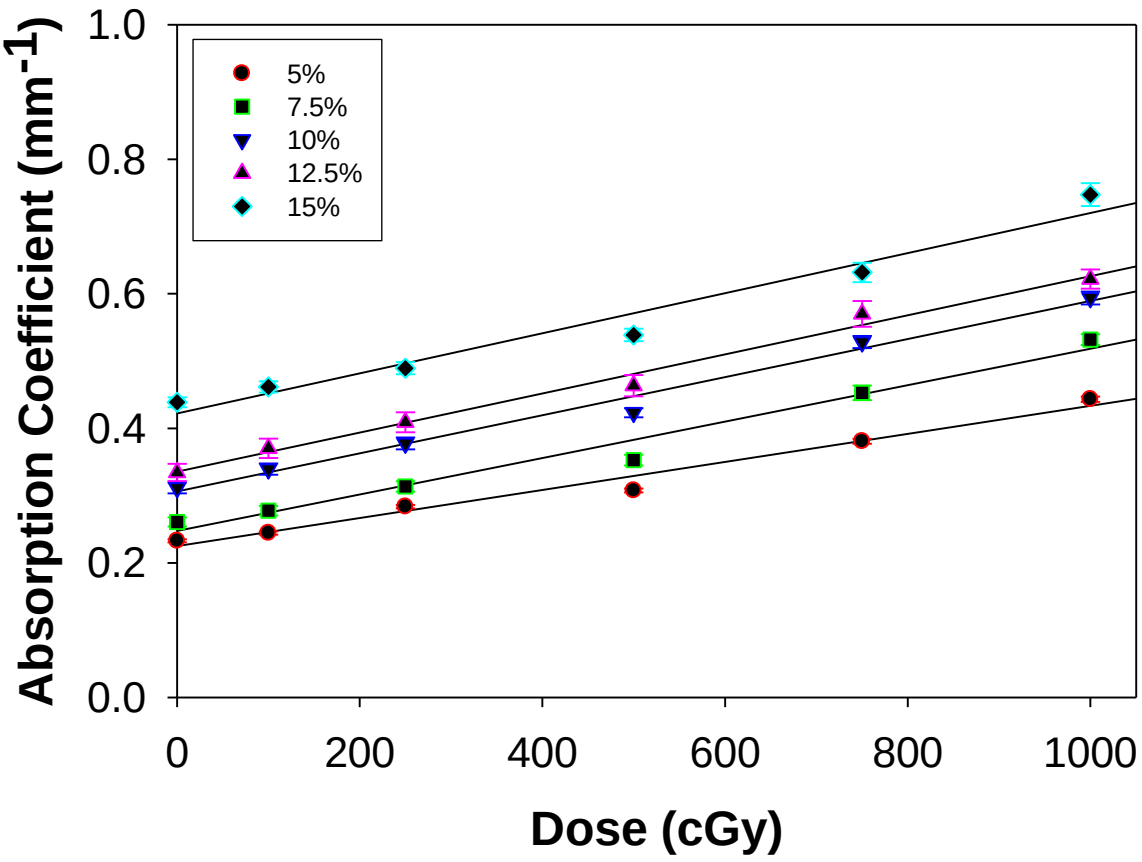

Figure 2.10. (a) The change in FBX-PVA cryogel absorption spectrum of the 5% PVA (three FTCs) 20/80 water/DMSO formulation due to irradiation. The absorption spectra of the unirradiated gel (0 cGy curve) and the irradiated gels (100, 250, 500, 750 and 1000 cGy curves) were measured using a colourless and transparent PVA-C sample as reference. (b) Dose-response curves of different dosimeter formulations for different concentrations of PVA. Different symbols represent different percentages of PVA used in the formulations for three FTCs, 20/80 water/DMSO formulation, and (c) three FTCs 30/70 water/DMSO formulation. Different symbols represent different percentages of PVA used in the formulations. Each data point represents the mean absorption coefficient averaged over 590 – 600 nm for three independent preparations measured at five locations on each sample (n = 15). The error bars are the standard errors of the plotted measured values.

For clarity, the sensitivities of the different formulations are shown in figure 2.11. The one FTC data in figure 2.11 seem to suggest a fundamental difference between it and the three and six FTCs samples. The number of crosslinks that form in the cryogel decreases with low PVA and FTCs compared with the higher PVA and FTCs dosimeters. So it is possible that, at low FTCs and PVA concentrations a small amount of radiochromic material bled from the matrix, resulting in a lower sensitivity than expected. While this situation is not ideal, it is highly reproducible from batch-to-batch and thus can be accounted for in the calibration process.

a)

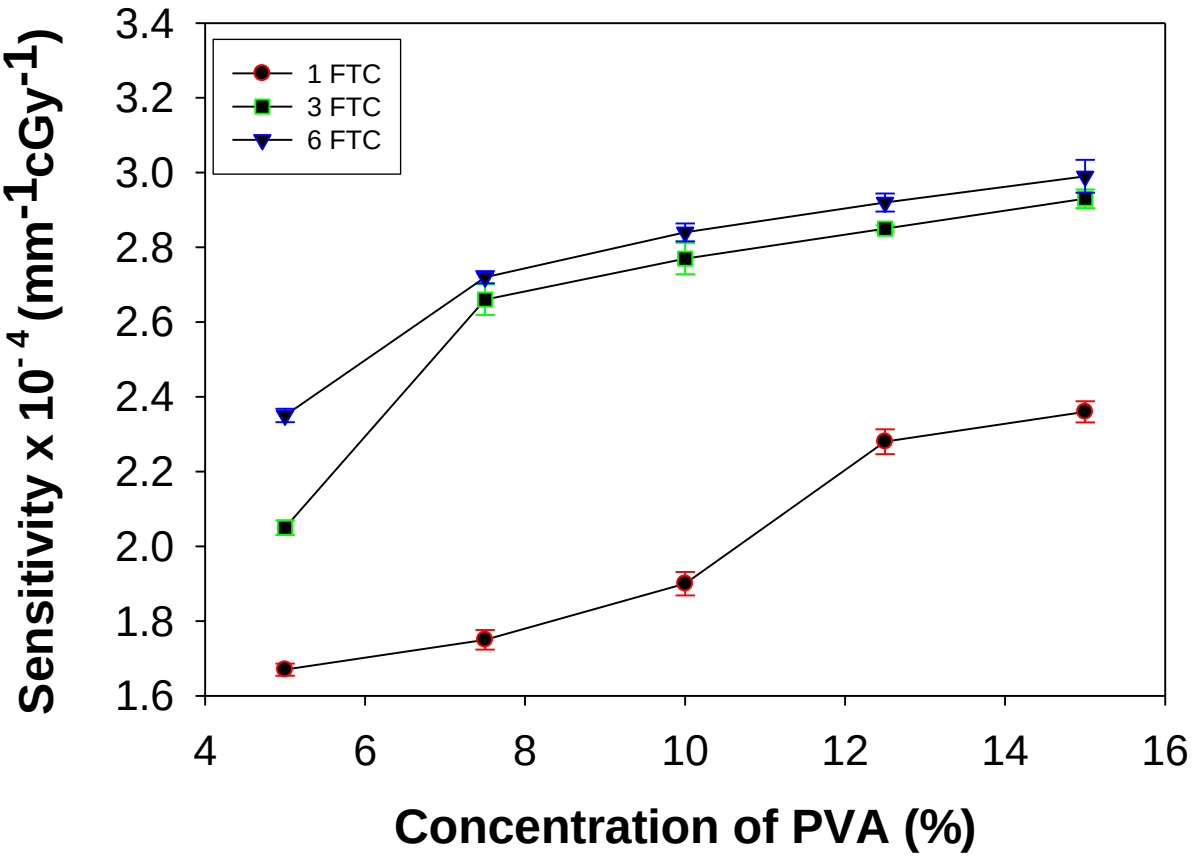

b)

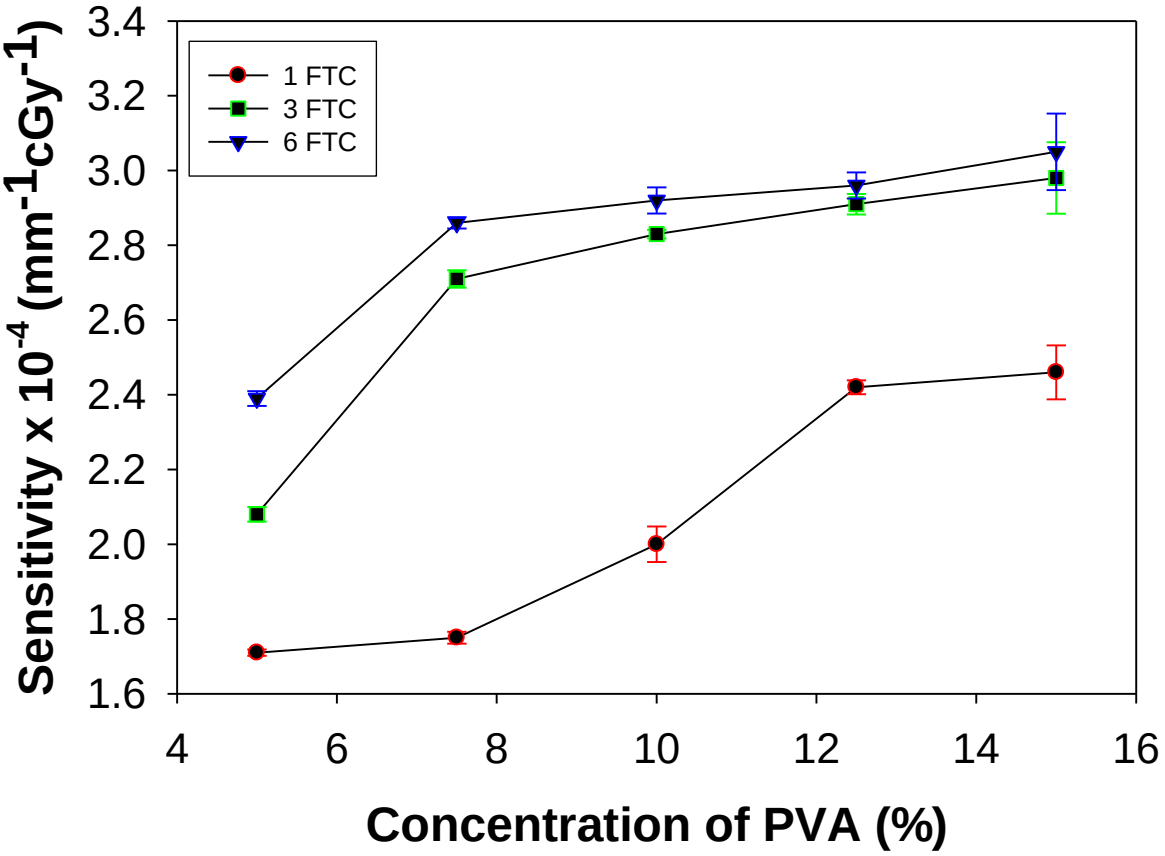

Figure 2.11. Sensitivity of different concentrations of PVA dosimeters. (a) 20/80 and (b) 30/70. Different symbols represent the number of FTCs.

The minimum detectable difference for dose was also determined for the different formulations using the standard deviations derived from the absorption measurements, where the averaged absorption coefficient measurements were used to estimate an error in dose. For the 20/80 formulations, the maximum relative error in dose found at 100 cGy was 2.1% and the minimum at 1000 cGy was 0.204%. Similarly, for the 30/70 formulations, the maximum at 100 cGy was 2.6% and the minimum at 1000 cGy was 0.244%. The difference in sensitivity between the different DMSO groups may be related to the free radical of scavenging properties of DMSO (Silva *et al.* 2011). Increased scavenger concentration should lead to a decrease in the oxidation of Fe^{2+} to Fe^{3+} (Jin *et al.* 2012), the mechanism for colour change in FBX-based dosimeters. The effect, however, is not large enough to preclude the use of the higher DMSO concentration, especially since it results in a more transparent matrix material. There is no obvious reason for the observed differences in sensitivity with PVA concentration and number of freeze-thaw- cycles. Additional PVA and freeze-thaw-cycles both lead to an increase in the number of crosslinks that form in the cryogel. It is possible that there is some interaction between the physical properties of the polymer and the FBX material suspended within. The measurements are consistent with related studies: Chu reported a small increase of sensitivity in PVA-C with increasing PVA concentration for some formulations, and Hill showed that increased numbers of freeze-thaw cycles resulted in a higher sensitivity for a certain PVA concentration. The salient difference between the current study and these two is that the dose was read using an accessible and inexpensive optical instrument rather than MRI.

Doses were extended up to 4000 cGy to investigate the onset of the chemical saturation region. The data are shown in figure 2.12 and demonstrate a linear dose response up to approximately 1000 cGy. The range of utility can be extended to higher doses by modeling the saturation region using an exponential function**.** Others have shown that, in a gelatin FX dosimeter, increasing the concentration of XO increases the linearity range (Davies and Baldock 2008).

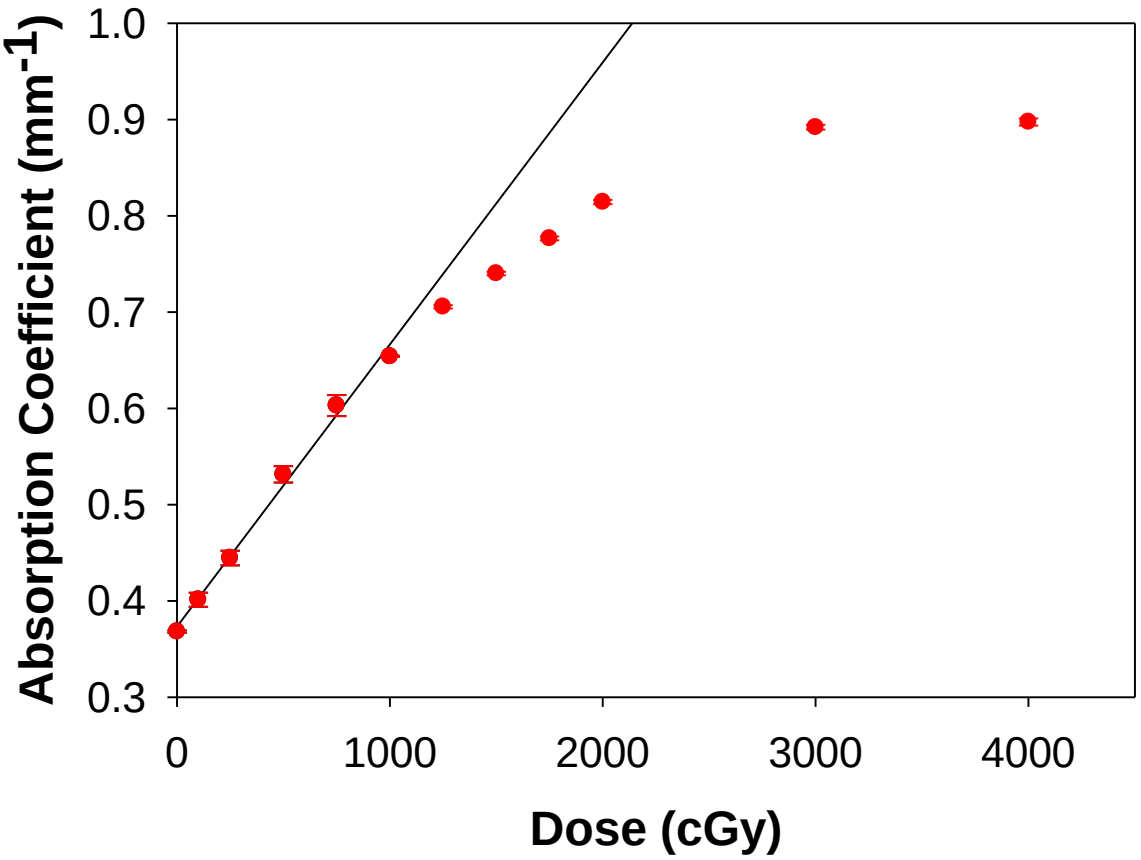

Figure 2.12. Dose-response curve of 15% PVA (three FTCs) using a 20/80 water/DMSO ratio formulation up to 40 Gy. Each data point represents the mean absorption coefficient averaged over 590 – 600 nm taken over a three locations on each sample. The error bars are the standard errors of the plotted measured values.

2.4.3 Dose Rate Effect

The effect of dose rate on the measured absorbance was studied using dose rates of 105, 316, 422, and 633 cGy/min (corresponding to machine settings of 100, 300, 400 and 600 MU/min respectively), 6 MV photons, and 500 cGy delivered dose. The samples were 15% (three FTCs) with 20/80 water/DMSO ratio. This particular formulation was selected due to its superior sensitivity, reasonable fabrication time, and it is a sturdy, easy to handle material. Figure 2.13 shows the mean absorbance with dose rate setting, averaged over a three day period after irradiation. The data suggest that there is no measurable effect in this range of dose rates.

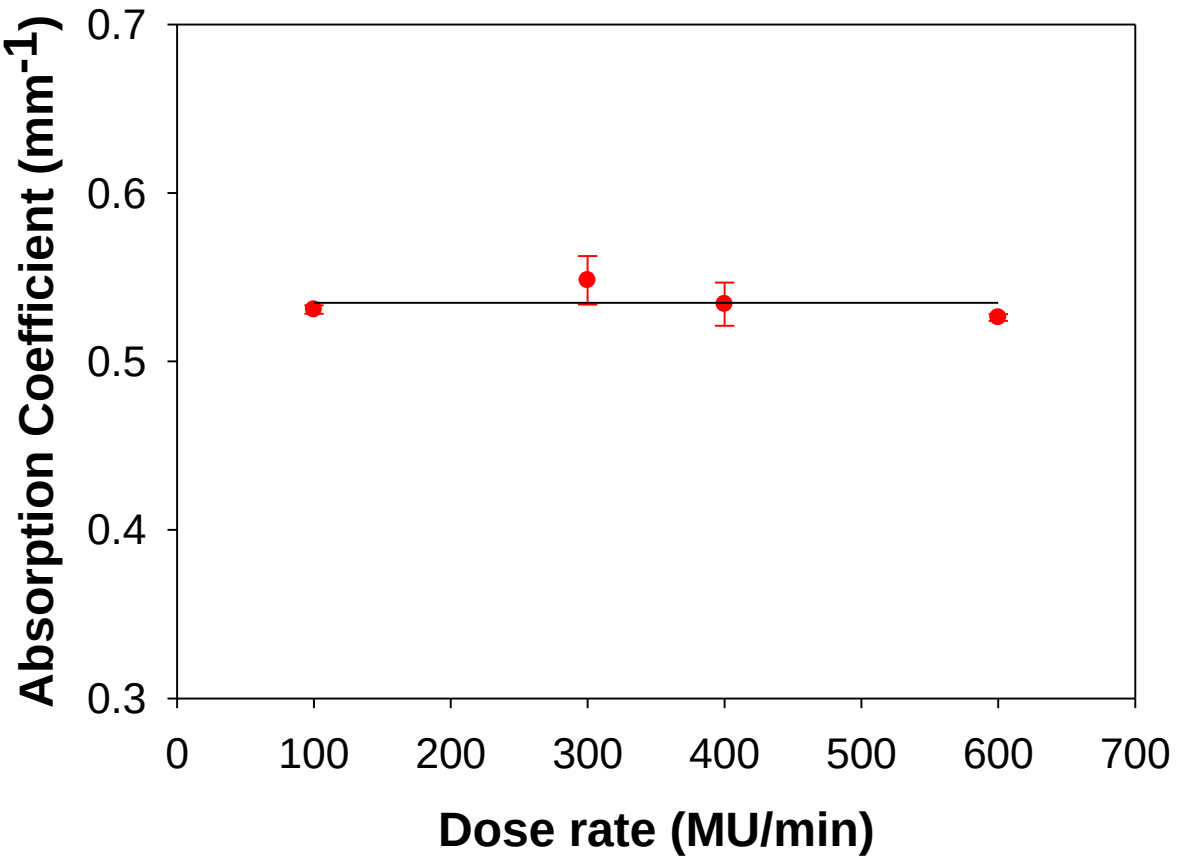

Figure 2.13. Absorbance of the gel dosimeter with different dose rate machine settings (100, 300, 400 and 600 MU/min), 6 MV, and 500 cGy delivered dose for sample of 15% (three FTCs) 20/80 water/DMSO dosimeter system. Each data point represents the mean absorption coefficient averaged over 590 – 600 nm and taken over a three day period post irradiation measured at three locations on each sample (n = 9). The error bars are the standard errors of the plotted measured values.

2.4.4 Energy Effect

The effect of energy on the dosimeter was evaluated using photon beams with nominal energies of 6, 10, and 18 MV, at a dose rate machine setting of 400 MU/min and nominal doses of 100, 250, 500, 750, and 1000 cGy. The samples were 15% PVA (three FTCs) using a 20/80 water/DMSO ratio. The auto oxidation at 500 cGy for the applied energies was studied in section 2.4.2.

The dose response of each energy was determined independently, yielding sensitivities of (3.00 ± 0.04) $x10^{-4}$, (3.00 ± 0.05) $x10^{-4}$, and (3.10 ± 0.05) $x10^{-4}$ $mm^{-1}cGy^{-1}$ for 6, 10, and 18 MV respectively. The dosimeter was found to be energy independent over the range of nominal photon energies examined in this study; figure 2.14 demonstrates the co-linearity of the dose response curves for the three different energies, with an overall sensitivity of (3.00 ± 0.04) $x10^{-4}$ $mm^{-1}cGy^{-1}$.

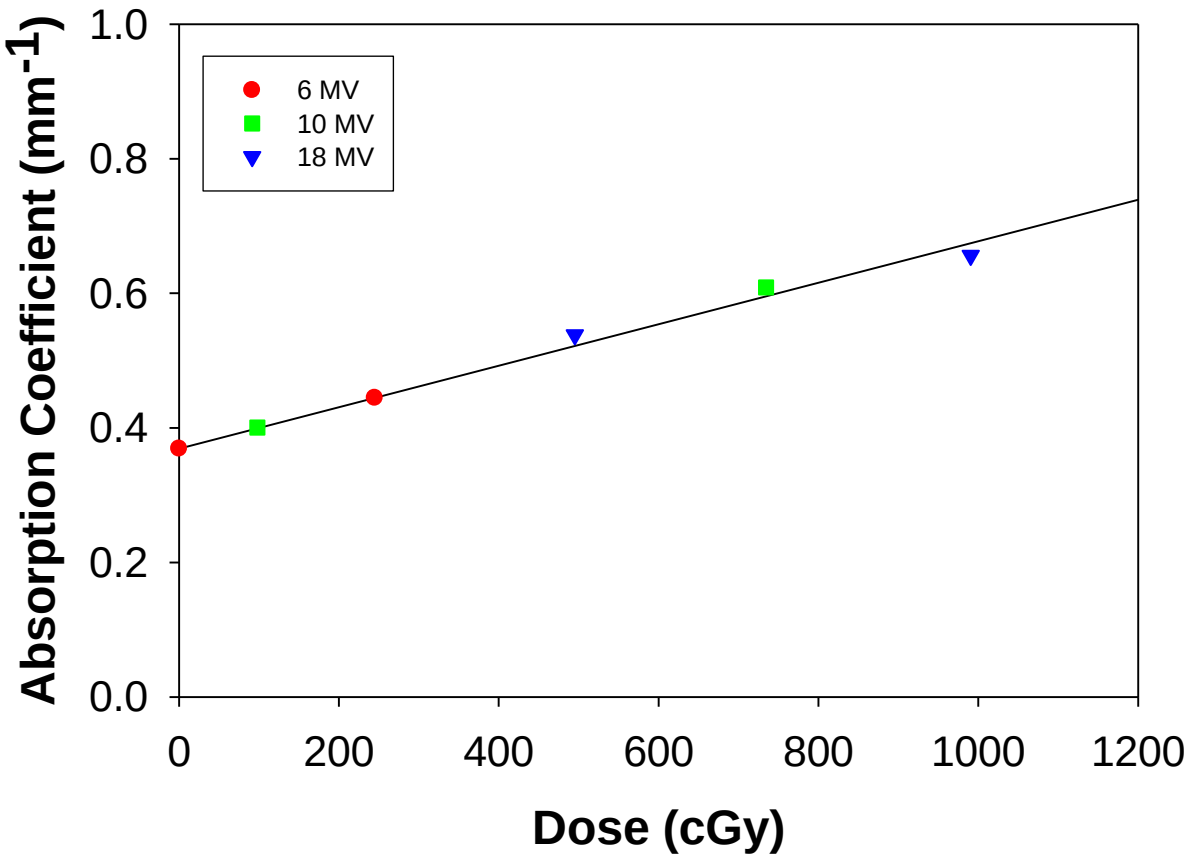

Figure 2.14. Evaluation of energy response of FBX-PVA-C using a 15% (three FTCs) 20/80 water/DMSO formulation**.**

2.5 Conclusion

A deformable radiochromic dosimeter with good stability and sensitivity was obtained by using FBX in a translucent poly(vinyl alcohol) cryogel. Of the two water/DMSO ratios tested, 80% DMSO by weight yielded a more transparent dosimeter, demonstrated by a lower pre-irradiation absorbance. This result is also consistent with the work of Hyon *et al*. Increasing the concentration of PVA and the number of FTCs resulted in higher

absorbance and sensitivity. The 30/70 dosimeter was slightly more sensitive than the 20/80 system. The dosimeter demonstrated a reproducible linear dose response up to approximately 1000 cGy, which is suitable for many therapeutic applications. No significant dose rate or energy dependence for this dosimeter was observed over the range studied. The diffusion coefficient of cryogel was found to be 0.152 mm^2 h^{-1} for 15% PVA (20/80 dosimeter, 3 FTCs), which is consistent with the observations of Chu *et al.* (2000).

This preliminary study has demonstrated that it may be possible to use a transparent PVA cryogel matrix loaded with FBX as a dosimeter, but optimization will be necessary in order to use the material in 3D applications. In the present formulations, the absorption coefficient of the unirradiated dosimeter is quite high (> 0.3 mm^{-1}), which would limit the thickness of material that could be imaged through. It is also challenging to produce pristine samples at high PVA concentrations since the hydrogel may retain bubbles even after evacuation. Different concentrations of XO and ferrous ammonium sulphate may lead to a reduction of the unirradiated absorbance. While translucent FBX-PVA-C is not yet suitable for 3D application, the use of transparent PVA cryogel as a general matrix material should be considered when developing new dosimeter models.

Acknowledgment

This work has been supported by the NSERC Discovery Grant program and the Yarmouk University Physics Department.

References

Appleby A and Leghrouz A 1991 Imaging of radiation dose by visible color development in ferrous-agarose-xylenol orange gels *Med. Phys.* **18** 309-12

Chu K C, Jordan K J, Battista J J, Van Dyk J and Rutt B K 2000 Polyvinyl alcohol Fricke hydrogel and cryogel:two new gel dosimetry systems with low Fe^{+3} diffusion *Phys. Med. Biol.* **45** 955-69

Davies J B and Baldock C 2008 Sensitivity and stability of the Fricke-gelation-Xylenol orange gel dosimeter *Radiat. Phys. Chem*. **77** 690-96

Doran S J, Rahman A A, Bräuer-Krisch E, Brochard T, Adamovics J, Nisbet A and Bradley D 2013 Establishing the suitability of quantitative optical CT microscopy of PRESAGE® radiochromic dosimeters for the verification of synchrotron microbeam therapy *Phys. Med. Biol*. **58** 6279-97

Farrell T J, Patterson M S and Wilson B 1992 A diffusion theory model of spatially resolved, steady-state diffuse reflectance for the noninvasive determination of tissue optical properties *in vivo Med. Phys.* **19** 879-88

Frick H and Hart E 1955 *Chemical Dosimetry* vol 2 ed F h Attix and W C Roesch (New York: Academic) (Chemical Dosimetry)

Frick H and Morse S 1927 The chemical action of Roentgen on dilute ferrous sulphate solutions as a measure of dose *Am. J. Roent. Radium Ther. Nucl. Med.* **18** 430-32

Gambarini G, Arrigoni S, Cantone M C, Molho N, Facchielli L and Sichirollo A E 1994 Dose-response curve slope improvement and result reproducibility of ferrous sulphate-doped gels analysed by NMR imaging *Phys. Med. Biol*. **39** 703-17

Gore J C and Kang Y S 1984 Measurement of radiation dose distributions by nuclear magnetic resonance (NMR) imaging *Phys. Med. Biol.* **29** 1189-97

Griffith P C, Stilbs P, Howe A M and Cosgrove T 1996 A self-diffusion study of the complex by sodium dodecyl sulphate and gelatin in aqueous solutions *Langmuir* **12** 2884-93

Gupta B L and Narayan G R 1985 G(Fe+3) values in the FBX dosimeter *Phys. Med. Biol*. **30** 337-40

Hazle J D, Hefner L, Nyerick C E, Wilson L and Boyer A L 1991Dose-response characteristics of a ferrous sulfate-doped gelation system for determining radiation

absorbed dose distributions by magnetic resonance imaging (FeMRI) *Phys. Med. Biol*. **36** 1117-25

Hill B, Bäck S Å J, Lepage M, Simpson J, Healy B and Baldock C 2002 Investigation and analysis of ferrous sulfate polyvinyl alcohol (PVA) gel dosimeter *Phys. Med. Biol.* **47** 4233-46

Hyon S H, Cha W I and Ikada Y 1989 Preparation of transparent poly (vinyl alchohol) hydrogel *Polym. Bull* **22** 119-22

Jiang S, Su Z, Wang X, Liu S and Yu Y 2013 Development of a new tissue-equivalent material applied to optimizing surgical accuracy *Mater. Sci. Eng.* C **33** 3768-74

Jin C, Chen J, Yang L, Luo W, Wu G and Zha Y 2012 Effect of DMSO on the sensitivity and diffusion of FPGX gel dosimeter *Radiat. Phys. Chem.* **81** 879-83

Kelly R G, Jordan K J and Battista J J 1998 Optical CT reconstruction of 3D dose distributions using the ferrous sulphate-benzoic acid-xylenol orange gel dosimeter *Med. Phys*. **25** 1741-50

Kharine A, Manohar S, Seeton R, Kolkman R G, Bolt R A, Steenbergen W and de Mul F F 2003 Poly (vinyl alcohol) gels for use as tissue phantoms in photoacoustic mammography *Phys. Med. Biol.* **48** 357-70

McJury M , Oldham M, Cosgrove V P, Murrphy P S, Doran S, Leach M O and Webb S 2000 Radiation dosimetry using polymer gels: methods and application *Br. J. Radiol.* **73** 919-29

Nazir A, Afzal M and Buzdar S A 2010 Effects of variation of MRI parameters of signal homogeneity: A Qualitative analysis for Ferrous Benzoic Xylenol Orange gel *JPMA* **60** 470-73

Niu C J, Foltz W D, Velec M, Moseley J L, Al-Maya A and Brock K K 2012 A novel technique to enable experimental validation of deformable dose accumulation *Med. Phys.* **39** 765-76

Olding T and Schreiner L J 2011 Cone-beam optical computed tomography for gel dosimetry II: imaging protocols *Phys. Med. Biol*. **56** 1259-79

Oliveira L N D, Calcina C S G, Cavalcante F, Almeida A D and Almeida C E D 2009 6 MV wedge photon beam profiles with the fricke xylenol gel dosimeter *Braz. J. Phys.* **39** 615-18

Olsson L E, Fransson A, Ericsson A and Mattsson S 1990 MR imaging of absorbed dose distribution for radiotherapy using ferrous sulfate gels *Phys. Med. Biol*. **35** 1623-31

Schreiner L J 2004 Review of Fricke gel dosimeters *J. Phys. 3rd Int. Conf. on Radiotherapy Gel Dosimetry* pp 9-21

Schreiner L J, Crooks I, Evans M D C, Keller B M and Parker W A 1994 Imaging of HDR brackytherapy dose distributions using NRM Fricke gelatin dosimetry *Magn. Reson. Imag*. **12** 901-7

Silva P P, Cuerra W, Silveria J N, Ferreira A M D C, Bortolotto T, Fischer F L, Terenzi H, Neves A and Pereira-Maia E C 2011 Two new ternary complexes of copper(II) with tetracycline or doxycycline and 1,10-phenanthroline and their potential as antitumoral : cytotoxicity and DNA cleavage *Inorg. Chem*. **50** 6414-24

Wang B H and Campbell G 2009 Formulations of polyvinyl alcohol cryogel that mimic the biomedical properties of soft tissues in the natural lumbar intervertebral disc *Spine* **34** 2745-53

Yeo U J, Taylor M L, Dunn L, Kron T, Smith R L and Franich R D 2012 A novel methodology for 3D deformable dosimetry *Med. Phys.* **39** 2203-13

Chapter 3

Paper II – Measurement of superficial dose distributions in radiation therapy using translucent cryogel dosimeters

Molham M Eyadeh, Marcin Wierzbicki and Kevin R Diamond

Department of Medical Physics and Applied Radiation Sciences, McMaster University and Juravinski Cancer Centre, 699 Concession St, Hamilton, ON, L8V 5C2, Canada

A version of this manuscript was submitted to Biomedical Physics & Engineering Express

3.0.1 Introduction to Paper II

Chu *et al.* (2000) suggested that PVA cryogel-based dosimeters may be employed as bolus for skin dose surface evaluation, without further investigation. This paper examines the ability of radiochromic bolus to monitor 2D surface dose distributions at superficial sites being treated using high energy photons in radiotherapy. The cryogels wrap easily around curved regions of the body compared to film and TLDs. 0.5 cm thick cryogels were used in place of bolus to perform *in vivo* dosimetry in regions where surface dose is important. IMRT radiation treatment fields were delivered to the head and neck region of a RANDO phantom. The radiochromic bolus samples were imaged using a charge coupled device (CCD) camera with a red light source in order to provide the highest sensitivity. In this manuscript, we proposed a method that generated a calibration factor to convert the dose measured using the 0.5 cm radiochromic bolus to the skin surface dose (which was estimated using Gafchromic EBT-2 film placed under the bolus). The proof-of-principle *in vivo* dosimetry IMRT measurements suggested that the radiochromic bolus may provide an accurate estimation of surface dose distribution using a simple single correction factor, and therefore, the radiochromic bolus may be used for skin surface dose evaluation purpose.

The experiments and analysis presented in this paper were performed by the author of this thesis under the supervision of Dr. Diamond. The manuscript was written by the author of this thesis and edited by Dr. Diamond and Dr. Wierzbicki. The manuscript has been changed slightly to conform to the style of the thesis.

3.0.2 Content of Paper II

3.1 Abstract

In external beam radiation therapy, skin dose measurement is important to evaluate dose coverage of superficial target volumes (Hsu *et al.* 2008). Treatment planning systems (TPSs) are often inaccurate in this region of the patient, so *in vivo* measurements are necessary for skin surface dose estimation (Fraass *et al.* 1989, Qi *et al.* 2009, Kry *et al.* 2011). Superficial dose distributions were measured using radiochromic translucent poly(vinyl alcohol) cryogels. The cryogels simultaneously served as bolus material, enabling *in vivo* dosimetry in regions where the surface dose was of interest. The relationship between skin surface and bolus doses was established using a series of oblique irradiations with gantry angles ranging from 0° to 90°. Gafchromic film was placed under the bolus to allow the computation of bolus-film dose ratios that ranged from 0.749 ± 0.005 to 0.930 ± 0.002 for 0° and 90° gantry angle, respectively. A single factor of 0.80 was used as the derived calibration factor to convert dose in bolus to dose to the skin surface. The calibration factor was used to estimate skin dose from head and neck intensity modulated radiation therapy (IMRT) treatments delivered to a RANDO phantom. The resulting dose distributions were compared to film using gamma analysis with a 3%/3mm tolerance and a 10% threshold. The minimum gamma pass rate was 95.2**%** suggesting that the radiochromic bolus may provide an accurate estimation of skin surface dose using a simple calibration factor. This study demonstrates the suitability of radiochromic cryogels for superficial dose measurements in megavoltge photon beams.

3.2 Introduction

In external beam radiation therapy, the dose deposited at the skin surface by megavoltage photons may be substantially lower than the underlying tissues due to a lack of electronic equilibrium. However, treatment of superficial disease, such as skin lesions or shallow lymph nodes, requires that the prescribed dose be delivered up to the skin surface. A layer of bolus may be placed on the skin to increase electron fluence, increasing the dose deposited in the superficial tissues (Moyer *et al.* 1983, Chang *et al.* 1992, Bentel 1996, Higgins *et al.* 2007, Khan 2010, Vyas *et al.* 2013). Other factors influencing the surface dose distribution include electron contamination from the linear accelerator, obliquity, field size, beam modifiers, air gap, and delivery technique (Biggs and Ling 1979, Pettit *et al.* 1983, Gerbi *et al.* 1987, Lamb and Blake 1998, Zhu and Palta 1998, Yang *et al.* 2004, Medina *et al.* 2005, Hsu *et al.* 2008). Accurate knowledge of dose to superficial tissues is necessary to ensure that shallow targets receive the prescribed dose while the dose to normal tissue is within tolerance (Lee *et al.* 2002, Jin *et al.* 2008). However, this is confounded due to the inaccuracy of most TPSs in the buildup region (Fraass *et al.* 1989).

Modern radiotherapy TPSs are able to calculate skin dose within ± 25% (Mutic and Low 2000, Dogan and Glasgow 2003, Chung *et al.* 2005, Court *et al.* 2008, Panettierei *et al.* 2009, Kry *et al.* 2011). Most TPSs estimate skin surface dose by extrapolating measured data with fitting functions (Chow *et al.* 2006, Device *et al.* 2006). Monte Carlo simulation is capable of calculating the dose in the buildup region accurately (Rogers *et al* 1995, Liu *et al.* 1997, Scalchi *et al.* 2005) but the use of these systems is limited in

the clinic due to the computational requirements (Qi *et al.* 2009). Therefore, *in vivo* measurements are desirable to verify the skin surface dose.

Several dosimeters are currently used in radiotherapy for surface skin dose estimation. Thermoluminescent detectors (TLDs) (Stathakis *et al.* 2006, Hsu *et al.* 2008, Kinhikar *et al.* 2009, Kry *et al.* 2011, Khanal *et al.* 2015), diodes (Yorke *et al.* 2005, Chan *et al.* 2006), and metal oxide semiconductor field effect transistors (MOSFETs) (Quach *et al.* 2000, Xiang *et al.* 2007, Qi *et al.* 2009, Falco *et al.* 2015) may be used to produce low resolution surface dose distributions. Radiographic or radiochromic film may be used to quantify the distribution of surface dose in two dimensions (Cheung *et al.* 2002, Chiu-Tsao and Chan 2010, Nakano *et al.* 2012, Morales *et al.* 2014). Radiochromic film has several advantages, such as tissue equivalency, self development, and high spatial resolution (Saur *et al.* 2009). However, film is difficult to form to surfaces that contain both convex and concave regions, which complicates dosimetry (Nakano *et al.* 2012). In these situations, a more flexible material is desirable.

Gel dosimeters can be used to measure absorbed dose distributions (Olsson *et al.* 1998). This is especially important for dosimetry of IMRT and stereotactic radiosurgery, where small fields and steep dose gradients exist (Ibbott 2006, Baldock *et al.* 2010, Adliene *et al.* 2014). Gel dosimeters such as cryogels are flexible and can easily conform to the skin over large, complex, curved regions. Furthermore, as suggested by Chu *et al.* (2000) without further investigation, poly(vinyl alcohol) cryogels (PVA-C) based dosimeters may be simultaneously employed as a dosimetric bolus. PVA-C is flexible and stable at 37 ^{o}C, and, when loaded with a radiosensitive material such as ferrous benzoic xylenol orange (FBX), is capable of recording dose in two and three

dimensions (Chu *et al.* 2000, Hill *et al.* 2002). Employing PVA-C based dosimeters as bolus has not received much attention in the literature.

The dose estimated using TPS at depths of 0.5 to 1.0 cm lacks the accuracy typically desired for radiotherapy targets. Thus, a dosimetric bolus material would be useful in simultaneously increasing dose to superficial targets and in ensuring these areas receive the prescribed dose. For megavoltage photon beams, the dose increases up to 60% within the first 0.5 cm depth, making the measured surface dose sensitive to the buildup thickness (Devic *et al.* 2006, Xiang *et al.* 2007, Qi *et al.* 2009). The requirement for a 0.5 cm thick bolus means that the dose will not be uniform throughout the material, and not equal to the actual surface dose. It may be possible, however, to derive a conversion factor from the dose measured in the gel dosimeter to the surface dose.

Eyadeh *et al.* (2014) described a FBX-PVA-C material that may be used as radiochromic bolus readable in two dimensions using a simple camera system. The material is translucent, allowing visualization of underlying skin marks to assist in patient and beam positioning. The purpose of this work is to evaluate the ability of FBX-PVA-C radiosensitive bolus material to measure skin dose during radiotherapy. The concept is demonstrated using previous patients' IMRT fields delivered to the head and neck region of a RANDO phantom (Phantom Laboratory, Salem, NY, United States).

3.3 Materials and Methods

3.3.1 Translucent FBX PVA-C Dosimeter Preparation

In this study, translucent FBX-PVA-C was used as radiochromic bolus. A detailed description of its production was described elsewhere (Eyadeh *et al.* 2014). Briefly, PVA concentration of 15% by weight was selected to optimize sensitivity, fabrication time, sturdiness, and ease of handling of the finished slabs of bolus.

The main ingredients of the formulation were all acquired from Sigma Aldrich, St. Louis, United States. The components were hydrolyzed PVA (molecular weight 146-188 kD), dimethyl sulfoxide (DMSO), ferrous ammonium sulphate (ammonium iron (II) sulphate hexahydrate), benzoic acid, and xylenol orange (XO) tetrasodium salt. Sulphuric acid of 95-98% purity was also used.

The PVA was dissolved in 25 mM sulphuric acid, water, and DMSO at 120 ^{o}C (70 mL of 20 water/80 DMSO by weight). The hydrogel was cooled to 50 ^{o}C, at which point a 10 mL solution of 0.55 mM ferrous ammonium sulphate, 5 mM benzoic acid, and 1 mM XO tetrasodium salt, all dissolved in 25 mM sulphuric acid, was added to the hydrogel. A solution of 25 mM sulphuric acid water/ DMSO was stirred in during the final 10 minutes to make up the desired total volume (100 mL). The mixture was then evacuated for 15 minutes to remove any visible air bubbles.

The hydrogel was decanted into custom plastic moulds with interior dimensions of 15 x 15 cm^2 and 0.5 cm thickness. The hydrogels were subjected to 3 cycles of 18 hour freezing at -80 ^{o}C and 6 hours thawing at room temperature (*i.e.* the moulds were allowed to thaw for 6 hours at room temperature after 18 hours of freezing at -80 ^{o}C). The finished cryogels were removed from their moulds and cut to size as necessary. To

ensure the uniformity of the cryogel samples, the homogeneity was studied by comparing the light transmission through different locations of the sample.

3.3.2 Radiochromic Bolus Read out Apparatus

The radiochromic bolus samples were imaged pre-and post-irradiation using the equipment shown in figure 3.1. A template was used to ensure reproducible placement of the radiochromic bolus. The apparatus was composed of a 1392 x 1024 pixel charged coupled device (CCD) camera (Nikon Corporation, Tokyo, Japan), a 28-105 mm, f/1.4-5.6, UC-II zoom lens (Sigma Corporation, Fukushima, Japan), a Lumen-Essence BK-600 uniform red LED array (620 – 645 nm bandwidth, Luminus Devices Inc., Billerica, MA, United States), and a light tight box. The linearity of the CCD was verified prior to use. A dark field was acquired at the start of each experiment and subtracted from all acquired images. The lens was focused on the centre of the radiochromic bolus. Images collected by the 16-bit CCD were stored as “Tiff gray image file”. Noise in the CCD images was reduced through post-processing; pre- and post-irradiation images were registered using a template that attached to the LED light source. Based on the CCD images, 2D absorption coefficient maps were computed using in house Matlab code (MathWorks Inc., Natick, MA, United States). All measurements and irradiations were performed at room temperature; post-irradiation imaging was performed two hours after irradiation.

Figure 3.1. In house 2D optical imaging apparatus. The lens is 61 cm away from the LED array, and the light box is 15.5 x 15.5 cm^2.

3.3.3 Calibration of Radiochromic Bolus and Film

The relationship between bolus absorption coefficient and delivered dose was established using a Varian iX linear accelerator (Varian Inc., Palo Alto, United States) with 6 MV photons and 20 x 20 cm^2 field size. The 0.5 cm thick samples of 7 x 7 cm^2 radiochromic bolus were sandwiched at isocentre between two 5.6 cm slabs of polystyrene. Doses ranging from 100 to 4000 cGy were applied with a dose rate of 633 cGy/min. The expected doses in cGy for this arrangement were computed using the Pinnacle v9.2 TPS (Philips, Amsterdam, Netherlands).

The same procedure was employed to relate optical density and dose in 7 x 7 cm^2 pieces of EBT-2 Gafchromic film (lot #A052810-01) [International Specialty Products, Wayne, New Jersey, United States]. 6 MV photons and a 20 x 20 cm^2 field size were used. Doses ranging from 100 to 1500 cGy were applied with a dose rate of 633 cGy/min (corresponding to machine settings of 600 MU/min). The expected doses in the film were also computed with the Pinnacle 9.2. As described later, film was used as the gold standard measurement of skin dose.

The process of film marking, read out, and analysis was consistent with the manufacturer's recommendations. EBT-2 film was also read prior to irradiation to obtain the background optical density; the net optical density of each irradiated film was obtained by subtracting the background optical density. The EBT-2 film was scanned using an Epson 11000XL Scanner (Proscan, Avision, Australia) and analyzed using Film QA^{TM} Pro (Ashland, Wayne, New Jersey, United States). The red channel data were used during film analysis at a resolution of 150 DPI; color correction was disabled. All films were read out approximately 24 hours after their irradiation. Calibration irradiations and subsequent read out were performed at room temperature. Subsequent comparisons of radiochromic bolus and film were also performed in the Film QA software suite.

3.3.4 Calibration of Radiochromic Bolus for Skin Surface Dosimetry

Open field irradiations with normal and oblique incidence were used to examine the relationship between the dose distribution recorded by the radiochromic bolus and the

true surface dose, which was estimated using EBT-2 film. The configuration of these measurements is shown in figure 3.2. A 0.5 cm thick, 7 x 7 cm^2 radiochromic bolus sample and 7 x 7 cm^2 piece of EBT-2 film were stacked on the surface of a 10.4 cm slab of polysterne. The film was positioned at isocentre, 100 cm away from the source. The irradiation was repeated with gantry angles of 0º, 22.5º, 45º, 67.5º, and 90º. At each angle, a 3 x 3 cm^2 field was formed using the jaw collimator and 1000 monitor units (MU) were delivered with a dose rate of 600 MU/min. This was also planned in Pinnacle to compute the surface dose distribution.

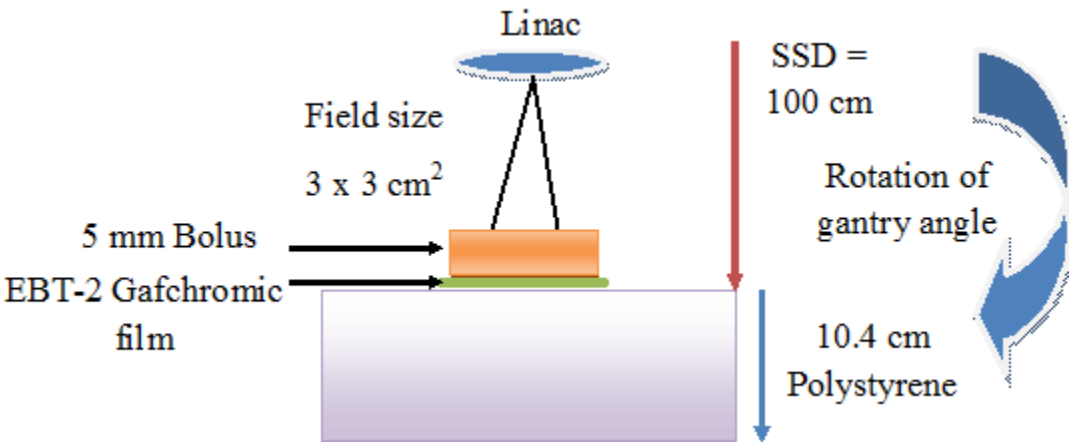

Figure 3.2. Schematic of the radiochromic bolus and EBT-2 film irradiation. A 3 x 3 cm^2 field was formed using the jaw collimator and 1000 MU were delivered with a rate of 600 MU/min. The procedure was repeated with gantry rotations ranging from 0º to 90º.

Optical density and absorption coefficient, measured in film and bolus, respectively, were converted to doses using the respective calibration curves. Finally, the ratio

between the film and radiochromic bolus dose distributions was obtained to serve as a calibration factor for scaling radiochromic bolus dose to dose on the skin surface.

3.3.5 Validation of Skin Surface Dosimetry Using Radiochromic Bolus

A Philips Brilliance Big Bore scanner was used to acquire 1 mm thick CT slices of the head and neck portion of a RANDO phantom. The CT data were exported to Pinnacle 9.2. Two simple static parallel-opposed-pair (POP) beam arrangements were planned for the neck region; two previously treated clinical cases with bolus including a 3-field larynx and a 9-field head and neck IMRT were selected and positioned on the RANDO data to approximate the arrangement on the patient. The use of the TPS in this part of the study was to locate and contour custom bolus for the various field arrangements: virtual bolus was drawn on the RANDO CT images to approximate the shape and size of the clinically used bolus material. These plans were then delivered to the phantom with EBT-2 film placed on the phantom surface below a layer of 0.5 cm radiochromic bolus to evaluate the skin surface dose directly under bolus. The bolus was manually cut to size on the phantom surface using orthogonal light field projections as a guide.

The two tangential POP static beams (0^o / 180^o and 90^o / 270^o) were delivered to the 0.5 cm radiochromic bolus and film stack on the surface of the RANDO phantom. The POP static beam arrangements consisted of 3 x 3 cm^2 open fields delivered to the neck with 6 MV photons and 250 MU with a rate of 600 MU/min. Figure 3.3 shows the placement of the radiochromic bolus for the static POP, as well as the two clinical beam arrangements.

The two clinical step-and-shoot IMRT plans were delivered as closely to the original planned conditions as possible. The larynx treatment included three step-and-shoot fields, with a total of 276 MU delivered at 400 MU/min. The head and neck treatment employed nine fields to deliver multiple dose levels to superficial disease and various neck nodes with total of 593 MU at 400 MU/min.

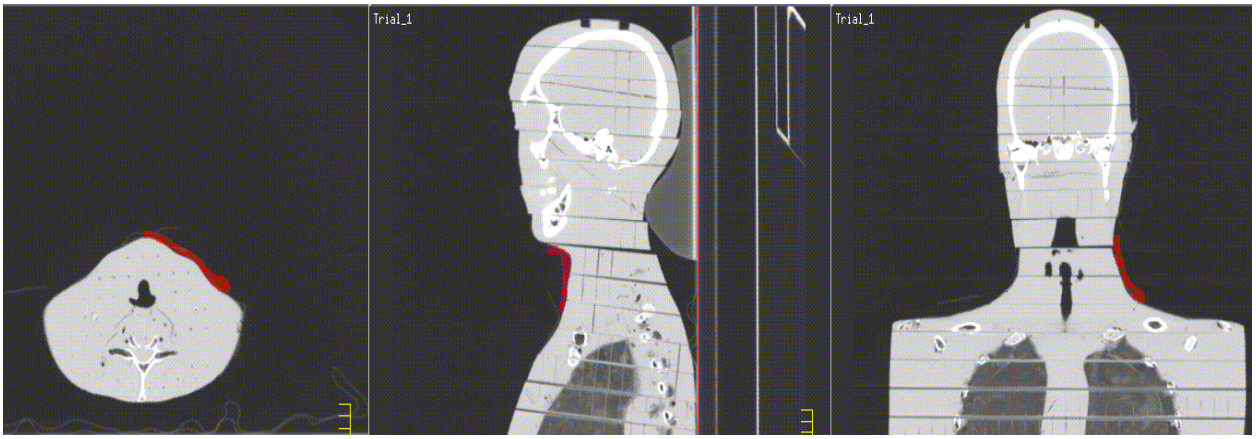

Figure 3.3. An example of radiochromic bolus definition for and AP/PA opposed pair. The bolus is 0.5 cm thick.

3.4 Results and Discussion

3.4.1 Calibration of radiochromic bolus for skin surface dosimetry

The relationship between absorption coefficient and dose delivered to the 0.5 cm slabs of radiochromic bolus in its linear range was (3.00 ± 0.04) $x10^{-4}$ mm^{-1} cGy^{-1}, which is consistent with our previous measurements (Eyadeh *et al.* 2014). The calibration curve was used to translate attenuation coefficient measured in radiochromic bolus to dose deposited in the bolus. A similar calibration curve was acquired for the Gafchromic film.

Figure 3.4 shows the irradiated radiochromic bolus and EBT-2 film with 1000 MU at gantry angles of 0, 45, and 90^{o}.

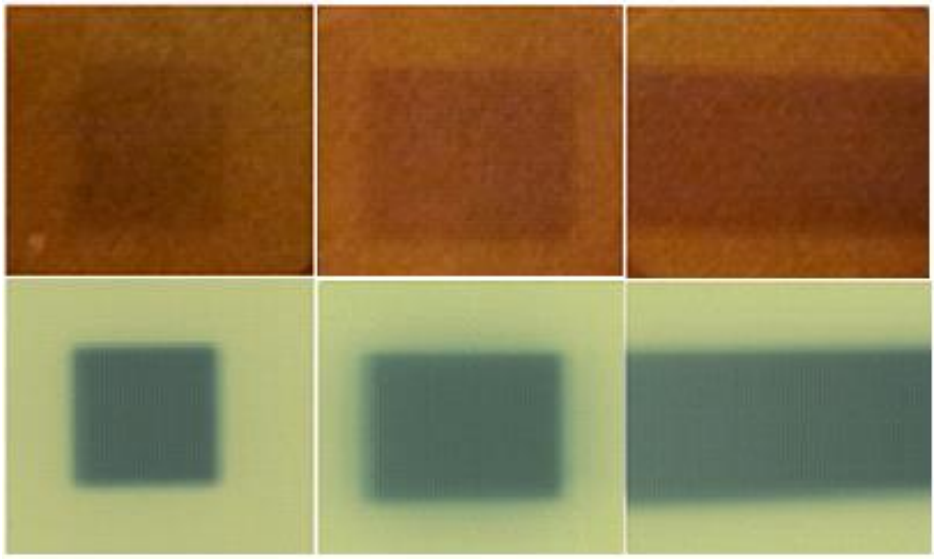

Figure 3.4. Photographs of irradiated radiochromic bolus and EBT-2 film arising from the configuration shown in figure 3.2: gantry angles of 0, 45, and 90^{o} from left to right.

Measurements correlating the dose distribution in bolus to the expected distribution at the underlying surface (estimated using Gafchromic EBT-2 film) indicated that dose increased with gantry angle. Dose increases because beam enters obliquely and has depth to build up. This is consistent with previous investigations that reported increasing surface doses with incident beam angles with a rapid increase beyond about 45^{o} incidence (Rinker and Grussel 1987, Lin *et al.* 2001, Hsu *et al.* 2008).

Film QA Pro software was used to visually align the radiochromic bolus and film dose maps. The point-by-point ratio was computed from these aligned images and shown in figure 3.5. The mean ratios for the irradiated areas (highlighted with a box) are summarized in Table 3.1. The goal of measuring these ratios was to develop a simple

approach to convert dose in bolus to dose on skin. To simplify, a single correction factor of 0.80 that is independent of the gantry angle was computed. This was done empirically, by minimizing the differences between the film and the calibrated bolus doses for all gantry angles. This factor was used to calibrate all subsequent bolus images. A calibration factor for normal incidence can be estimated by integrating over the percent depth dose (PDD) data and dividing by the dose at the underlying surface (in this case, depth 0.5 cm). For the linear accelerator used in this study, the estimated dose ratio was 0.739, which agrees well with the measured value of 0.749 ± 0.005.

a) b)

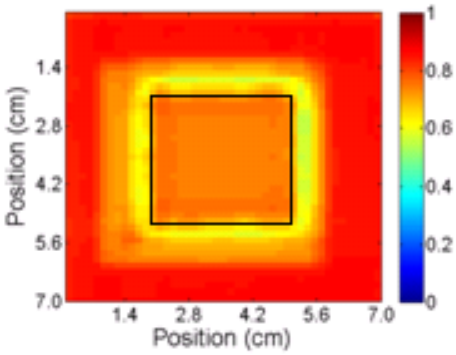

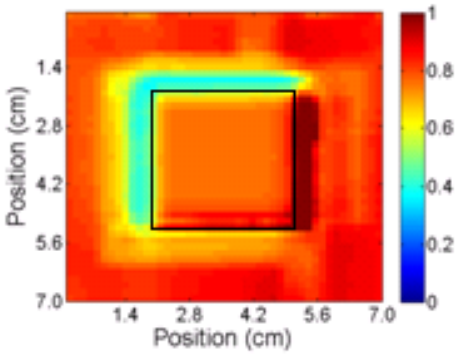

c) d)

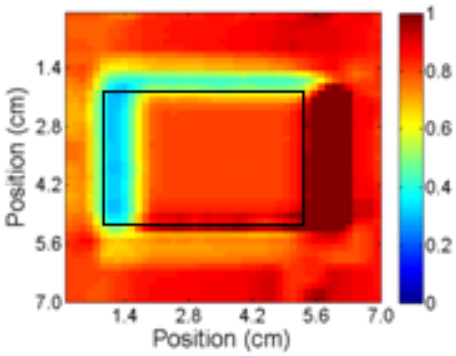

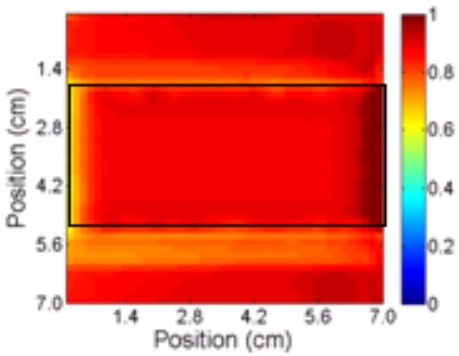

e)

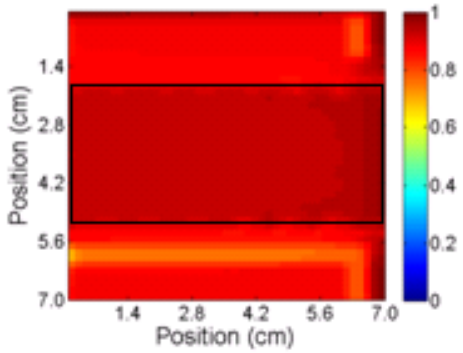

Figure 3.5. The ratio of the measured dose distribution in a radiochromic bolus to the surface dose distribution estimated using Gafchromic EBT-2 film for gantry angles of a) 0 ,b) 22.5, c) 45, d) 67.5, and e) 90^{o}. The irradiated area regions of interest(ROI) are included.

Table 3.1. The mean ratio between surface dose and the dose measured in the radiochromic bolus at different gantry angles ranging from 0 to 90^{o}.

Gantry angle (deg)	Mean ratio ± Standard deviation
0	0.749 ± 0.005
22.5	0.760 ± 0.005
45	0.802 ± 0.009
67.5	0.890 ± 0.016
90	0.930 ± 0.002

The central inline (y-axis) and cross line (x-axis) of absolute dose distributions were found for 0 and 90^{o} gantry angles in Gafchromic film, radiochromic bolus, calibrated radiochromic bolus using derived scaling factor of 0.80, and those computed using the TPS at the surface. Figure 3.6 shows the central cross line profiles; figure 3.7 shows the central in line profiles corresponding to figure 3.6.

a)

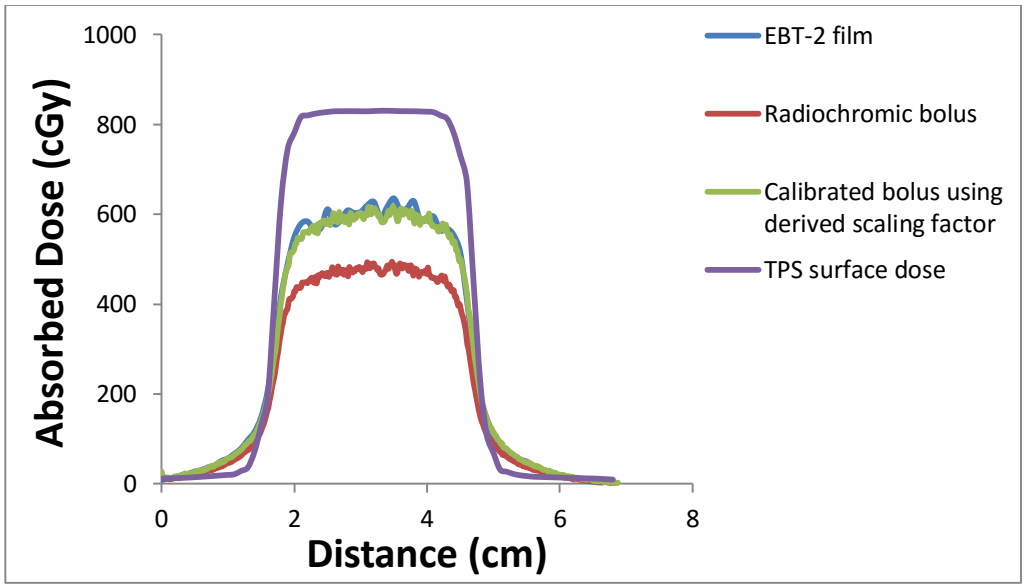

b)

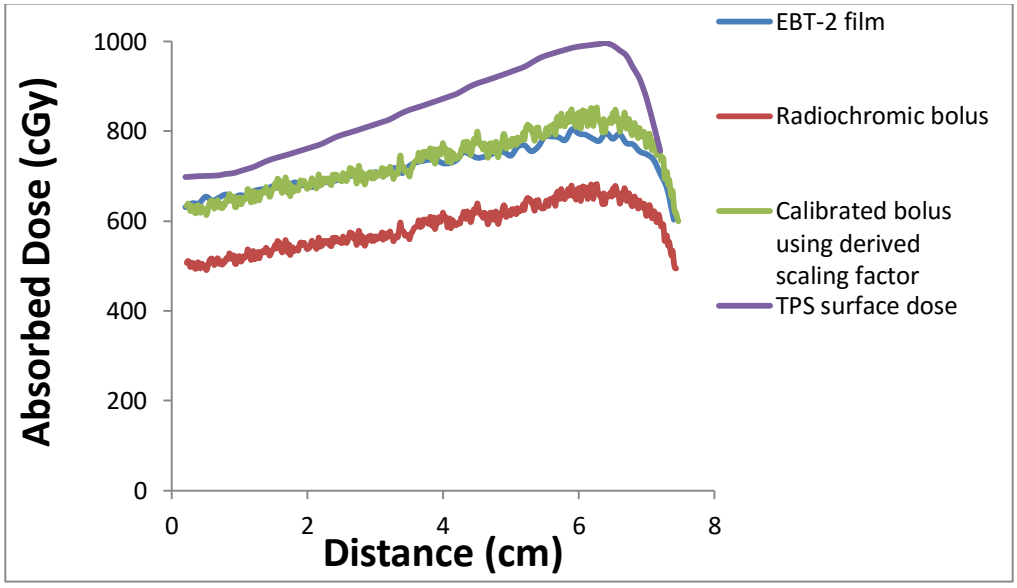

Figure 3.6. Cross line profiles (x-axis) of absolute dose distributions extracted from Gafchromic film, radiochromic bolus, calibrated radiochromic bolus using derived scaling factor of 0.80, and TPS surface dose for a) 0 and b) 90^{o} gantry angles.

a)

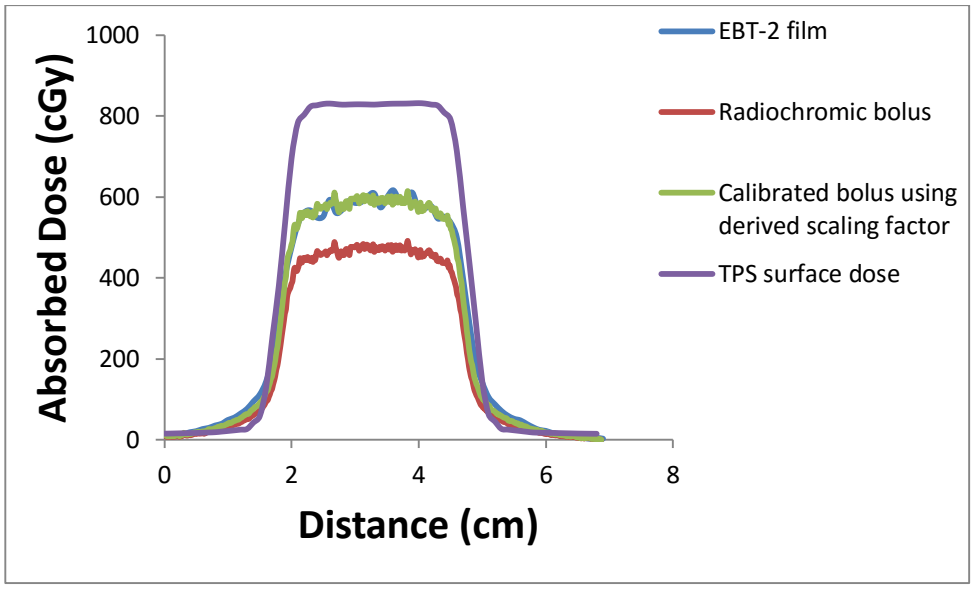

b)

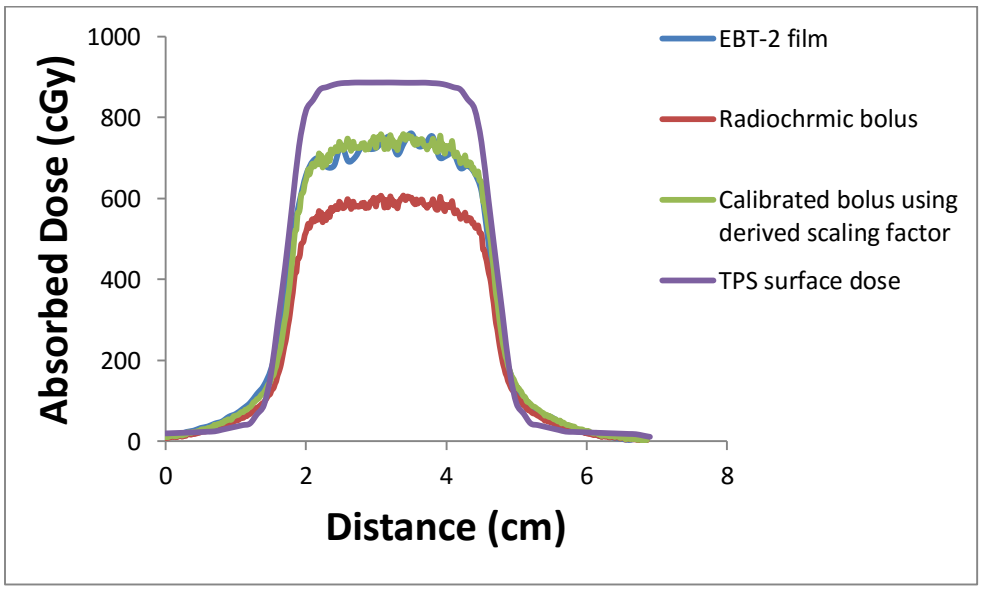

Figure 3.7. Inline profiles (y-axis) of absolute dose distributions extracted from Gafchromic film, radiochromic bolus, calibrated radiochromic bolus using derived scaling factor of 0.80, and TPS surface dose for a) 0 and b) 90^{o} gantry angles.

For all gantry angles cases, the maximum difference between absorbed doses in film and TPS computation ranged from 14.3 to 25.6% overestimate depending on the gantry angle. This was consistent with related studies with various dosimeters; Dogan and Glasgow (2003) observed that the TPS overestimated surface dose by 25% compared to a parallel plate ion chamber measurement. Chung *et al.* (2005) reported that two TPSs overestimated surface dose by up to 18.5% when compared to Gafchromic film measurements. Court *et al.* (2008) showed that the agreement between TPS calculated skin surface dose was within 20% of doses measured using MOSFETs. Kry *et al*. (2011) reported an overall 22% difference surface dose between TPS and TLDs.

Using the calibration factor of 0.80 allowed us to match the absolute dose distributions measured using radiochromic bolus with the skin dose distribution measured using Gafchromic film. Good agreement in central and cross line profiles between the calibrated bolus and Gafchromic film was observed, with average differences ranging from 1.4 to 1.9%. This suggests that a 0.5 cm radiochromic cryogel should be able to predict dose deposited at the bolus-skin interface. Even though the irradiation geometry was quite simple, it was dosimetrically more challenging than realistic treatment geometries where exit dose from some beams may help to mitigate the large differences in buildup seen due to beam obliquity.

3.4.2 Validation of Skin Surface Dosimetry Using Radiochromic Bolus

The calibration factor of 0.80 was applied to the radiochromic bolus measurements for the four treatment plans. Figure 3.8 compares the absolute dose distributions of the

POP beams measured using calibrated radiochromic bolus and film. The larynx is shown in figure 3.9, and the neck is shown in figure 3.10.

a)

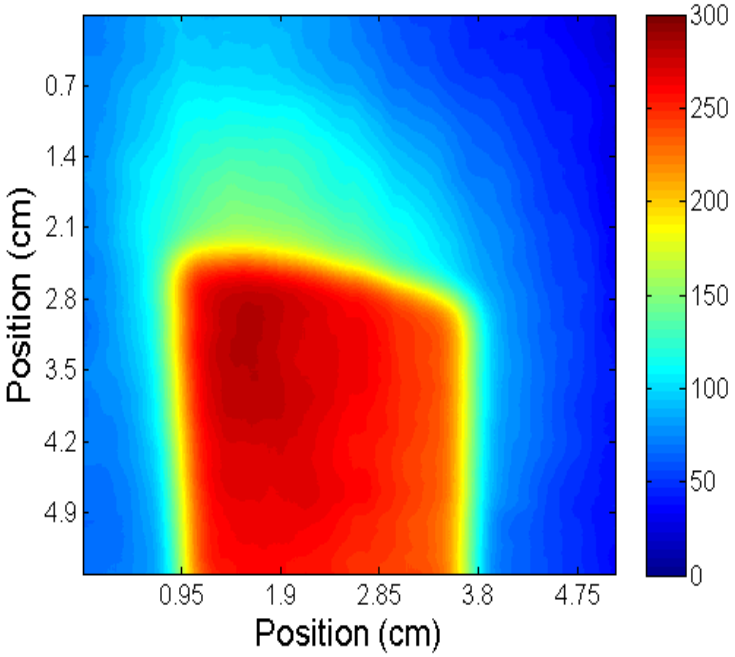
Position (cm)
0.7
1.4
2.1
2.8
3.5
4.2
4.9
0.95
1.9
2.85
3.8
4.75
Position (cm)
300
250
200
150
100
50
0

b)

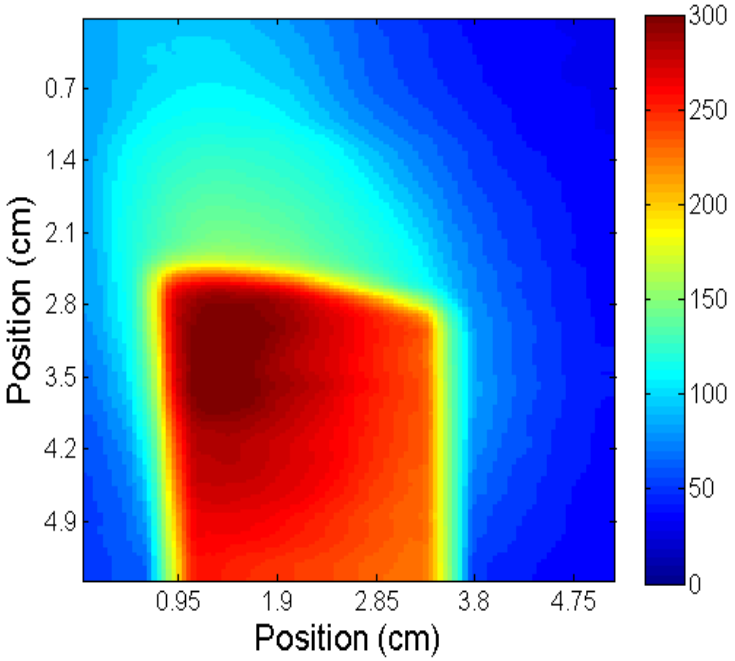
Position (cm)
0.7
1.4
2.1
2.8
3.5
4.2
4.9
0.95
1.9
2.85
3.8
4.75
Position (cm)
300
250
200
150
100
50
0

c)

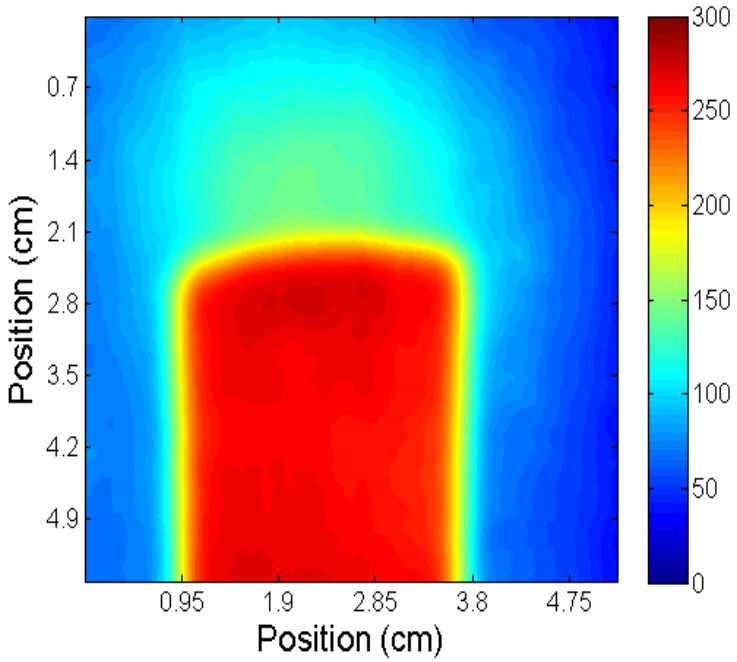
Position (cm)
0.7
1.4
2.1
2.8
3.5
4.2
4.9
0.95
1.9
2.85
3.8
4.75
Position (cm)
300
250
200
150
100
50
0

d)

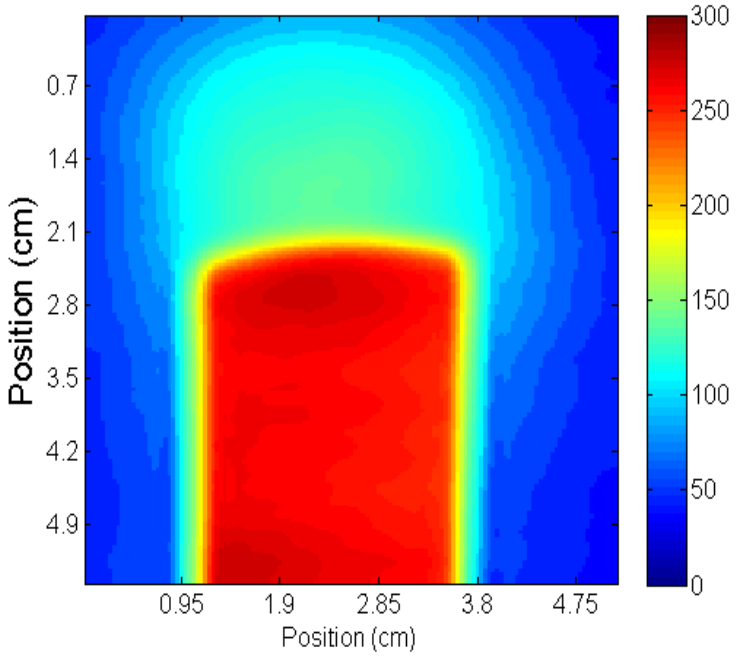
Position (cm)
0.7
1.4
2.1
2.8
3.5
4.2
4.9
0.95
1.9
2.85
3.8
4.75
Position (cm)
300
250
200
150
100
50
0

Figure 3.8. Absorbed dose in cGy from calibrated measured radiochromic bolus (a,c) and the measured Gafchromic EBT-2 film (b,d) for two tangential POP static beams of (0^o / 180^o) and (90^o / 270^o) respectively.

a)

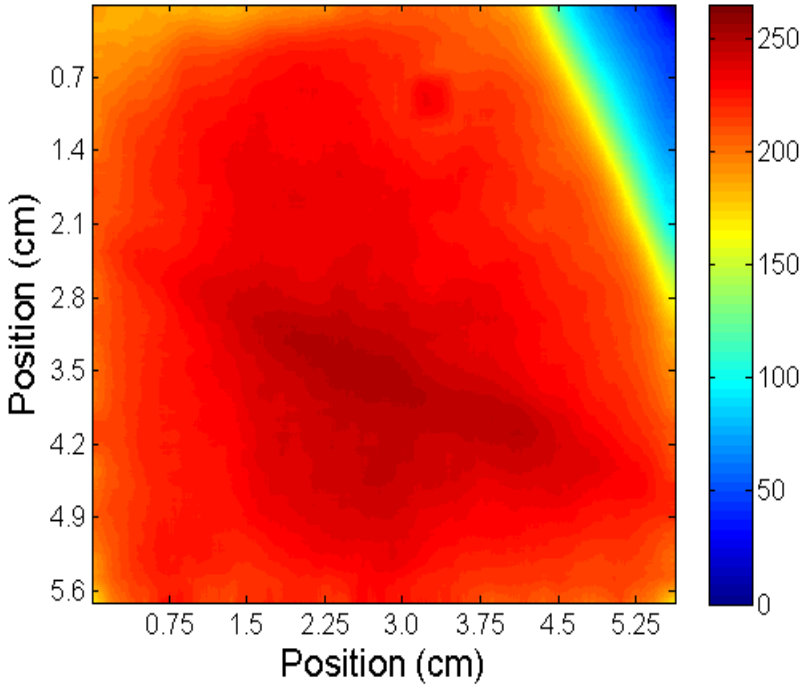
Position (cm)
0.7
1.4
2.1
2.8
3.5
4.2
4.9
5.6
0.75
1.5
2.25
3.0
3.75
4.5
5.25
Position (cm)
250
200
150
100
50
0

b)

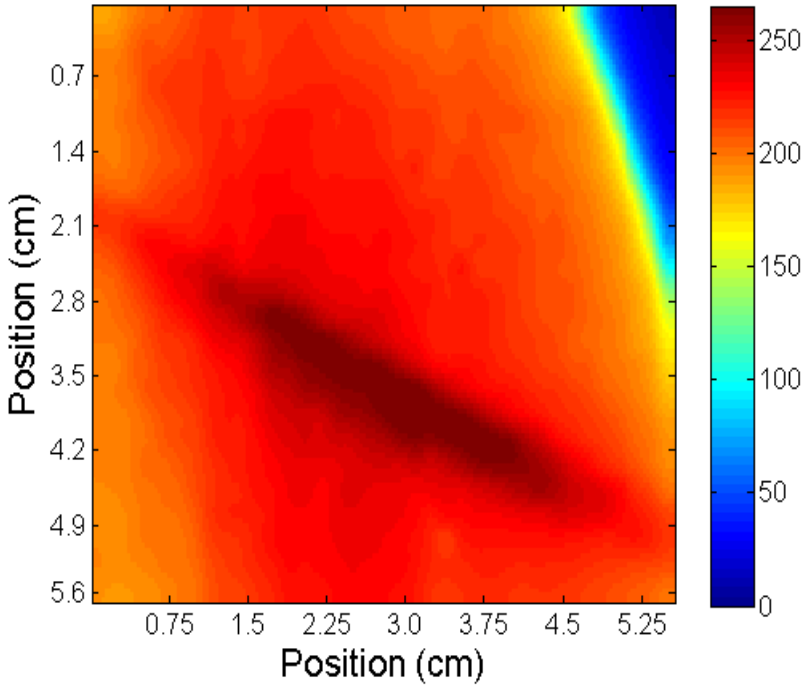
Position (cm)
0.7
1.4
2.1
2.8
3.5
4.2
4.9
5.6
0.75
1.5
2.25
3.0
3.75
4.5
5.25
Position (cm)
250
200
150
100
50
0

Figure 3. 9. Absorbed dose in cGy from calibrated measured radiochromic bolus (panel a) and the measured Gafchromic EBT-2 film (panel b) for step-and-shoot IMRT larynx treatment.

a)

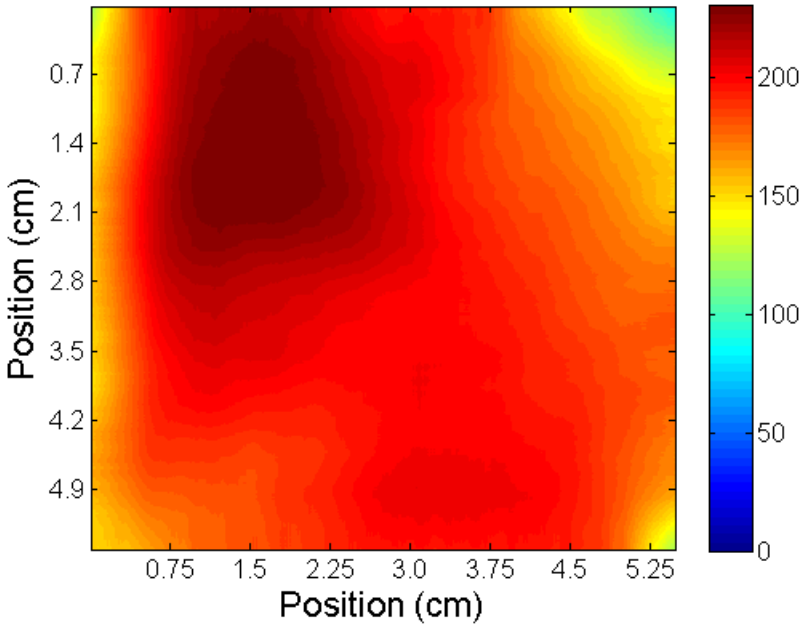

b)

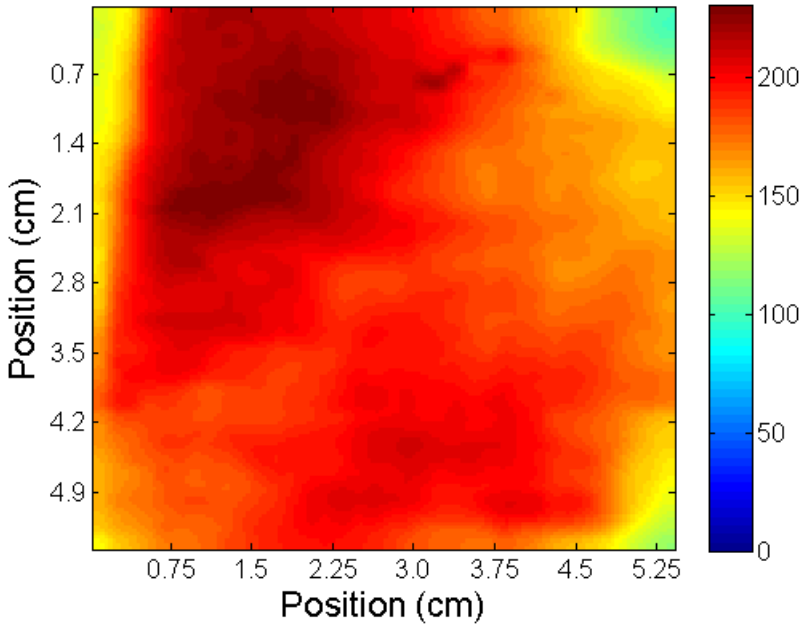

Figure 3.10. Absorbed dose in cGy from calibrated measured radiochromic bolus (panel a) and the measured Gafchromic EBT-2 film (panel b) for step-and-shoot IMRT neck treatment.

Gamma analysis is typically used to judge the agreement between treatment plans and dose measurements (Low *et al.* 1998). In our study, it was used to evaluate the agreement between the calibrated radiochromic bolus and EBT-2 film (*i.e.* comparing independent measurements to one another). A 2D gamma analysis was performed using the Film QA Pro software using 3%/3mm criteria and a 10% dose threshold. The percentage of pixels passing *versus* the total numer of tested pixels ranged from 95.2 to 96.4% as shown in Table 3.2.

Table 3.2. Gamma pass rates for comparisons of calibrated radiochromic bolus and EBT-2 Gafchromic film (3%/3mm, 10% threshold) for different field arrangements.

Irradiation Geometry	Gamma passing rate (%)
0^o / 180^o POP, static beams	96.1
90^o / 270^o POP, static beams	96.4
3-field beams larynx, IMRT	95.2
9-field beams neck, IMRT	95.5

The above results suggest that the radiochromic bolus measures skin dose with sufficient accuracy for clinical use. The disagreement between calibrated bolus and film is around the level of uncertainity in film dosimetry, optically simulated luminescence detectors (OSL), and ionization chambers (Buston *et al.* 1999, Quach *et al.* 2000, Devic *et al.* 2006, Schembri and Heijmen 2007, Nakano *et al.* 2012, Morales *et al.* 2014, Louwe *et al.* 2015).

Furthermore, the FBX PVA-C material is more flexible than film, providing improved skin contact. It can be wrapped easily around curved surfaces and provide *in vivo* dosimetry in areas where skin dose quantification is desired. Finally, our system employs a simple calibration process and one correction factor for accurate skin dose estimation.

3.5 Conclusion

Skin dosimetry is an important aspect in radiotherapy of superficial targets considering that treatment planning systems are inaccurate in this region of the patient. A comparison of EBT-2 Gafchromic film and FBX-PVA-C radiochromic bolus suggests that the latter may provide an accurate estimation of skin surface dose distribution using a simple correction factor. Radiochromic bolus can then be used in place of more traditional forms of bolus to perform *in vivo* dosimetry in regions where the skin dose is important. The main advantage of this system over film is that it is more flexible, allowing it to be wrapped around complex curved surfaces. It may be possible to improve agreement between radiochromic bolus and EBT-2 film using a more complex, angle dependent correction scheme, but this may overcomplicate the dose estimation process. In this study, the dose distributions recorded in the calibrated cryogels and film were not compared with the Pinnacle skin dose, as this requires projecting a flattened 2D dose image onto the original 3D surface. It may be necessary to evaluate the calibration factor for different parts of the body. For example, quantifying skin dose in tangential irradiation of the chest wall, where the beams are quite oblique to the skin surface. However, we feel that it is feasible to use a radiochromic cryogel as an *in vivo* dosimeter to evaluate superficial dose distributions.

Acknowledgment

This work has been supported by the NSERC Discovery Grant program and the Yarmouk University Physics Department.

References

Adliene D, Jakstas K and Vaiciunaite N 2014 Application of optical methods for dose evaluation in normoxic polyacrylamide gels irradiated at two different geometries *Nucl. Instru. Meth. Phys.* **741** 88-94

Baldock C. De Deene Y, Doran S, Ibbott G, Jirasek A, Lepage M and Schreiner L J 2010 Polymer gel dosimetry *Phys. Med. Biol.* **55** R1-R63

Bentel G C 1996 *Radiation therapy planning* vol 162 (New York: McGraw-Hill).

Biggs P J and Ling C C 1979 Electrons as the cause of the observed d_{max} shift with field size in high energy photon beams *Med. Phys.* **6** 291-95

Buston M J, Yu P K N and Metcalfe P E 1999 Extrapolated surface dose measurements with radiochromic film *Med. Phys.* **26** 485-88

Chan M, Song Y, Meli J, Huang Y and Burman C 2006 TU-FF-A1-02: Estimating Dose to ICD outside the Treatment Fields Using Skin QED Diode *Med. Phys.* **33** 2218-2218

Chang F, Chang P and Benson K 1992 Study of Elasto-Gel pads used as surface bolus material in high energy photon and electron therapy *Int. J. Radiat. Oncol. Biol. Phys.* **22** 191-92

Cheung T, Buston M J and Yu P Y N 2002 Multilayer Gafchromic film detectors for breast skin dose determination in vivo *Phys. Med. Biol.***47** N31-N37

Chiu-Tsao S T and Chan M F 2010 Evaluation of two-dimensional bolus effect of immobilization/support devices on skin doses: A radiochromic EBT film dosimetry study in phantom *Med. Phys*. **37** 3611-20

Chow J, Grigorov G and Branett R 2006 Study on surface dose generated in prostate intensity-modulated radiation therapy treatment *Med. Dosim.* **31** 249-58

Chu K C, Jordan K J, Battista J J, Van Dyk J and Rutt B K 2000 Polyvinyl alcohol-Fricke hydrogel and cryogel: two new gel dosimetry systems with low Fe^{+3} diffusion *Phys. Med. Biol.* **45** 955-69

Chung H, Jin H, Dempsey J F, Liu C, Palta J, Suh T S and Kim S 2005 Evaluation of surface and build-up region dose for intensity modulated radiation therapy in head and neck cancer *Med. Phys.* **32** 2682-89

Court L E, Tishler R B, Xiang H, Allen A M, Makrigiorgos M and Chin L 2008 Experimental evaluation of the accuracy of skin dose calculation of a commercial treatment planning system *J. Appl. Clin. Med. Phys.* **9** 29-35

Devic S, Seuntjens J, Abdel-Rahman W, Evans M, Olivares M, Podgorsa E B, Vuong Té and Soares C G 2006 Accurate skin dose measurements using radiochromic film in clinical applications *Med. Phys.* **33** 1116-24

Dogan N and Glasgow G P 2003 Surface and build-up region dosimetry for obliquely incident intensity modulated radiotherapy 6 MV x rays *Med. Phys.* **30** 3091-96

Eyadeh M M, Farrell T J and Diamond K R 2014 Evaluation of a ferrous benzoic xylenol orange transparent PVA cryogel radiochromic dosimeter *Phys. Med. Biol*. **59** 1773-87

Falco M D, Masala S, Stefanini M, Fiori R, Gandini R, Bagalà P, Morosetti D, Calabria E, Tonnetti A, Verona-Rinati G, Santoni R and Simonetti G 2015 Patient skin dose measurements using a cable free system MOSFETs based in fluoroscopically guided percutaneous vertebroplasty, percutaneous disc decompression, radiofrequency medial branch neurolysis, and endovascular critical limb ischemia *J. Appl. Clin. Med. Phys*. **16** 298-10

Fraass B, Doppke k, Hunt M, Kutcher G, Starkschall G, Stern R and Van Dyke J 1998 American Association of Physicists in Medicine Radiation Therapy Committee Task Group 53:quality assurance for clinical radiotherapy treatment planning *Med. Phys.* **25** 1173-822

Gerbi B J, Meigooni A S and Khan F M 1987 Dose build up for obliquely incident photon beams *Med. Phys.* **14** 393-9

Higgins P D, Han E Y, Yuan J L, Hui S and Lee C K 2007 Evaluation of surface and superficial dose for head and neck treatments using conventional or intensity-modulated techniques *Phys. Med. Biol*. **52** 1135-46

Hill B, Bäck S Å J, Lepage M, Simpson J, Healy B and Baldock C 2002 Investigation and analysis of ferrous sulfate polyvinyl alchohol (PVA) gel dosimeter *Phys. Med. Biol*. **47** 4233-46

Hsu S H, Roberson P L, Chen Y, Marsh R B, Pierce L J and Moran J M 2008 Assessment of skin dose for breast chest wall radiotherapy as a function of bolus material *Phys. Med. Biol.* **53** 2593-06

Ibbott G S 2006 Clinical applications of gel dosimeters *J. Phys. Conf. on Radiotherapy Gel Dosimetry* **56** pp108

Jin H, Palta J, Suh T S, and Kim S 2008 A generalized a priori dose uncertainty model of IMRT delivery *Med. Phys.* **35** 982-96

Khanal S P, Ouhib Z, Benda R K and Leventouri T 2015 Evaluation of surface dose outside the treatment area for five breast cancer irradiation modalities using thermo-luminescent dosimeters *Int. J. Canc. Thera. Oncol.* **3** ISSN 2330-49

Kinhikar R A, Murthy V, Goel V, Tambe C M, Dhote D S and Deshpande D D 2009 Skin dose measurements using MOSFET and TLD for head and neck patients treated with tomotherapy *Appl. Radiat. Isot*. **67** 1683-85

Khan F M 2010 The Physics of Radiation Therapy 4th ed Lippincott Williams & Wilkins, Baltimore, MD, USA.

Kry S F, Smith S A, Weathers R and Stovall M 2011 Skin dose during radiotherapy: a summary and general estimation technique *J. Appl. Clin. Med. Phys.* **13** 20-34

Lamb A and Blake S 1998 Investigation and modeling of the surface dose from linear accelerator produced 6 and 10 MV photon beams *Phys. Med. Biol*. **43** 1133-46

Lee N, Chuang C, Quivey J M, Phillips T L, Akazawa P, Verhey L J and Xia P 2002 Skin toxicity due to intensity-modulated radiotherapy for head-and-neck carcinoma *Int. J. Radiat. Oncol. Biol. Phys.* **53** 630-37

Lin J P, Chu T C, Lin S Y and Liu M T 2001 Skin dose measurement by using ultra thin-TLDs *Appl. Radiat. Isot.* **55** 383-91

Louwe R J, Wendling M, Monshouwer R, Satherley T, Day R A and Greig L 2015 Time-resolved dosimetry using a pinpoint ionization chamber as quality assurance for IMRT and VMAT *Med. Phys*. **42** 1625-39

Low D A, Harms W B, Mutic S and Purdy J A 1998 A technique for the evaluation of dose distributions *Med. Phys*. **25** 656-61

Liu H H, Mackie T R and McCullough E C 1997 A dual source photon beam model used in convolution/superposition dose calculations for clinical megavoltage x-ray beams *Med. Phys.* **24** 1960-74

Medina A L, Teijeiro A, Garcia J, Esperon J, Terron J A, Ruiz D P and Carrion M C 2005 Characterization of electron contamination in megavoltage photon beams *Med. Phys.* **32** 1281-92

Morales J E, Hill R, Crowe S B, Kairn T and Trapp J V 2014 A comparison of surface doses for very small field size x-ray beams: Monte Carlo calculations and radiochromic film measurements *Austra.Phys. Eng. Sci. Medic.* **37** 303-09

Moyer R F, McElroy W R, O'Brien J E and Chamberlain C C 1983 A surface bolus material for high-energy photon and electron therapy *Radiol.* **146** 531-32

Mutic S and Low D A 2000 Superficial doses from serial tomotherapy delivery *Med. Phys.* **27** 163-65

Nakano M, Hill R F, Whitaker M, Kim J H and Kuncic Z 2012 A study of surface dosimetry for breast cancer radiotherapy treatments using Gafchromic EBT2 film *J. Appl. Clinic. Med. Phys*. **13** 3727

Olsson L, Baeck S, Magnussen P and Haraldsson P 1998 3D-Dosimetry using gels and MRI. *Imag. Rad. Ther. AAPM Monograph.* **24** 475-04

Penettierei V, Barsoum P, Westermark M, Brulla L and Lax I 2009 AAA and PBC calculation accuracy in the surface build-up region in tangential beam treatments. Phantom and breast case study with the Monte Carlo code PE-NELOPE *Radiother. Oncol.* **93** 94-01

Pettit P L, Goodman M S, Gabriel T A and Mohan R 1983 Investigation of build up dose from electron contamination of clinical photon beams *Med. Phys.* **10** 18-24

Qi Z Y, Deng X W, Huang S M, Zhang L, He Z C, Li X A, Kwan L, Lerch M, Cutajar D, Metcalfe P and Rosenfeld A 2009 In vivo verification of superficial dose for head and neck treatments using intensity-modulated techniques *Med. Phys*. **36** 59-70

Quach K Y, Morales J, Buston M J, Rosenfeld A B and Metcalfe P E 2000 Measurement of radiotherapy skin dose x-ray skin dose on a chest wall phantom *Med. Phys.* **27** 1676-80

Rinker G and Grussel E 1987 Patient dose measurements in photon fields by means of silicon semiconductor detectors *Med. Phys.* **14** 870-73

Rogers D W O, Faddegon B A, Ding G X, Ma C M, Wei J, and Mackie T R 1995 BEAM: A Monte Carlo Code to simulate radiotherapy treatment units *Med. Phys.* **22** 503-24

Saur S, Fjellsboe L M B, Lindmo T and Frengen J 2009 Contralateral breast doses measured by film dosimetry: tangential techniques and an optimized IMRT technique *Phys. Med. Biol*. **54** 4743 -58

Scalchi P, Francescon P and Rajaguru P 2005 Characterization of a new MOSFET detector configuration for in vivo skin dosimetry *Med. Phys.* **32** 1571-78

Schembri V and Heijmen B J M 2007 Optically stimulated luminescence (OSL) of carbon-doped aluminum oxide (Al2O3: C) for film dosimetry in radiotherapy *Med. Phys.* **34** 2113-18

Stathakis J S, Li K, Paskalev J, Yang L, Wang and Ma C M 2006 Ultra thin TLDs for skin dose determination in high energy photon beams *Phys. Med. Biol*. **51** 3549-67

Vyas V, Palmer L, Mudge R, Jiang, R, Fleck, A, Schaly B and Charland P 2013 On bolus for megavoltage photon and electron radiation therapy *Med.Dosim.***38** 268-73

Xiang H F, Song J S, Chin D W, Cormack R A, Tishler R B, Makrigiorgos G M and Chin L M 2007 Build-up and surface dose measurements on phantoms using micro-MOSFET in 6 and 10MV x-ray beams and comparisons with Monte Carlo calculations *Med. Phys.* **34** 1266-73

Yang J, Li J S, Qin L, Xiong W and Ma C M 2004 Modelling of electron contamination in clinical photon beams for Monte Carlo dose calculations *phys. Med. Biol*. **49** 2657-73

Yokoyama S, Roberson P L, Litzenberg D W, Moran J M and Fraass B A 2004 Surface build dose dependence on photon field delivery technique for IMRT *J. Appl. Clin. Med. Phys.* **5** 71-81

Yorke E, Alecu R, Ding L, Fontenla D, Kalend A, Kaurin D, Masterson-McGary M E, Marinello G, Matzen T, Saini A, Shi J, Simon W, Zhu T C, Zhu X R, Rikner G and Nilsson G 2005 Diode in vivo dosimetry for patients receiving external beam radiation therapy: Report of Task group 62 of the AAPM Radiation Therapy Committee AAPM Report **87** *Med. Phys. Publish.* Madison, WI

Zhu T C and Palta J R 1998 Electron contamination in 8 and 18 MV photon beams *Med. Phys*. **25** 12-9

Chapter 4

Paper III – Translucent poly(vinyl alcohol) cryogel dosimeters for simultaneous dose build up and monitoring during chest wall radiation therapy

Molham M Eyadeh, Mark A Weston, Janos Juhasz and Kevin R Diamond

Department of Medical Physics and Applied Radiation Sciences, McMaster University and Juravinski Cancer Centre, 699 Concession St, Hamilton, ON, L8V 5C2, Canada

A version of this manuscript was submitted to the Journal of Applied Clinical Medical Physics

4.0.1 Introduction to Paper III

The following paper employs the radiochromic bolus developed in paper II to evaluate setup errors and uncertainties in chest wall position for patients performing deep inspiration breath hold (DIBH). Measurements were conducted on the chest wall region of a RANDO phantom using forward planned tangential IMRT fields delivered at the planned position and at small anterior/posterior (A/P) shifts from the planned position (±2 mm, ±3 mm, and ± 5 mm). Two dimensional absolute dose maps at the planned position were compared with doses at all shifts for the radiochromic cryogels (measurements to measurements), and Pinnacle dose surfaces (calculation to calculation). The Pinnacle dose planes were computed using the skin surface and mid-cryogel for all A/P shifts.

The results of this study showed that cryogels may be used for simultaneous dose build up and monitoring during chest wall radiotherapy. The cryogels were capable of detecting A/P positioning errors of 3 mm, which may be enable the quantification of potentially clinically relevant errors.

The experiments and analysis presented in this paper were performed by the author of this thesis under the supervision of Dr. Diamond. The manuscript was written by the author of this thesis and edited by Dr. Diamond; Dr. Juhasz, and Dr Weston. The manuscript has been changed slightly to conform to the style of the thesis.

4.0.2 Content of Paper III

4.1 Abstract

Chest wall radiotherapy under deep inspiration breath-hold (DIBH) was monitored using a 5 mm thick radiochromic poly(vinyl alcohol) cryogel that also provided build up material. The cryogels were used to detect positioning errors and measure the impact of shifts for a chest wall treatment that was delivered to a RANDO phantom. The phantom was shifted by ±2, ±3, and ±5 mm from the planned position in the anterior/posterior (A/P) direction; these shifts represent setup errors and the uncertainty associated with lung filling during DIBH. The two dimensional absolute dose distributions measured in the cryogel at the planned position were compared with the distributions at all shifts from this position using gamma analysis (3%/3 mm, 10% threshold). For shifts of ±2, ±3, and ±5 mm the passing rates ranged from 94.3% to 95.6%, 74.0% to 78.8%, and 17.5% to 22.5%, respectively. These results are consistent with the same gamma analysis performed on dose planes calculated in the middle of the cryogel and on the phantom surface using our treatment planning system, which ranged from 94.3% to 95.0%, 76.8% to 77.9%, and 23.5% to 24.3%, respectively. The results of this study suggest that cryogels may be used as both a build up material and to evaluate errors in chest wall treatment positioning during deep inspiration breath hold delivery. The cryogels are sensitive to A/P chest wall shifts of less than 3 mm, which potentially allows for the detection of clinically relevant errors.

4.2 Introduction

The organs of the cardiopulmonary system are at risk during radiation therapy of the thorax. Previous studies have shown a strong correlation between the irradiated cardiac volume with cardiac mortality (Gagliardi *et al*. 1996, Gyenes *et al*. 1998), and the irradiated lung volume associated with functional lung damage (Gagliardi *et al*. 2000, Ooi *et a*l. 2000). Meta analyses have shown cardiac deaths following breast radiotherapy are associated with the volume of the heart receiving dose in excess of 5 Gy (Clarke *et al*. 2005). Cardiac toxicity may be exacerbated during radiation therapy to the left breast or chest wall (Recht 2006) Thus, there is a desire to balance the dose delivered to the clinical target volume (CTV) and dose to the healthy organs at risk (OAR) (Bentzen *et al*. 2001, Shah *et al*. 2014).

Patients receiving mastectomies often receive adjuvant radiotherapy to reduce their risk of local recurrence and in turn this improves long term survival (Whelan *et al*. 2000, Vin-Hung *et al*. 2002, Darby *et al*. 2011, Rudat *et al.* 2011, Swamy *et al.* 2014). Radiation therapy of the chest wall is typically delivered by using photon beams and three dimensional conformal radiation radiotherapy or forward planned intensity modulated radiation therapy (IMRT) (Al-Rahbi *et al.* 2013, Fassi *et al.* 2014, Mansouri *et al.* 2014).

The dose delivered by these techniques may be affected by respiratory motion of the thorax during treatment (Korreman *et al.* 2005, Månsson *et al.* 2005, Latty *et al.* 2015) These movements may be accounted for using breathing adapted radiotherapy (BART) techniques such as respiratory gating, breath hold (BH), and deep inspiration breath hold (DIBH) (Ohara *et al.* 1989, Wong *et al.* 1999, Pedersen *et al*. 2004, Prabhakar *et*

al. 2007, Korreman *et al.* 2005, Fassi *et al*. 2014, Shah *et al.* 2014, Latty *et al.* 2015). DIBH is a technique used in the treatment of left sided breast cancer that allows for cardiac sparing by increasing the distance between the chest wall target and heart. During DIBH, the patient takes a deep breath and holds it during CT simulation and subsequently during treatment; the treatment is delivered as long as the chest wall remains within a certain range of positions, usually 5 – 10 mm, which is tracked using an external fiducial on the thorax or abdomen with accuracy up to 2 mm. The implementation of DIBH is managed by instructing the patient to hold their breath during the treatment; the resulting doses delivered to the cardiac and pulmonary volumes are reduced when compared with free-breathing (Hanley *et al.* 1999, Sixel *et al.* 2001, Remouchamps *et al.* 2003, Fassi *et al*. 2014, Latty *et al.* 2015). Different BH methods have been used, such as the spirometry-based active breathing coordinator (ABC) system (Elekta, Stockholm, Sweden) and the video-based real-time position management (RPM) system (Varian Medical Systems, Palo Alto, CA). Both systems are viable options for delivery of a DIBH treatment (Hanley *et al.* 1999, Sixel *et al.* 2001, Remouchamps *et al.* 2003, Fassi *et al*. 2014, Latty *et al.* 2015). The dosimetric effect of DIBH depends on patient anatomy, lung capacity, and pulmonary function (Latty *et al.* 2015).

The dose to the heart may also be reduced using techniques such as IMRT or volumetric modulated arc therapy (VMAT). The DIBH-IMRT decreases the maximum dose to the heart for left sided patients compared with DIBH three dimensional conformal radiation radiotherapy, but the treatment time is often much longer (Rudat *et al.* 2011, Fassi *et al.* 2014, Mansouri *et al.* 2014). With VMAT, the target coverage is

improved with substantial reduction in treatment time (Swamy *et al.* 2014). Given the level of modulation in these types of treatment fields, all uncertainties and setup errors should be well understood in order to limit the potential risk of geographical misses leading to the under dosing of the target tissues and/or overdosing of healthy tissues (Saliou *et al.* 2005): positioning uncertainties and breathing motions can introduce a significant deviation between planned and delivered dose distribution (Mavroidis *et al.* 2002). The typical maximum uncertainties/set up errors involved in left breast and chest wall treatment in the A/P direction (vertical chest wall excursion over the treatment duration) have been reported to be as large as 5 mm. Patient-induced chest wall shifts of a similar magnitude during DIBH have also been reported (Mitine *et al.* 1991, Van Tienhoven *et al.* 1991, Westbrook *et al.* 1991, Gagliardi *et al.* 1992, Creutzberg *et al.* 1993, Lirette *et al.* 1995, Fein *et al.* 1996, Pouliot *et al.* 1996, Hurkmans *et al.* 2001, Mavroidis *et al.* 2002, Pedersen *et al.* 2004, Korrreman *et al.* 2005, Korrreman *et al.* 2006, Alderliesten *et al.* 2013, Fassi *et al.* 2014, Brouwers *et al.* 2015).

A variety of dosimetric systems are used currently during radiotherapy for dose verification purposes, including thermoluminescent detectors (TLDs) (Sathakis *et al.* 2006, Hsu *et al.* 2008, Kinhikar *et al.* 2009, Kry *et al.* 2011, Khanal *et al.* 2015), metal oxide semiconductor field effect transistors (MOSFETs) (Quach *et al.* 2000, Xiang *et al.* 2007, Falco *et al.* 2015), and radiographic or radiochromic film (Chiu-Tsao et al. 2010, Nakano *et al.* 2012, Morales *et al.* 2014). An alternative approach would be to use gel dosimeters (Chu *et al.* 2000)

In principle, dosimetric gels such as cryogels may be used as both a build up material and to act as an *in vivo* dosimeter to monitor the treatment delivery (Chu *et al.* 2000). In

regions where the surface dose is of interest, a dosimetric gel may provide an accurate estimation of superficial dose distributions (Eyadeh *et al.* 2015). Dosimetric gels may also be used to quantify setup uncertainties or breathing irregularities during left breast or chest wall DIBH radiation therapy. Build up materials are often used for chest wall radiation therapy to deliver the full prescribed dose up to the target tissue surface (Hsu *et al.* 2008), where the typical thicknesses of build up used for megavoltage photon beams range from 5-10 mm, depending on in house practices (Frass *et al.* 1998).

The purpose of the work presented here is to use a translucent poly(vinyl alcohol) cryogel (PVA-C) containing ferrous benzoic xylenol orange (FBX) (Eyadeh *et al.* 2014) to provide build up and to monitor treatment delivery. The concept is demonstrated using radiation treatment fields delivered to the left chest wall region of a RANDO phantom (Phantom Laboratory, Salem, NY, United States). To simulate setup errors in chest wall position during DIBH, irradiations were conducted at both the planned position and with minimal A/P shifts.

4.3 Materials and Methods

4.3.1 Treatment Planning System and Dose Delivery

CT images of the RANDO phantom with a cryogel placed over the chest area (5 mm thick piece 15 x 15 cm^2) were acquired with a 3 mm slice thickness (Brilliance Big Bore, Philips Radiation Oncology Systems). The CT data set was exported to our radiation treatment planning system (Pinnacle 9.2, Phillips Radiation Oncology Systems) to generate a forward planned IMRT tangential chest wall treatment plan using a 10 x 10 cm^2 6 MV photon beams, at angles of $140^o/314^o$, with no collimator or couch rotation

segmented fields. Dose evaluation surfaces were defined in Pinnacle at the chest wall surface and in the centre of the cryogel as part of a planning study; the procedure is described below. An 8 x 12 mm^2 reference beam was included in the plan outside of the irradiated region to act as a registration point. A prescribed dose of 1000 cGy was planned for delivery to the surface of the chest wall. Figure 4.1 shows the treatment planning parameters used in this study.

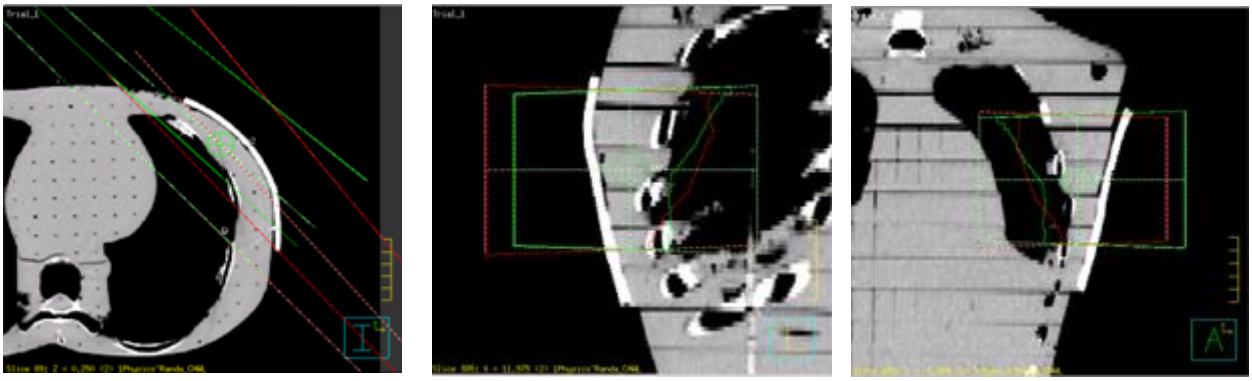

Figure 4.1 Treatment planning used in this study. Three plan view of the two tangential beam arrangments.

The treatment was delivered using a Varian TrueBeam™ STx linear accelerator and the A/P shifts were performed using the PerfectPitch 6 degree-of-freedom couch, which has a resolution of 0.1 mm (Varian Inc., Palo Alto, CA, United States). In addition to delivering the treatment at the correct position, the couch height was adjusted so that the phantom was shifted A/P by ±2 mm, ±3 mm, and ±5 mm to simulate errors in chest wall position during treatment.

4.3.2 Planar Dose Calculation Using Dose Evaluation Surfaces

Two dimensional dose maps were generated using Pinnacle's planar dose calculation tool. The dose evaluation surfaces were derived in a semi-automated manner. First, the external contour of the physical body, in this case the RANDO phantom, was generated and confined to a bounding region of interest corresponding to the radiochromic cryogel. A contour representing the mid-thickness of the cryogel was generated by expanding the external contour by 2.5 mm (*i.e.* to the centre of the 5 mm thick cryogel) and confining the expansion to the cryogel. The physical coordinates corresponding to the cryogel-RANDO interface, as well as the center of the cryogel, were extracted from the region of interest file (*.roi) and arranged in a manner that was readable by the planar dose calculation utility. These surfaces were used to record the dose delivered in the planned position and with the isocentre shifted by ±2, ±3, and ±5 mm from the planned position in the A/P direction to simulate chest wall positioning errors during DIBH. This planning study was used to establish the minimum required performance of the cryogel dosimeter system.

4.3.3 Radiochromic Cryogel Dosimeter Preparation

The cryogel dosimeter was prepared from a mixture of PVA, water, dimethyl sulfoxide (DMSO), and radiochromic FBX. The mixing procedure has been presented elsewhere (Eyadeh *et al.* 2014), 15% PVA by weight was selected for its reasonable fabrication time, sturdiness, ease of handling, and sensitivity. All chemicals used in the formulation were obtained from Sigma Aldrich (St. Louis, USA). The hydrogel was poured into custom plastic moulds with dimensions of 15 x 15 cm^2 and 5 mm thickness. The

samples were then subjected to 3 freeze-thaw cycles with each cycle consisting of a period of freezing for 18 hours at -80 ^{o}C and 6 hours thawing at room temperature.

4.3.4 Measurement of Cryogel Dosimeter Using a Charged Coupled Device (CCD) Camera Apparatus

Pre and post irradiation scans of the cryogel dosimeter were acquired using the imaging system presented in figure 4.2. The imaging apparatus consists of a CCD camera (Nikon Corporation model 1002584, Tokyo, Japan); a 28-105 mm, f/1.4-5.6, a (UC-II) zoom lens (Sigma Corporation, Fukushima, Japan); and a Lumen-Essence BK-600 uniform red LED array (Luminus Devices Inc., Billerica, MA, United States) housed in a light tight box. The lens was focused onto the centre of the cryogel dosimeter to optimize the resolution; 16-bit tiff gray scale images were obtained. Absorption coefficient maps were generated using an in house Matlab program (MathWorks Inc., Natick, MA, United States) after registering the pre- and post-irradiation images. The CCD camera had a resolution of 1392 X 1024. The pre- and post-irradiation measurements were performed at ambient room temperature. The pre-measurements were acquired 10 minutes before irradiation, and the post measurements were acquired two hours after irradiation.

Figure 4.2. 2D optical imaging apparatus consisting of a diffuse red light surface and a lens coupled CCD. Excess area on the light surface was masked using black construction paper to improve the dynamic range of the system.

4.3.5 Calibration of Cryogel Dosimeter

Translucent cryogel dosimeter samples were irradiated with a 6 MV photon beam at 20 x 20 cm^2 field size. The dose response was measured to establish the relationship between absorption coefficient and dose measured using the cryogel dosimeter. The calibration samples were 5 mm thick with a cross sectional area of 7 x 7 cm^2. Calibrations were performed at isocentre height (1 m source-to-axis distance) with the samples sandwiched between 5.6 cm slabs of polystyrene. Doses ranging from 100 to 4000 cGy were applied with a dose rate of 633 cGy/min (corresponding to a machine

setting of 600 MU/min). The expected doses in the cryogel samples were computed with the treatment planning software.

4.3.6 Two Dimensional Dose Analysis

Gamma analysis was used to judge the agreement between measured and calculated dose planes. Pixels that satisfied the evaluation criteria were assigned a value falling between 0 and 1; failing pixels are represented by values greater than 1 (Low *et al.* 1998). The passing rate represents the percentage of pixels passing compared to the total numer of tested pixels (*i.e.* those pixels above the threshold dose) (Low *et al.* 1998). In our study, gamma analysis was performed to compare planned and A/P shifted dose distributions, either computed with the treatment planning software or delivered to the radiochromic cryogel build up material. All images were aligned using the dose resulting from the 8 x 12 mm² reference beam. The gamma analysis was restricted to the irradiated area excluding the reference beam.

The gamma analysis was performed with the Film QA^{TM} Pro (Ashland, United States) analysis suite using 3%/3 mm criteria and a 10% threshold dose. It is important to emphasize that the dose distributions recorded in the radiochromic cryogels were not compared directly with the Pinnacle dose surfaces: it is challenging to project a flattened 2D dose image onto the original 3D surface and is beyond the intent of this study.

4.4 Results and Discussion

It is reasonable to expect that Pinnacle treatment planning system be able to predict differences between the planned position and with A/P shifts, in spite of any deficiencies

that may exist in the treatment planning beam model. The treatment planning system was used to generate 2D dose planes at the surface of the phantom and in the middle of the cryogel dosimeter. The absolute dose distributions were calculated at seven different A/P positions (0, ±2 mm, ±3 mm, and ±5 mm with respect to the planned treatment). Figure 4.3 shows examples of the absolute dose distributions at the surface of the phantom at different A/P positions (0, +2, -3, and +5 mm).

a) 0 mm

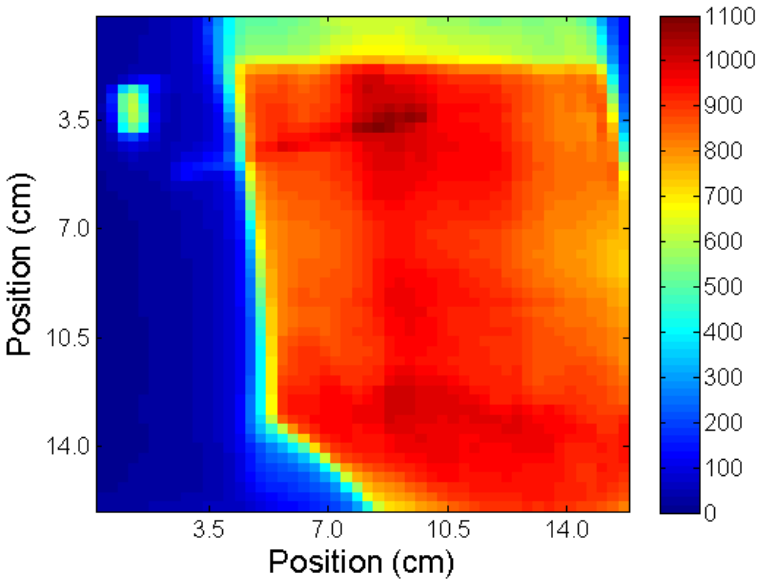
Position (cm)
3.5
7.0
10.5
14.0
Position (cm)
3.5
7.0
10.5
14.0
1100
1000
900
800
700
600
500
400
300
200
100
0

b) +2 mm

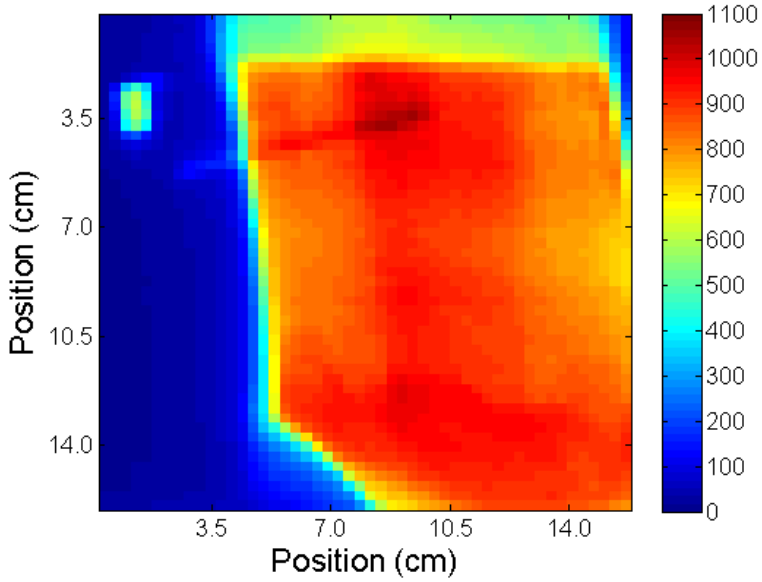
Position (cm)
3.5
7.0
10.5
14.0
Position (cm)
3.5
7.0
10.5
14.0
1100
1000
900
800
700
600
500
400
300
200
100
0

c) -3 mm

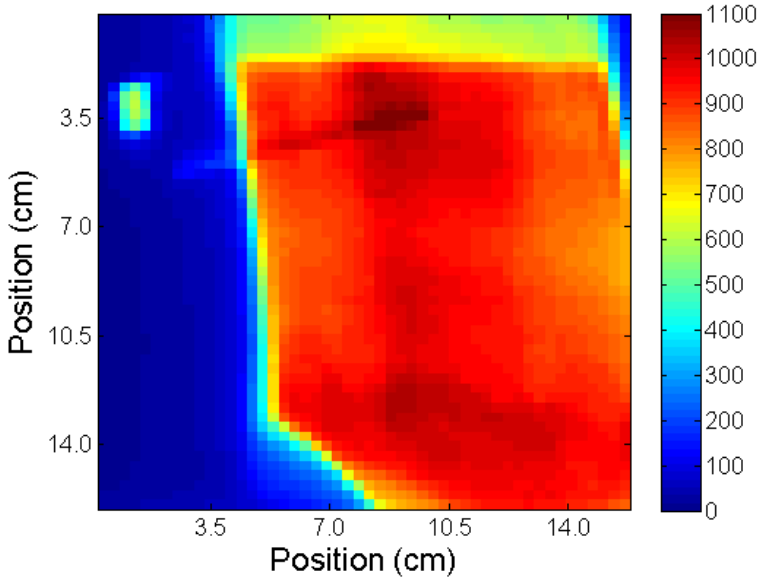

d) +5 mm

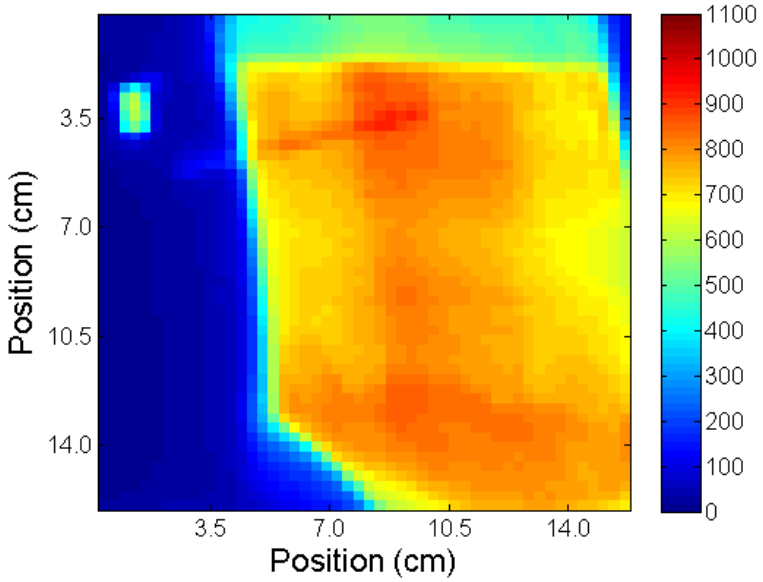

Figure 4.3. Absolute dose distributions maps in cGy calculated in Pinnacle at phantom-cryogel interface at the different A/P positions from the planned position a) 0 mm, b) +2 mm, c) -3 mm, and d) +5 mm.

Figure 4.4 shows examples of the 2D gamma maps at phantom-cryogel interface, at the planned treatment position compared to +2, and -3 mm. The passing rates ranged from 94.3% to 95.0%, 76.8% to 77.9%, and 23.5% to 24.3% at both the middle of cryogel and the surface of the phantom for shifts of ±2, ±3, and ±5 mm. The results of the gamma analysis for both series of Pinnacle dose planes (phantoms surface and middle of cryogel) are summarized in Table 4.1. A 3 mm A/P shift resulted in a gamma pass rate below 80%, suggesting that an unacceptable fraction of the irradiated area at the chest wall surface may have been over or under dosed.

a) +2 mm

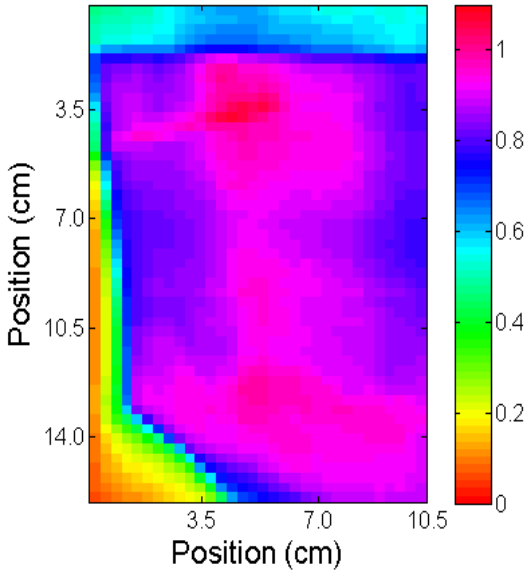

b) -3 mm

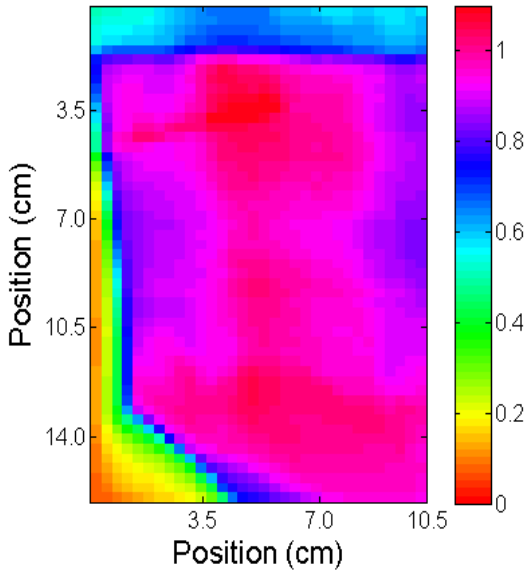

Figure 4.4. 2D gamma maps (3%/3 mm, 10% threshold) that compare absolute dose planes at the phantom-cryogel interface generated in Pinnacle. The dose plane corresponding to the treatment position was compared to (A/P) shifts of a) +2 and b) -3 mm.

Table 4.1. Gamma analyses (3%/3 mm, 10% threshold) passing rate of absolute dose planes created in Pinnacle for all A/P shifts compared to the planned A/P position.

Shift (mm)	Surface of Phantom (%)	Middle of cryogel (%)
-2	95.0	94.7
+2	94.6	94.3
-3	78.9	78.5
+3	77.5	77.1
-5	24.3	24.1
+5	23.8	23.5

The clinical significance of the A/P shifts on the chest wall dose was examined using a simple planning study. The 95% isodose line arising from the planned position was converted in to a volume representing the target tissue. The plan was delivered at the different positions as described above, and the respective 95% isodose volumes compared to the planned “target”. The fraction of the target covered by the shifted 95% isodose levels is shown in figure 4.5 as function of A/P shift. The data suggest that a 3 mm shift results in a reduction in coverage of approximately 7%, which may be considered clinically significant.

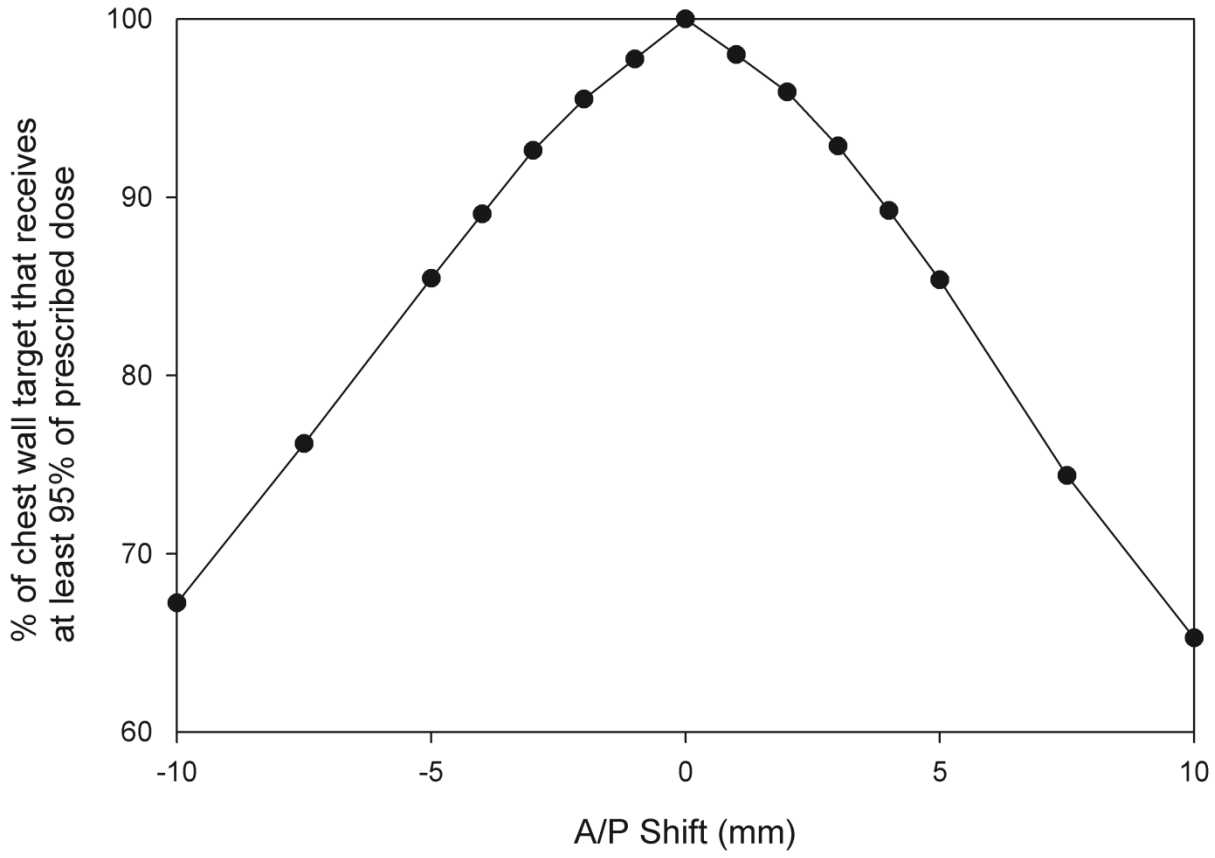

Figure 4.5. The fraction of chest wall target covered by the shifted 95% isodose levels as a function of A/P shift

The cryogel was calibrated under full scatter conditions using 7 x 7 x 0.5 cm^3 samples. The relationship between the measured absorption coefficient and expected dose in the linear range was (3.00±0.04) $x10^{-4}$ mm^{-1} cGy^{-1}, which is consistent with our previous measurements (Eyadeh *et al.* 2014).

The treatment was delivered to the RANDO phantom (with cryogel over the left chest wall) at the planned position and for all of the different A/P offsets (*i.e.* ±2, ±3, and ±5 mm). For each different A/P position the treatment was repeated 3 times, each with an unirradiated cryogel dosimeter. Figure 4.6 shows examples of the absolute dose distributions measured at different A/P positions (0, +2, -3, and +5 mm).

a) 0 mm

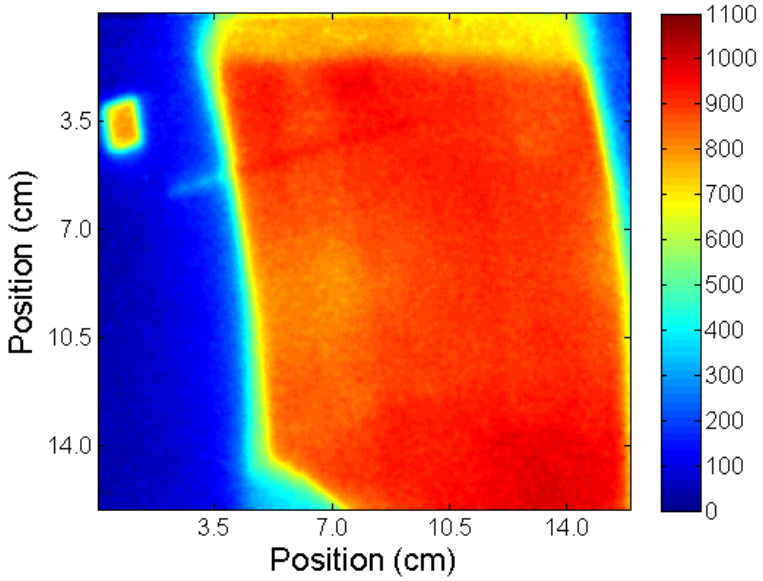
Position (cm)
3.5
7.0
10.5
14.0
Position (cm)
3.5
7.0
10.5
14.0
1100
1000
900
800
700
600
500
400
300
200
100
0

b) + 2 mm

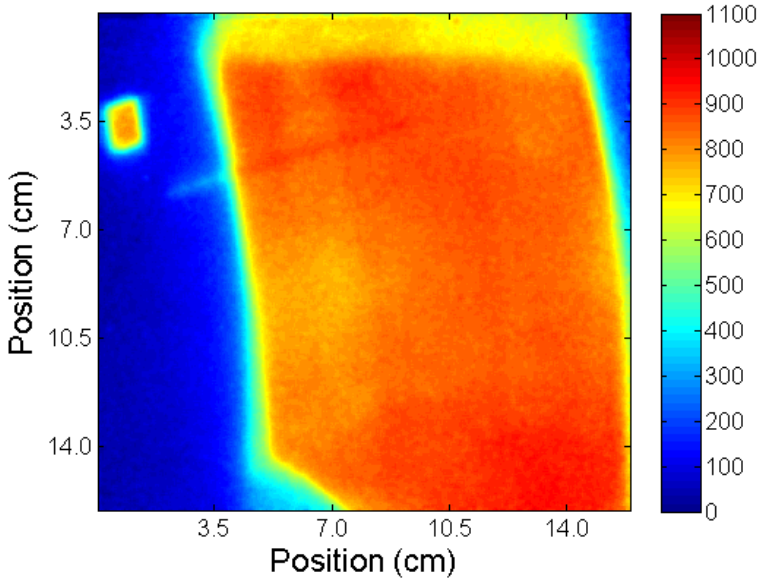
Position (cm)
3.5
7.0
10.5
14.0
Position (cm)
3.5
7.0
10.5
14.0
1100
1000
900
800
700
600
500
400
300
200
100
0

c) - 3 mm

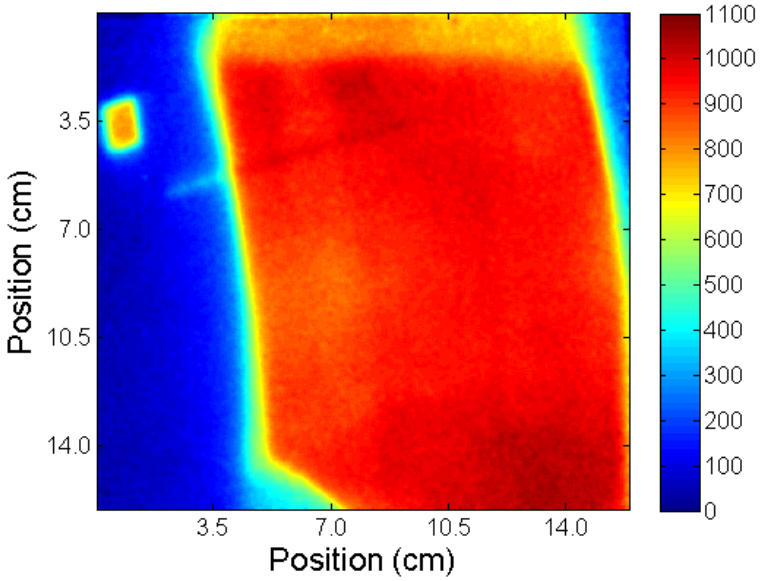

d) + 5 mm

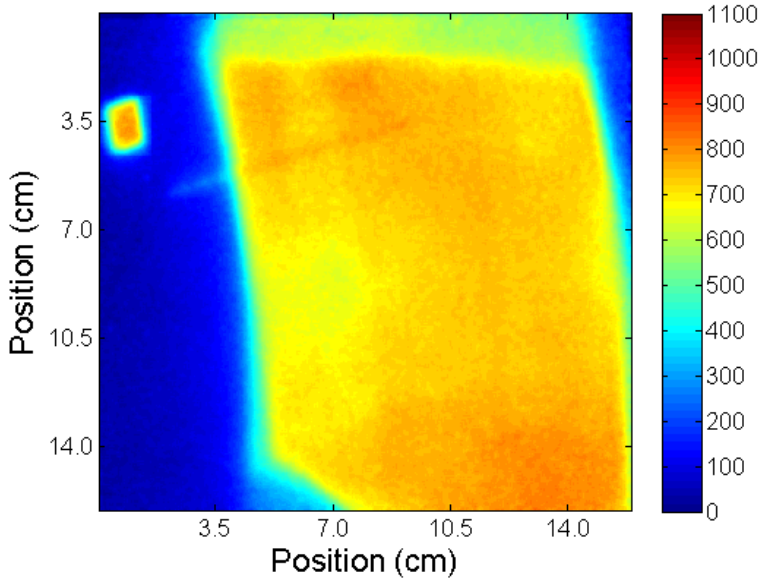

Figure 4.6. Absolute dose distributions maps in cGy measured using the cryogel dosimeter at different A/P shifts from the planned position: a) 0 mm, b) +2 mm, c) -3 mm, and d) +5 mm.

Figure 4.7 shows cross line and inline directions used to extracted profiles for comparison, which are shown in figure 4.8. For the extracted profiles, the average dose difference from the planned treatment position was -2.8, -7.8, and -17.2% for the +2, +3, and +5 mm shifts respectively. Similarly, the average dose difference from the planned treatment position was +2.6, +7.3, and +16.9% for the -2, -3, and -5 mm shifts respectively.

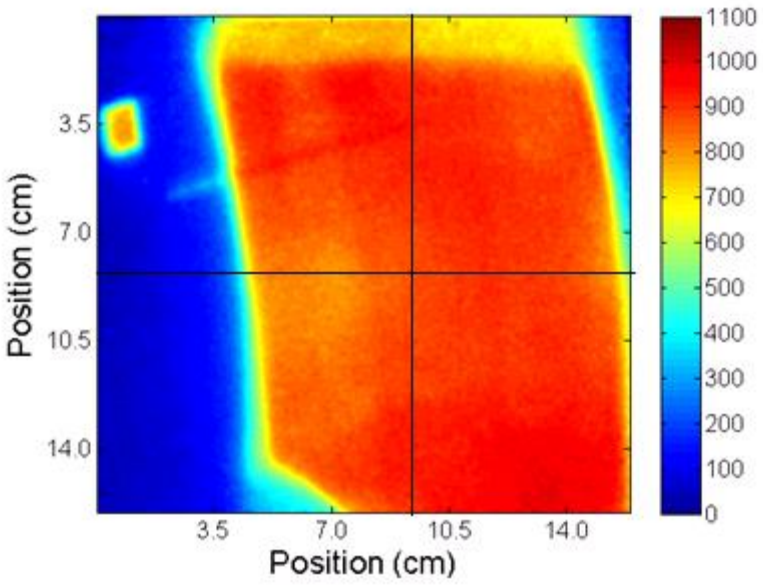

Figure 4.7. The 0 mm offset measured cryogel dose distribution map in cGy with black lines showing the cross line (horizontal) and inline (vertical) axes used to extract profiles at different A/P shifts, shown in figure 4.8.

a)

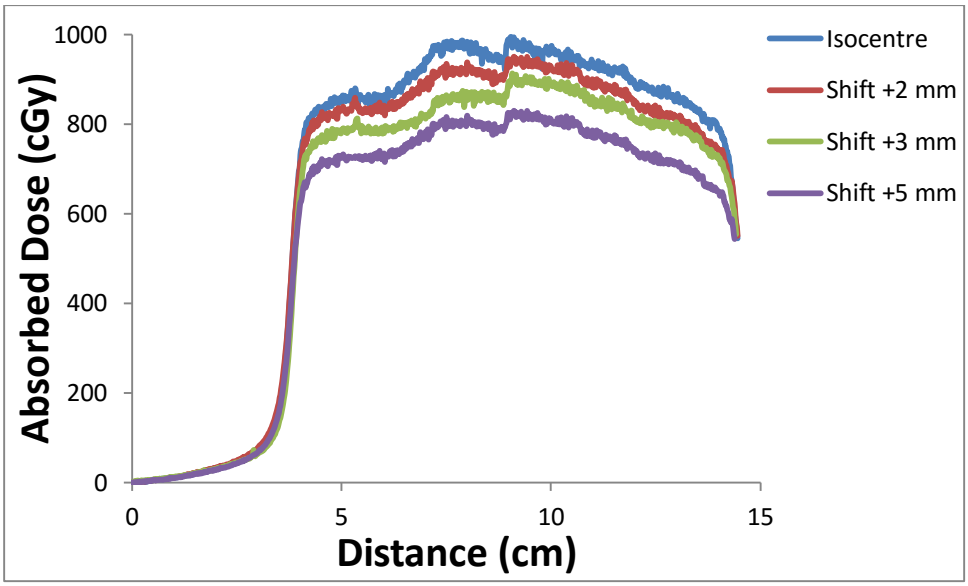

b)

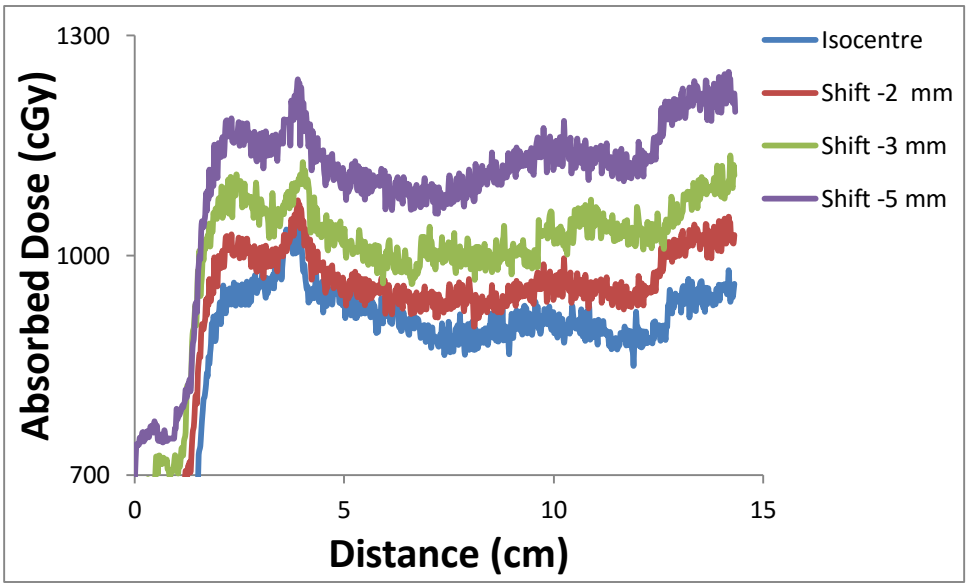

Figure 4.8. a) The cross line profiles and b) inline profiles extracted from absolute measured cryogel dose distribution images at different A/P shifts. The cross line profiles are taken from cryogels where the table was raised (+A/P couch shifts) and the inline profiles when the table was lowered (-A/P couch shifts).

The measured absolute dose distributions at the planned treatment position were compared to those that were acquired at different A/P positions using gamma analysis. For each shift there are 9 corresponding gamma analyses, where each measurement is compared to all 3 planned position measurements to demonstrate reproducibility. For shifts of ±2, ±3, and ±5 mm the passing rates ranged from 94.3% to 95.6%, 74.0% to 78.8%, and 17.5% to 22.5% respectively. A summary of these data is shown in Table 4.2. Figure 4.9 shows examples of the 2D gamma maps comparing the treatment position to shifts of +2 and -3 mm.

a)

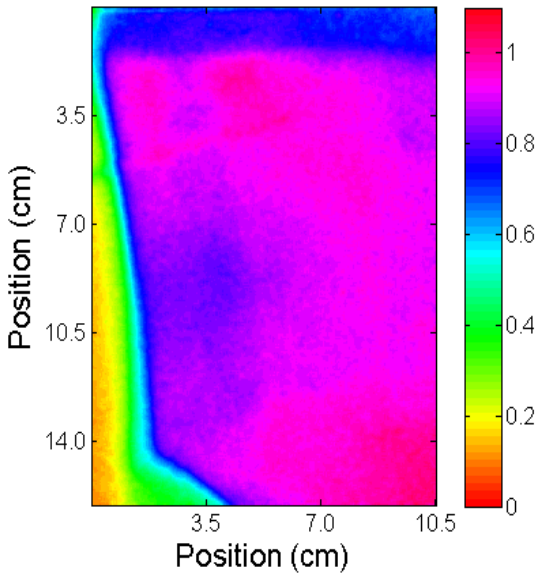

b)

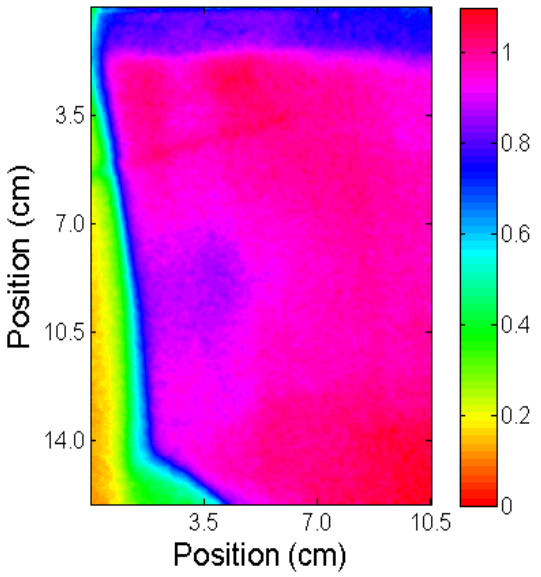

Figure 4.9. 2D gamma maps (3%/3 mm, 10% threshold) comparing dose measured using the cryogel dosimeter at the planned treatment position to A/P shifts of a) +2 and b) -3 mm.

Table 4.2. Summary of gamma analyses (3%/3 mm, 10% threshold) passing rate comparing the measured absolute doses acquired at different A/P shifts to those acquired at the planned position. For each (A/P) shift a total of 9 gamma analyses were performed.

Shift (mm)	Mean ± standard deviation (%)	Minimum (%)	Maximum (%)
-2	95.2 ± 0.6	94.4	95.6
+2	95.0 ± 0.7	94.3	95.2
-3	76.4 ± 1.7	74.4	78.8
+3	75.6 ± 1.0	74.0	76.7
-5	19.6 ± 1.3	17.9	22.5
+5	18.9 ± 0.9	17.5	20.2

The reproducibility of the treatment geometry and gel fabrication methodology was also validated by performing gamma analyses between all the cryogels acquired at the same A/P position. By this measure, the setups were highly reproducible as the lowest passing rate for any treatment setup was 97.6%. A summary of these data is shown in Table 4.3.

Table 4.3. Summary of gamma analyses (3%/3 mm, 10% threshold) passing rate comparing absolute doses measured at the same A/P position using the cryogel.

Shift (mm)	Mean ± standard error (%)	Minimum (%)	Maximum (%)
0	98.9 ± 0.3	98.8	99.1
-2	98.6 ± 0.2	98.3	99.0
+2	98.8 ± 0.2	98.5	99.1
-3	98.6 ± 0.3	98.3	99.2
+3	98.8 ± 0.3	98.5	99.3
-5	98.5 ± 0.2	98.2	98.9
+5	98.5 ± 0.4	97.6	98.7

It is interesting to note that the gamma pass rates are consistent between measurements using the radiochromic cryogel and the Pinnacle dose surfaces. Both studies suggest that a 3 mm A/P offset from the planned position may lead to an unacceptable difference in dose at the chest wall surface (*i.e.* gamma passing rate below 80%). Existing studies suggest that setup errors in the A/P direction can range from approximately 2 to 5 mm (Westbrook *et al.* 1991, Gagliardi *et al.* 1992, Creutzberg *et al.* 1993, Lirette *et al.* 1995, Fein *et al.* 1996, Pouliot *et al.* 1996, Hurkmans *et al.* 2001, Korrreman *et al.* 2006, Alderliesten *et al.* 2013, Brouwers *et al.* 2015). Additional studies have shown that patients may shift their chest wall position during free breathing (FB), BH, and DIBH by 2.5 2.7 and 4.6 mm, respectively (Pedersen *et al.* 2004, Korrreman *et al.* 2005, Korrreman *et al.* 2006, Alderliesten *et al.* 2013, Fassi *et al.* 2014 Brouwers *et al.* 2015). Our data suggest that the larger A/P variations associated with DIBH would be readily discerned. Thus, the cryogel could be used to verify patient positioning during treatment delivery and possibly identify clinically relevant errors.

4.5 Conclusion

Radiochromic cryogels were used to evaluate potential dosimetric errors observed during tangential irradiation of the chest wall arising from A/P shifts. A comparison of absolute dose measured using the cryogels for planned and shifted positions (±2, ±3, and ±5 mm) resulted in gamma passing rates that ranged from 94.3% to 95.6%, 74.0% to 78.8%, and 17.5% to 22.5%, respectively. Similar results were obtained in the associated planning study, where the gamma pass rates ranged from 94.3% to 95.0%,

76.8% to 77.9%, and 23.5% to 24.3% respectively, in the middle of the cryogel as well as at the surface of phantom. These results suggest that the radiochromic cryogel used in this study can detect errors in chest wall position, and that an error as small as 3 mm in the A/P direction may represent a clinically relevant over or under dosing of the chest wall target. A 3 mm offset may arise from a number of sources, whether it is an error in patient setup, breathing irregularity, or for DIBH the patient may shift their body position to mimic a deeper inspiration that they may have achieved during the planning phase. The reproducibility of the radiochromic cryogel measurements was verified by intercomparing the triplicate irradiations performed for each shifted position. Using the same gamma metric as the A/P shift analysis, a minimum pass rate of 97.6% was observed, suggesting excellent reproducibility in cryogel formulation and phantom setup. Given an increased interest of DIBH for left chest wall irradiation and escalating complexity of the associated radiation fields (*e.g.* VMAT), an *in vivo* dosimetry tool that provides build up material and records dose in two dimensions to monitor treatment delivery may be desirable. While radiochromic films satisfy the 2D side of the equation, it may be difficult to place in a predictable position on the skin surface under added build up material, whereas we are proposing a unified system that could be incorporated into the planning process more readily.

Acknowledgment

This work has been supported by the NSERC Discovery Grant program and the Yarmouk University Physics Department.

References

Alderliesten T, Betgen A, Elkhuizen P H, van Vliet-Vroegindeweij C, Remeijer P. Estimation of heart-position variability in 3D-surface-image-guided deep-inspiration breath-hold radiation therapy for left-sided breast cancer. *Radiother. Oncol.* 2013; 109(3):442-447.

Al-Rahbi Z S, Al Mandhari Z, Ravichandran R, Al-Kindi F, Davis C A, Bhasi S, Satyapal N, Rajan B. Dosimetric comparison of intensity modulated radiotherapy isocentric field plans and field in field (FIF) forward plans in the treatment of breast cancer. *J. Med. Phys/Assoc. Med. Phys. India.* 2013; 38(1):22-29.

Bentzen S M and Dische S Late morbidity: the Damocles sword of radiotherapy?. *Radiother. Oncol.* 2001; 61(3):219-221.

Brouwers P J, Lustberg T, Borger J H, van Baardwijk A A, Jager J J, Murrer L H, Nijsten S M, ReymenB H, Van Loon J G M, Boersma L J. Set-up verification and 2-dimensional electronic portal imaging device dosimetry during breath hold compared with free breathing in breast cancer radiation therapy. *Prac. Radiat. Oncol.* 2015; 5(3):e135-e141.

Chiu-Tsao S T, Chan M F. Evaluation of two-dimensional bolus effect of immobilization/support devices on skin doses: A radiochromic EBT film dosimetry study in phantom. *Med. Phys.* 2010; 37(7):3611-3620.

Chu K C, Jordan K J, Battista J J, Van Dyk J, Rutt B K. Polyvinyl alcohol-Fricke hydrogel and cryogel: two new gel dosimetry systems with low Fe^{+3} diffusion. *Phys. Med. Biol.* 2000; 45(4):955-969.

Clarke M, Collins R, Darby S, et al. Effects of radiotherapy and of differences in the extent of surgery for early breast cancer on local recurrence and 15-year survival: an overview of the randomized trials. *Lancet.* 2005; 366 (9503):2087–2106.

Creutzberg C L, Althof V G M, Huizenga H, Visser A G, Levendag P C. Quality assurance using portal imaging: the accuracy of patient positioning in irradiation of breast cancer. *Int. J. Radiat. Oncol. Biol. Phys.* 1993; 25(3):529-539.

Darby S, Mcgale P, Correa C, et al. Early Breast Cancer Trialists' Collaborative Group. Effect of radiotherapy after breast-conserving surgery on 10-year recurrence and 15-year breast cancer death: meta-analysis of individual patient data for 10 801 women in 17 randomised trials. *Lancet.* 2011; 378(9804):1707-1716.

Eyadeh M M, Farrell T J, Diamond K. Evaluation of a ferrous benzoic xylenol orange transparent PVA cryogel radiochromic dosimeter. *Phys. Med. Biol*. 2014; 59(7):1773-1787.

Eyadeh M M, Wierzbicki M, Diamond K R. Measurement of superficial dose distributions in radiation therapy using translucent cryogel dosimeters. Paper submitted to *Biom. Phys. Eng. Exp.* 2015.

Falco M D, Masala S, Stefanini M, Fiori R, Gandini R, Bagalà P, Morosetti D, Calabria E, Tonnetti A, Verona-Rinati G, Santoni R, Simonetti G. Patient skin dose measurements using a cable free system MOSFETs based in fluoroscopically guided percutaneous vertebroplasty, percutaneous disc decompression, radiofrequency medial branch neurolysis, and endovascular critical limb ischemia. *J. Appl. Clin. Med. Phys.* 2015; 16(1):298-310.

Fassi A, Ivaldi G B, Meaglia I, Porcu P, de Fatis P T, Liotta M, Ribold M, Baroni G. Reproducibility of the external surface position in left-breast DIBH radiotherapy with spirometer-based monitoring. *J. Appl. Clin. Med. Phys*. 2014; 15(1):130-140.

Fein D A, McGee K P, Schultheiss T E, Fowble B L, Hanks G E. Intra-and interfractional reproducibility of tangential breast fields: a prospective on-line portal imaging study. *Int. J. Radiat. Oncol. Biol. Phys.* 1996; 34(3):733-740.

Fraass B, Doppke k, Hunt M, Kutcher G, Starkschall G, Stern R,Van Dyke J. American Association of Physicists in Medicine Radiation Therapy Committee Task Group 53:Quality assurance for clinical radiotherapy treatment planning. *Med. Phys*. 1998 25(10):1173-1822.

Gagliardi G, Bjöhle J, Lax I, Ottolenghi A, Eriksson F, Liedberg A, Lind P, Rutqvist L E. Radiation pneumonitis after breast cancer irradiation: analysis of the complication probability using relative seriality model. *Int. J. Radiat. Oncol. Biol. Phys.* 2000; 46(2):373-381.

Gagliardi G, Lax I, Ottolenghi A, Rutqvist L E. Long-term cardiac mortality after radiotherapy of breast cancer-application of the relative seriality model. *Br. J. Radiol.* 1996*;* 69(825):839-846.

Gagliardi G, Lax I, Rutgvis L E. Radiation therapy of stage I breast cancer: analysis of treatment technique accuracy using three-dimensional treatment planning tools. *Radiother. Oncol.* 1992; 24(2):94-101.

Gyenes G, Rutqvist L E, Liedberg A, Fornader T. Long-term cardiac morbidity mortality in a randomized trial of pre-and postoperative radiation therapy versus surgery alone in primary breast cancer. *Radiother. Oncol*. 1998; 48(2):185-190.

Hanley J, Debois M M, Mah D, Mageras G S, Raben A, Rosenzweig K, Mychalczak B, et al. Deep inspiration breath-hold technique for lung tumors: The potential value of target immobilization and reduced lung density in dose escalation. *Int. J. Radiat. Oncol. Biol. Phys.* 1999; 45(3):603–611.

Hsu S H, Roberson P L, Chen Y, Marsh R B, Pierce L J, Moran J M. Assessment of skin dose for breast chest wall radiotherapy as a function of bolus material. *Phys. Med. Biol.* 2008; 53(10):2593-2606.

Hurkmans C W, Remeijer P, Lebesque J V, Mijnheer B J. Set-up verification using portal imaging; review of current clinical practice. *Radiother. Oncol.* 2001; 58(2):105-120.

Khanal S P, Ouhib Z, Benda R K and Leventouri T 2015 Evaluation of surface dose outside the treatment area for five breast cancer irradiation modalities using thermo-luminescent dosimeters. *Int. J. Canc. Thera. Oncol*. 2015; 3(1):ISSN 2330-4049.

Kinhikar R A, Murthy V, Goel V, Tambe C M, Dhote D S, Deshpande D D. Skin dose measurements using MOSFET and TLD for head and neck patients treated with tomotherapy. *Appl. Radiat. Isot*. 2009; 67(9):1683-1685.

Korreman S S, Pedersen A N, Aarup L P, Nottrup T J, Specht L, Nystrom H. Reduction of cardiac and pulmonary complication probabilities after breathing adapted radiotherapy for breast cancer. *Int. J Radiat. Oncol. Biol. Phys.* 2006; 65(5):1375-1380.

Korreman S S, Pedersen A N, Nottrup T J, Specht L, Nystrom H. Breathing adapted radiotherapy for breast cancer: Comparison of free breathing with the breath hold-technique. *Radiother. Oncol.* 2005; 76(3):311-318.

Kry S F, Smith S A, Weathers R, Stovall M. Skin dose during radiotherapy: a summary and general estimation technique. *J. Appl. Clin. Med. Phys.* 2011; 13(3):20-34.

Latty D, Stuart K E, Wang W, Ahern V. Review of deep inspiration breath-hold techniques for the treatment of breast cancer. *J. Med. Radiat. Sci*. 2015; 62(1):74-81.

Lirette A, Pouliot J, Aubin M, Larochelle, M. The role of electronic portal imaging in tangential breast irradiation: a prospective study. *Radiother. Oncol.* 1995; 37(3): 241-245.

Low D A, Harms W B, Mutic S, Purdy J A. A technique for the evaluation of dose distributions. *Med. Phys.* 1998; 25(5):656-661.

Månsson S, Karlsson A, Gustavsson H, Christensson J, Bäck, S Å J. Dosimetric verification of breathing adapted radiotherapy using polymer gel. *J. Phys*.: *Conf* series (Vol. 56, No. 1, p. 300). 2005; IOP Publishing

Mansouri S, Naim A, Glaria L, Marsiglia H. Dosimetric evaluation of 3-D conformal and intensity-modulated radiotherapy for breast cancer after conservative surgery. *Asian. Pac. J. Cancer .Prev*.2014; 15(11):4727-4732.

Mavroidis P, Axelsson S, Hyödynmaa S, Rajala J, Pitkänen M A, Lind B K, Brahme A. Effects of positioning uncertainty and breathing on dose delivery and radiation pneumonitis prediction in breast cancer. *Acta. Oncol.* 2002; 41(5):471-485.

Mitine C, Leunens G, Verstraete J, Blanckaert N, Dam J B, Dutreix A, Der Schueren E B. Is it necessary to repeat quality control procedures for head and neck patients?. *Radiother. Oncol.* 1991; 21(3):201-210.

Morales J E, Hill R, Crowe S B, Kairn T and Trapp J V 2014 A comparison of surface doses for very small field size x-ray beams: Monte Carlo calculations and radiochromic film measurements. *Austra. Phys. Engin. Sci. Med.* 2014; 37(2):303-309.

Nakano M, Hill R F, Whitaker M, Kim J H, Kuncic Z. A study of surface dosimetry for breast cancer radiotherapy treatments using Gafchromic EBT2 film. *J. Appl. Clinic. Med. Phys.* 2012; 13(3):3727:3727.

Ohara K, Okumura T, Akisada M, Inada T, Mori T, Yokota H, Calaguas M J. Irradiation synchronized with respiration gate. *Int. J. Radiat. Oncol. Biol. Phys.* 1989; 17(4):853-857.

Ooi G C, Kwong D L W, Chan K N, Ngan H, Lock D T W, Lam W K, Chan F L,Au G and Tsang, K W T Serial HRCT lung changes after 3-field radiation treatment of breast cancer. *Clin. Radiol*. 2000; 55(11):817-824.

Pedersen A N, Korreman S S, Nystrom H, Specht L. Breathing adapted radiotherapy of breast cancer: reduction of cardiac and pulmonary doses using voluntary inspiration breath-hold. *Radiother. Oncol.* 2004; 72(1):7253-7260.

Pouliot J, Lirette A. Verification and correction of setup deviations in tangential breast irradiation using EPID: gain versus workload. *Med. Phys*. 1996; 23(8):1393-1398.

Prabhakar R, Tharmar G, Julka P K, Rath G K, Joshi R C, Bansal A K, Bisht R K, Gopishankar N, Pant G S, Thulkar S. Impact of different breathing conditions on the dose to surrounding normal structures in tangential field breast radiotherapy. *J. Med. Phys.* 2007; 32(1):24–28.

Quach K Y, Morales J, Buston M J, Rosenfeld A B, Metcalfe P E. Measurement of radiotherapy skin dose x-ray skin dose on a chest wall phantom. *Med. Phys*. 2000; 27(7):1676-1680.

Recht A. Which breast cancer patients should really worry about radiation-induced heart disease — and how much?. *J. Clin. Oncol.* 2006; 24(25):4059–4061.

Remouchamps V M, Vicini F A, Sharp M B, Kestin L L, Martinez A A, Wong J W. Significant reduction in heart and lung doses using deep inspiration breath hold with active breathing control and intensity-modulated radiation therapy for patients treated with locoregional breast irradiation. *Int. J. Radiat. Oncol. Biol. Phys.* 2003; 55(2):392-406.

Rudat V, Alaradi A, Mohamed A, Yahay K, Altuwaijri S. Tangential beam IMRT versus tangential beam 3D-CRT of the chest wall in postmastectomy breast cancer patients: a dosimetric comparison. *Radiat. Oncol.* 2011; 6(26):717X-6.

Saliou M G, Giraud P, Simon L, Fournier-Bidoz N, Fourquet A, Dendale R, Cosset J M. Radiotherapy for breast cancer: respiratory and set-up uncertainties. *Canc. Radiother.* 2005; 9(6):414-421.

Shah C, Badiyan S, Berry S, Khan A J, Goyal S, Schulte K, Nanavati A, Lynch M, Vicini F A. Cardiac dose sparing and avoidance techniques in breast cancer radiotherapy. *Radiother. Oncol.* 2014; 112(1):9-16.

Sixel K E, Aznar M C, Ung Y C. Deep inspiration breath hold to reduce irradiated heart volume in breast cancer patients. *Int. J. Radiat. Oncol. Biol. Phys*. 2001; 49(1):199-204.

Stathakis J S, Li K, Paskalev J, Yang L, Wang and Ma C M 2006 Ultra thin TLDs for skin dose determination in high energy photon beams. *Phys. Med. Biol.* 2006; 51(14):3549-3567.

Swamy S T, Radha C A, Kathirvel M, Arun G, Subramanian S. Feasibility study of deep inspiration breath-hold based volumetric modulated arc therapy for locally advanced left sided breast cancer patients. *Asian. Pac. J. Cancer. Prev*. 2014; 15(20):9033-9038.

Van Tienhoven G, Lanson J H, Crabeels D, Heukelom S, Mijnheer B J. Accuracy in tangential breast treatment set-up: a portal imaging study. *Radiother. Oncol.* 1991; 22(4):317-322.

Vinh-Hung V, Burzykowski T, Van de S J, Storme G, Soete G. Post-surgery radiation in early breast cancer: survival analysis of registry data. *Radiother. Oncol.* 2002; 64(3) 281-290.

Westbrook C, Gildersleve J, Yarnold J. Quality assurance in daily treatment procedure: patient movement during tangential fields treatment. *Radiother. Oncol.* 1991; 22(4): 299-303.

Whelan T J, Julian J, Wright J, Jadad A R, Levine M L. Dose locoregional radiation therapy improve survival in breast cancer? A meta analysis. *J. Clin. Oncol.* 2000; 18(6):1220-1229.

Wong J W, Sharpe M B, Jaffray D A, Kini V R, Robertson J M, Stromberg J S, Martinez A A. The use of active breathing control (ABC) to reduce margin for breathing motion. *Int. J. Radiat. Oncol. Biol. Phys*. 1999; 44(4), 911-919.

Xiang H F, Song J S, Chin D W, Cormack R A, Tishler R B, Makrigiorgos G M, Chin L M. Build-up and surface dose measurements on phantoms using micro-MOSFET in 6 and 10MV x-ray beams and comparisons with Monte Carlo calculations. *Med. Phys.* 2007; 34(4):1266-1273.

Chapter 5

Conclusions and Future Directions

5.1 Summary and Conclusions

The primary objective in radiotherapy is to deliver the prescribed dose to a tumour while minimizing the dose delivered to the surrounding healthy tissues (Jin *et al.* 2008). Current radiotherapy techniques such as IMRT have led to improved tumour control by conforming the dose distribution to the target volume (Ibbott 2006, Baldock *et al.* 2010). *In vivo* dosimeters currently in use in radiotherapy such as TLDs and films are limited to one and two dimensions. Gel dosimeters are capable of recording dose distributions in three dimensions and can be formed into a variety of shapes by choosing an appropriate mould (Schreiner 2009). Gel dosimeters may also be used to evaluate the delivered dose distribution under realistic treatment conditions, as designed in the original treatment plan, where film and TLDs may not be able to achieve the same coverage.

The overall objective of this thesis was to develop a transparent PVA cryogel radiochromic dosimeter that could be read optically and characterize its radiosensitivity. It was also desirable that the dosimeter have adjustable, tissue-like mechanical properties. The radiochromic cryogel developed in the first section of this thesis was then evaluated for its potential use as an *in vivo* dosimeter.

Chapter 2 describes the development of a translucent PVA cryogel loaded with radiochromic ferrous-benzoic-xylenol orange (FBX-PVA-C). The cryogel was made translucent by adding DMSO to the formulation. A wide range of PVA concentrations and thermal cycles were studied, both of which affect the mechanical properties of the cryogel. Samples were prepared using 5% to 15% by weight PVA, for two different ratios of water/DMSO (20/80 and 30/70 by weight), and were subjected to one, three, or six FTCs. Each cycle contains a period of freezing for 18 hours at -80^{o}C and thawing at room temperature for 6 hours. The irradiated gels have an absorbance band over the range of 590-600 nm. The absorption coefficient at 595 nm was calculated from pre- and post-irradiation transmission measurements using a colourless and transparent PVA-C sample as reference.

A deformable radiochromic dosimeter was obtained that was stable pre- and post-irradiation: stability was evaluated over a two day period prior to irradiation and seven days afterwards for a particular formulation (15% PVA, 3 FTCs, 20/80 DMSO). The dose response was dependent on PVA concentration and thermal cycling: the sensitivity of the radiochromic cryogel increased with PVA concentration and #FTCs. The 30/70 dosimeter was more sensitive than the more transparent 20/80 system due to increased oxidation from Fe^{2+} to Fe^{3+}.

Reproducible linear relationships between dose and absorption coefficients up to 1000 cGy were obtained. The dosimeter was found to be energy independent over the range of nominal photon energies of 6, 10, and 18 MV with an overall sensitivity of (3.00±0.04) $x10^{-4}$ mm^{-1} cGy^{-1} for particular formulation. The study also suggested that there was no significant effect of dose rate on the measured response.

The results obtained in this study were consistent with related studies (Chu *et al.* 2000, Hill *et al.* 2002), except the dose was read using a simple, accessible optical instrument rather than MRI. Overall, this study showed that it is feasible to use a transparent PVA cryogel matrix loaded with FBX as a deformable radiochromic dosimeter.

In Chapter 3, the translucent FBX-PVA-C described in Chapter 2 was studied in an *in vivo* dosimetry context. Typically, a piece of film would be used to measure a 2D skin surface distribution; however, film does not wrap well around irregularly curved surfaces, whereas FBX-PVA-C does. The translucent cryogels were formed into 5 mm thick sheets of radiochromic bolus and evaluated for their ability to quantify superficial dose distributions arising from irradiations with high energy photons. The study was performed in two sections: first, a relationship between the dose delivered to the bolus/surface interface and the dose recorded by the bolus was determined; and second, a series of proof of principle measurements were performed on the head and neck region of an anthropomorphic phantom. The radiochromic bolus samples were imaged pre- and post-irradiation using a charge coupled device (CCD) camera, illuminated using a uniform, red LED array. In the first section of this study, the ratios between surface dose (estimated using Gafchromic EBT-2 film on the surface of a polystyrene phantom) and the dose measured in the overlying 5 mm sheet of radiochromic bolus were measured for a series of open field irradiations with gantry angles of 0^o, 22.5^o, 45^o, 67.5^o, and 90^o.

The dose measured in the radiochromic bolus and the dose at the underlying surface both increased with increasing gantry angle, consistent with the observations of Hsu *et al.* (2008). The measured ratio ranged from 0.749 ± 0.005 at 0^o to 0.930 ± 0.002 at 90^o.

To convert dose in bolus to dose to the skin surface, a single correction factor of 0.80 was computed empirically by minimizing the differences between the film and the calibrated bolus doses for all gantry angles. Inline and cross line profiles were extracted from the film and calibrated bolus. The average differences between Gafchromic film and calibrated bolus profiles ranged from 1.4 to 1.9%.

The calibration factor was applied to clinical head and neck IMRT treatment plans that were delivered to a RANDO phantom to demonstrate the cryogel's potential for *in vivo* dosimetry measurements. The radiochromic bolus was added electronically to the CT scan of the RANDO phantom to approximate the conditions of the actual patient treatments. A gamma comparison between the calibrated radiochromic bolus and film was performed to evaluate the performance of the bolus. The pass rate ranged from 95.2 to 96.4% for different IMRT fields arrangements (3%/3mm evaluation criteria, 10% dose threshold). These comparisons suggested that the radiochromic bolus provided an accurate estimation of skin surface dose using a simple correction factor.

In conclusion, a comparison of EBT-2 Gafchromic film and translucent FBX-PVA-C suggests that the radiochromic bolus may used in place of more conventional models of bolus to conduct *in vivo* dosimetry in regions where skin surface dose is of interest.

In Chapter 4, the radiochromic bolus developed in Chapter 3 was used to study a clinical problem related to chest wall irradiation during deep inspiration breath hold (DIBH). CT images of the RANDO phantom with a cryogel placed over the chest wall were acquired and a forward planned IMRT tangential chest wall treatment plan generated. The radiation beams were delivered in the planned position, and with the

phantom shifted in the A/P direction by ±2 mm, ±3 mm, and ±5 mm to simulate errors in chest wall position during DIBH. The effect of these shifts was studied using the treatment planning software along with measurements using the radiochromic bolus. The dose planes in the middle of cryogel and on the phantom surface were calculated using Pinnacle 9.2. Two dimensional images at the planned position were compared with the distributions at all shifts from this position using gamma analysis (3%/3mm, 10% threshold).

For shifts of ±2, ±3, and ±5 mm, the gamma pass rates resulting from the cryogel measurements ranged from 94.3% to 95.6%, 74.0% to 78.8%, and 17.5% to 22.5%. The cryogel measurements were consistent with dose planes calculated in Pinnacle, which ranged from 94.3% to 95.0%, 76.8% to 77.9%, and 23.5% to 24.3% at both the middle of cryogel and the surface of the phantom. The gamma analysis suggested that A/P shifts of the chest wall of less than 3 mm may lead to an inferior treatment, as the 3 mm shift results in a reduction in coverage of the 95% isodose line of approximately 7% compared to the planned position, which may be considered clinically significant. The maximum chest wall A/P displacement reported in the literature for DIBH and setup error falls between 4 – 5 mm (Mavroidis *et al.* 2002, Korreman *et al.* 2005, Alderliesten *et al.* 2013, Fassi *et al.* 2014, Brouwers *et al.* 2015). The results of our study suggest that errors of this magnitude may be clinically unacceptable. We may conclude, then, that the radiochromic cryogel bolus employed in this study is capable of quantifying clinically relevant errors in patient position (setup or breath hold).

As an overall conclusion of this thesis, a stable, rubbery cryogel dosimeter with good sensitivity, that can be read optically, was developed using FBX in a transparent PVA

cryogel matrix. This dosimeter is accurate enough to be used to perform *in vivo* dosimetry, as demonstrated using examples of head and neck IMRT and DIBH tangential chest wall irradiations, and may be used to monitor superficial dose distribution in the clinical setting.

5.2 Future Directions

Gel dosimetry provides the promise of accurate and convenient dosimetry under several circumstances, where robust and convenient dosimetry tools are required to record complex three dimensional dose distributions (Guo *et al.* 2006). In three dimensional radiochromic gel dosimetry, there are two areas of concern: development of optical read out techniques and development of accurate three dimensional dosimeters (Vandecasteele *et al.* 2011). The translucent FBX-PVA-C dosimeter developed as part of this thesis should be optimized for its use in three dimensional verification. This is due to two reasons: first, the absorption coefficient at the read out wavelength of the unirradiated dosimeter is high, which may limit the thickness of material that could be imaged. Different concentrations of XO and ferrous ammonium sulphate may lead to a reduction of the unirradiated absorbance. Second, it is not easy to produce perfect samples at high PVA concentrations; the hydrogel may hold bubbles even after evacuation. Future studies should focus on modifying the formula to get lower attenuation while maintaining good dose response. We believe that our approach is capable of creating translucent FBX-PVA-C dosimeter for three dimensional verification.

DMSO is not the only option to clarify PVA cryogels for optical read out techniques. Other solvents, acetone, ethylene glycol, and glycerine for example, should also be

investigated for use in future formulations. One significant advantage of a non-DMSO solvent is that there may be an increase in radiosensitivity of the dosimeter compared to DMSO: DMSO is a known free radical scavenger, so eliminating it from the formulation may be desirable. Future studies should focus on improving the sensitivity of existing optical measurement systems that would permit the detection of lower levels of transmitted light. This would allow larger samples to be measured, enabling the simulation of larger organs. Along this vane, most optical CT systems require regularly shaped phantoms (e.g. cylinders). Future work should also focus on models of light propagation that would allow for 3D reconstructions of arbitrarily shaped phantoms. Similarly, realistic tissue-mimicking 3D dosimeters should also be modeled; this could be achieved by exploiting the relationships between PVA concentrations, thermal cycling, and the radiochromic formulation.

The translucent FBX-PVA-C dosimeter is promising for dosimetric quality assurance of complex radiation treatments for different parts of patient's body, including the deformability of the phantom. The implementation of PVA-C dosimetry into the clinical radiotherapy environment is possible, but more research is required. The findings of this thesis lay the groundwork toward the successful implementation of PVA-C dosimetry in clinical radiotherapy.

References

Alderliesten T, Betgen A, Elkhuizen P H M, van Vliet-Vroegindeweij C and Remeijer P 2013 “Estimation of heart-position variability in 3D-surface-image-guided deep-inspiration breath-hold radiation therapy for left-sided breast cancer”, *Radiother. Oncol*. 109(3) 442-447

Baldock C, De Deene Y, Doran S, Ibbott G, Jirasek A, Lepage M, McAuley K B, Oldham M and Schreiner L J 2010 “Polymer gel dosimetry”, *Phys. Med. Biol*. 55(5) R1-R63

Brouwers P J, Lustberg T, Borger J H, van Baardwijk A A, Jager J J, Murrer L H, Nijsten S M, ReymenB H, Van Loon J G M and Boersma L J 2015 “Set-up verification and 2-dimensional electronic portal imaging device dosimetry during breath hold compared with free breathing in breast cancer radiation therapy”, *Pract. Radiat. Oncol.* 5(3) e135-e141

Chu K C, Jordan K J, Battista J J, Van Dyk J and Rutt B K 2000 “Polyvinyl alcohol Fricke hydrogel and cryogel:two new gel dosimetry systems with low Fe^{+3} diffusion”, *Phys. Med. Biol.* 45(4) 955-969

Fassi A, Ivaldi G B, Meaglia I, Porcu P, de Fatis P T, Liotta M, Ribold M and Baroni G 2014 “Reproducibility of the external surface position in left-breast DIBH radiotherapy with spirometer-based monitoring”, *J. Appl. Clin. Med. Phys*. 15(1) 130-140

Guo P Y, Adamovics J A and Oldham M 2006 “Characterization of a new radiochromic three dimensional dosimeter”, *Med. Phys*. 33(5) 1338 –1345

Hill B, Bäck S Å J, Lepage M, Simpson J, Healy B and Baldock C 2002 “Investigation and analysis of ferrous sulfate polyvinyl alcohol (PVA) gel dosimeter”, *Phys. Med. Biol.* 47(23) 4233-4246

Hsu S H, Roberson P L, Chen Y, Marsh R B, Pierce L J and Moran J M 2008 “Assessment of skin dose for breast chest wall radiotherapy as a function of bolus material”, *Phys. Med. Biol.* 53(10) 2593-2606

Ibbott, G S 2006 “Clinical applications of gel dosimeters”, *J. Phys. Conf* (Vol. 56, No. 1, p. 108). IOP Publishing

Jin H, Palta J, Suh T S, and Kim S 2008 “A generalized a priori dose uncertainty model of IMRT delivery”, *Med. Phys.* 35(3) 982-996

Korreman S S, Pedersen A N, Nottrup T J, Specht L and Nystrom H 2005 “Breathing adapted radiotherapy for breast cancer: Comparison of free breathing with the breath hold-technique”, *Radiother. Oncol.* 76(3) 311-318

Mavroidis P, Axelsson S, HyödynmaaS, Rajala J, Pitkänen M A, Lind B K, and Brahme A 2002 “Effects of positioning uncertainty and breathing on dose delivery and radiation pneumonitis prediction in breast cancer”, *Acta. Oncol.* 41(5) 471-485

Schreiner L J “Where does gel dosimetry fit in the clinic?”, 2009 *J. Phys. 5th Int. Conf. on Radiotherapy Gel Dosimetry* , Conf series 164

Vandecasteele J, Ghysel S, Baete S H and De Deene Y 2011 “Radio-physica properties of micelle leucodye 3D integrating gel dosimeters”, *Phys. Med. Biol*. 56(3) 627 –651

Appendix I

Transparent FBX-PVA-C radiochromic cryogel manufacture

A) 20/80 (water/DMSO) stock by weight

Distilled water	100 mL
DMSO	362.32 mL
Sulphuric acid (18M)	642.63 μL

The resulting solution is equivalent to 25 mM sulphuric acid.

B) 10 mL stock solution

Distilled water	10 mL
Sulphuric acid (18M)	139 μL
Benzoic acid	0.061 g
Xylenol Orange	0.076 g

The resulting stock solution is equivalent to 25 mM sulphuric acid.

C) Ferrous ammonium sulphate stock solution

Stock solution	1 mL
Ferrous ammonium sulphate	0.0028 g

D) Manufacturing process

The manufacturing process begins with preparation of 20/80 (water/DMSO) stock by weight consists of water, DMSO, and sulphuric acid, followed by the addition of PVA (*e.g.* 15% by weight) to 80 mL of water/DMSO stock. The mixture should stir at 120^{o}C for 120 min under normal atmospheric pressure using a hot plate stirrer. The volume of the hydrogel is monitored during stirring and sulphuric water/DMSO mixture should be added to replace any evaporated liquid.

10 mL stock solution consists of water, benzoic acid, xylenol orange, and sulphuric acid will be prepared in a volumetric flask and kept at room temperature.

In another beaker, ferrous ammonium sulphate will be dissolved in 1 mL of the stock solution (benzoic acid, xylenol orange, and sulphuric acid) and then will be added to the PVA hydrogel after it had cooled to 50 ^{o}C. The process will be completed by adding sulphuric water/DMSO mixture (*e.g.* 20 mL) to the hydrogel and mixing slowly at 50 ^{o}C for another 10 min.

The warm hydrogel is subsequently evacuated for 15 min to remove unwanted air bubbles. The hydrogel is then poured into moulds. The samples were then subjected to one, three, or six freeze-thaw-cycles.

Clear and colourless reference samples are also produced using the same procedure as above omitting the stock solution and ferrous ammonium sulphate (*i.e.* without xylenol orange, ferrous ammonium sulphate, and benzoic acid).

E) Thermal cycling

One Freeze-thaw-cycle (FTC) for the purposes of this thesis consists of 18 hours freezing at -80^{o}C and thawing at room temperature for 6 hours. Freezing may be performed at a higher temperature (-20^{o}C) in a conventional freezer or in an environmental chamber (*e.g.* TestEquity 107 chamber).